Spring 1995

Excited-State Magnesium-Rare Gas Optical Collisions

Rosemary A. Lasell
Old Dominion University

EXCITED-STATE MAGNESIUM–RARE GAS OPTICAL COLLISIONS

by

Rosemary A. Lasell
B.S. May 1985, Bob Jones University
M.S. May 1992, Old Dominion University

A Dissertation Submitted to the Faculty of Old Dominion University
in Partial Fulfillment of the Requirement for the Degree of

DOCTOR OF PHILOSOPHY

PHYSICS

OLD DOMINION UNIVERSITY
May, 1995

Approved by:

Mark D. Havey (Director)

ABSTRACT

EXCITED-STATE MAGNESIUM–RARE GAS OPTICAL COLLISIONS

Rosemary A. Lasell
Old Dominion University, 1995
Director: Dr. Mark D. Havey

Polarization and intensity spectra have been obtained for excited-state magnesium ($3s3p\ ^1P_1$) – rare gas optical collisions. The magnesium was excited by a linearly polarized laser tuned to the $3s^2\ ^1S_0 \rightarrow 3s3p\ ^1P_1$ atomic transition at 285 nm. A second linearly polarized laser was tuned near the $3s3p\ ^1P_1 \rightarrow 3s5s\ ^1S_0$ transition at 571 nm (experiment A) and near the $3s3p\ ^1P_1 \rightarrow 3s4d\ ^1D_2$ transition at 553 nm (experiment B). The polarization vector of the second laser was oriented either parallel or perpendicular to the polarization direction of the first laser. The absorption of nonresonant light from the second laser, possible only during a collision, was monitored by cascade fluorescence from the $3s^2\ ^1S_0 \leftarrow 3s4p\ ^1P_1$ transition at 203 nm. For each detuning of the second laser from resonance, the degree of linear polarization and the intensity were measured. For experiment A, argon and neon were used as rare gases. For experiment B, argon was the rare gas used. For experiment B, fluorescence from the $3s3p\ ^1P_1 \leftarrow 3s5s\ ^1S_0$ transition, and the $3s3p\ ^3P_j \leftarrow 3s5s\ ^3S_1$ transition at 333 nm were also measured in an attempt to observe the region of inelastic transitions in the molecular states. No inelastic branching was observed in this experiment.

ACKNOWLEDGMENTS

I would like to thank Dr. Mark Havey, my research advisor, for his guidance in this research and his encouragement in my studies. I am also grateful to the other committee members, Dr. L. Vušković, Dr. C. Hyde-Wright, Dr. R. Schiavilla, and Dr. A. Dharamsi, for reading this dissertation and making helpful comments. I greatly appreciate the help and support of my fellow graduate students, especially Mr. David Olsgaard and Mrs. Burçin Bayram, who worked with me on these experiments. Finally, I would like to thank my parents, Stanley and Marvine Lasell, and my siblings, Leona, Horace, and Orvil Lasell, for their moral support during my graduate work.

This research was supported by the National Science Foundation.

TABLE OF CONTENTS

LIST OF TABLES

LIST OF FIGURES

Chapter 1

Introduction

The study of collisional line broadening has a long history[1], but there are still areas to be investigated in the field. Since the line shape is affected by the dynamics of the collision, measuring the line broadening has been important in improving collision theories and calculated molecular potentials. More recently, measurements of the angular distribution of the emitted light, or light absorbed in a second excitation, have increased the details that can be discerned by experiment [2]. Interactions of molecular systems with light have practical applications as well. If the details of the interactions are known, it may be possible to use an interaction to produce a desired light output, for example, in lamps; or it may be possible to use light to produce a desired type of interaction, for example, in excimer lasers.

Several different kinds of collision studies have been performed, each with advantages. In a full collision, the characteristics of each atom are measured before and after the collision. These were the first experiments in the field, but full collision studies can still give useful information about the collision, especially if it involves using atomic beams to select the initial velocity, polarization, and atomic state of the atoms [3,4]. These experiments have been called "complete," in that initial and final quantum numbers are selected, along with initial and

final velocities. However, measuring the system during the collision gives even more information.

Light that is absorbed during a collision may be spectrally far from an atomic resonance; hence the name collisional line broadening. The process, also called an optical collision, has been studied by several experimental and theoretical groups [5-7]. One type of optical collision, a half collision, begins with both atoms in their ground state. During the collision a photon is absorbed, leaving the system in an excited state. After the collision the molecule dissociates to an excited atomic state, then emits a photon, or is probed by a photon with an atomic resonance frequency. Knowing the characteristics, the frequency and polarization, of the absorbed photon and measuring the multipolar intensity of the emitted photon or knowing the characteristics of the probe photon and transition gives information about the collision from the time the photon was absorbed until the collision has ended [8-11].

A variation of the half-collision technique is a fractional collision, in which two photons that are off atomic resonance are absorbed during a single collision [12-14]. The time between the two absorptions is a fraction of the total collision time. Fractional collisions may also be studied by using extremely short-pulse lasers, and adjusting their timing so that both are absorbed during a single collision [15].

Half collision effects need not be confined to scattering states of the molecular system. In some cases, a photon can excite the molecular system to a

bound upper state, a process called photoassociation. States formed by photoassociation are called excimers, and are often used to make high-power lasers. In contrast, a photon may excite a bound molecule to an unbound upper state, a process known as photodissociation [16-18].

Another variation of the half collision is to use a laser to prepare one of the atoms participating in the process in a polarized excited state. This method allows the observation of the transport of atomic alignment into the molecular system. The experiments reported here are of this type.

Theories as well as experiments have been developed for the field of optical collisions. The theories range from formal, fully quantum calculations [19-21] to simpler, more intuitive semiclassical models [22]. Experimental data is used to test and refine the calculations to improve the understanding of the optical collisions process.

This dissertation discusses optical collisions of excited-state ($3s3p\ ^1P_1$) magnesium with argon or neon. During the collision the molecular system is excited to the $3s5s\ ^1\Sigma_0^+$ state or the $3s4d\ ^1\Sigma_0^+$, $3s4d\ ^1\pi_1$, or $3s4d\ ^1\Delta_2$ state. The main results are polarization spectra, and I interpret these using the adiabatic reorientation model of Lewis *et al* [22], as extended by Kupriyanov [23]. In the experiments, I made measurements which are sensitive to inelastic transitions among the $3s5s\ ^1\Sigma_0^+$ state, the $3s4d\ ^1\Sigma_0^+$ and $3s4d\ ^1\pi_1$ states, and the $3s5s\ ^3\Sigma_1$ state.

The remainder of this dissertation is organized as follows. Chapter two covers some relevant theoretical concerns. It includes the concepts of polarization

and alignment of states, selection rules, the adiabatic reorientation model, and the Landau-Zener model of non-adiabatic transitions. Chapter three discusses the experimental apparatus and methods. It includes the special challenges of producing variable-polarization, variable-frequency light with minimized background. Chapter four presents the results and their interpretation. These consist of the polarization and intensity spectra, the disalignment rates, and the inelastic transition data. Systematic influences on the data are also discussed here. Chapter five provides a summary of the results. It further suggests improvements to the experiment and ideas for future experiments.

Chapter 2

Theoretical Background

This chapter provides some background for the ideas explored in the experiments. It begins by discussing the absorption of light during a collision. This is followed by a discussion of the usefulness of polarized light in optical collision studies. Then the adiabatic reorientation model of optical collisions is explained. Finally there is a brief discussion of inelastic branching, including the Landau-Zener Model.

Optical Collisions

Figure 1 shows a partial energy level diagram for magnesium [24]. An electron may gain or lose energy only in amounts corresponding to differences between energy levels. Therefore, a magnesium atom can absorb or emit light with frequencies specified by

$$h\nu = E_2 - E_1 \tag{2.1}$$

where h is Planck's constant, ν is the frequency of the light, and E_1 and E_2 are the energies of two levels. An absorption or emission spectrum of the atom, where

FIGURE 1
Partial energy level diagram for magnesium.

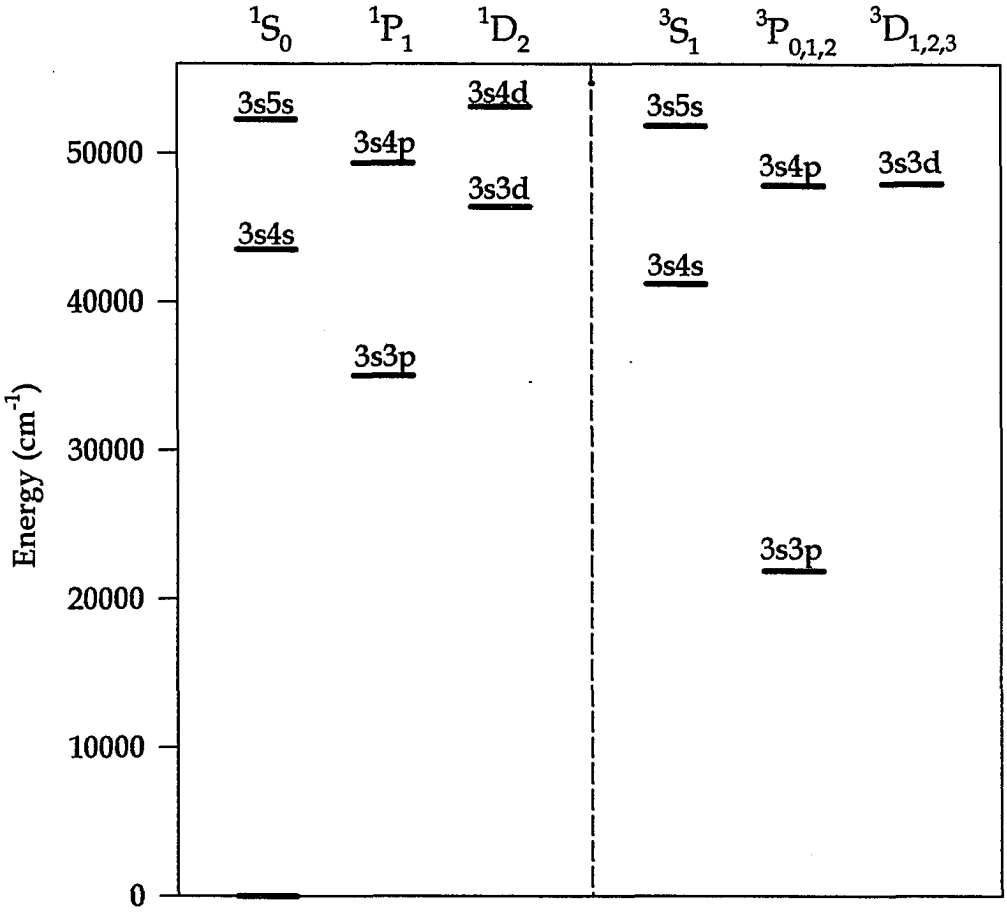

intensity of absorbed or emitted light is plotted versus frequency, will consist of a series of intensity maxima at frequencies given by the above equation. The width of each peak depends on the lifetimes of the states involved, according to the uncertainty principle. The width can also be affected by the conditions of the measurement; for example, the relative motion of the atom and light source, and interactions with other atoms.

During a binary collision, the system energy changes with the distance between the atoms. Figure 2 qualitatively shows the potential energy for a magnesium-rare gas pair, as a function of the distance between the nuclei; that is, a partial molecular potential diagram [25-27]. The ground and first excited states have been determined by spectroscopy, but the upper states are estimated from calculations for the 3s4s $^1\Sigma_0$ state. For very small distances, the atoms repel each other. For very large distances, the effect of the rare gas atom on the magnesium atom is negligible. For intermediate distances, the atoms may either attract or repel. An attraction at intermediate distances forms a well in the potential for that energy level, which allows the formation of bound states for the magnesium-rare gas molecule. In these experiments, the main concern is not bound states, but rather the free states describing the collision.

The molecular system can absorb a photon that makes up the energy difference between two electronic potentials (Figure 3). According to the Classical Franck-Condon Principle, the absorbed frequencies ν' can be related to the upper and lower state potentials, $V_u(R)$ and $V_l(R)$:

FIGURE 2
Qualitative interaction potentials for selected magnesium - rare-gas molecular states. Axes are not to scale.

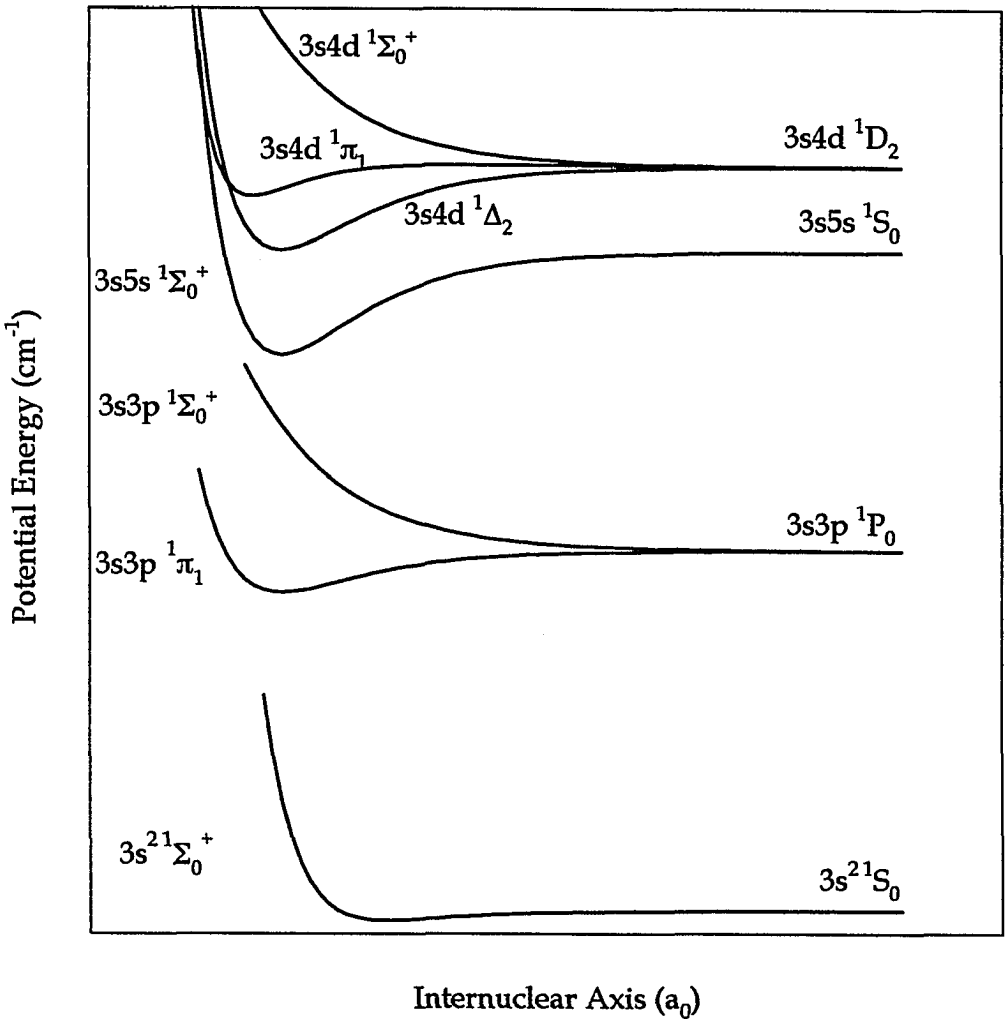

FIGURE 3
Illustration of the Classical Franck-Condon Principle. The potentials V(R) are measured from the atomic energy levels.

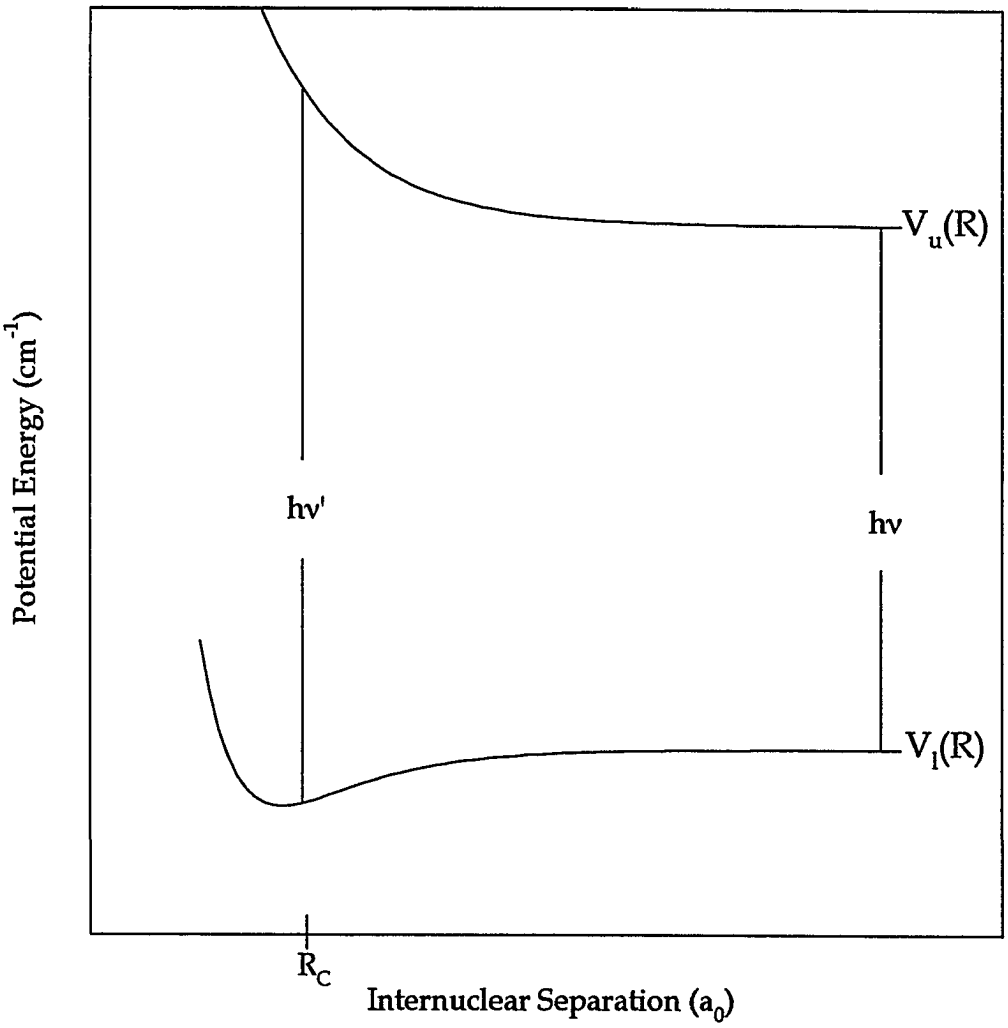

$$h\nu' - h\nu = V_u(R) - V_l(R) \tag{2.2}$$

where ν is an atomic resonance frequency. The assumption is that the absorption takes place much faster than the atoms move, so that the internuclear separation R is about the same for both potentials. The location R at which a given ν' may be absorbed is called a Condon point; these are also the stationary points for the optical transition. Thus during a collision the molecular system can be excited by light of frequencies that neither atom can absorb when it is isolated. The assumption that the excitation takes place much faster than the atoms move depends on the relation between the duration of the collision, t_c, and the characteristic time associated with the absorbed frequency, t_f. This characteristic time is the inverse of the detuning of the light from resonance, Δ

$$t_f = \frac{1}{\Delta} \tag{2.3}$$

$$\Delta = \omega' - \omega \tag{2.4}$$

where ω' is the frequency of the light, and ω is the resonance frequency of the atom. For the Franck-Condon Principle to hold, t_f must be smaller than t_c. The duration of the collision in the experiments is on the order of a picosecond, so $1/t_c$ is ~ 10 cm^{-1}. Detunings less than this are said to be approaching the impact limit, where the integrated effect of the entire collision is important. Detunings approximately equal to $1/t_c$ are termed intermediate, and there is as yet no satisfactory theory explaining all observed effects in the intermediate region.

Detunings greater than $1/t_c$ are said to be approaching the quasi-static limit, where the atoms are essentially stationary as far as the absorption is concerned. The experiments concentrate on the quasi-static region.

If the molecular potentials are known, then the internuclear separations where optical transitions occur can be estimated for a given absorption frequency. Occasionally there are multiple Condon points; that is, equation (2.2) is satisfied for more than one R. Some potentials are approximately parallel for a range of R. These regions, called satellite regions, lead to increased absorption for a given frequency of light, but they also increase the spread in R for an optical transition.

Optical Polarization Effects

Using polarized light can increase the information gathered about the collision. For electric dipole transitions, the interaction operator is

$$e\vec{E} \cdot \vec{r} \tag{2.5}$$

where e is the charge of the electron, $\vec{r}$ is its position vector, and E is the electric field of the light. It can be rewritten as

$$eE\hat{\epsilon} \cdot \vec{r} \tag{2.6}$$

where $\hat{\epsilon}$ is a unit vector in the direction of E, which is the light's polarization direction. For linearly polarized light, E varies only along a straight line; for other polarizations, its variation is more complex. The polarization direction is usually

specified in terms of cartesian coordinates, since these are more natural laboratory coordinates, but spherical coordinates are often more useful in calculating matrix elements for the interaction. Therefore consider $eE\hat{\epsilon}\cdot\vec{r}$, expressed in spherical coordinates, for $\hat{\epsilon}$ along x, y, and z axes.

$$\begin{aligned} x&: \; eE\hat{\epsilon}\cdot\vec{r} = eE(1/\sqrt{2})(r^1_{-1} - r^1_1) \\ y&: \; eE\hat{\epsilon}\cdot\vec{r} = eE(1/\sqrt{2})(r^1_{-1} - r^1_1) \\ z&: \; eE\hat{\epsilon}\cdot\vec{r} = eEr^1_0 \end{aligned} \tag{2.7}$$

This interaction connects two states in the atom:

$$\langle l_1 m_1 | eE\hat{\epsilon}\cdot\vec{r} | l_2 m_2 \rangle \tag{2.8}$$

Substituting the expressions for $\hat{\epsilon}$ along x, y , and z axes gives

$$\begin{aligned} x&: \; \langle l_1 m_1 \mid eE(1/\sqrt{2})(r^1_{-1} - r^1_1) \mid l_2 m_2 \rangle \\ y&: \; \langle l_1 m_1 \mid eE(1/\sqrt{2})(r^1_{-1} + r^1_1) \mid l_2 m_2 \rangle \\ z&: \; \langle l_1 m_1 \mid eEr^1_0 \mid l_2 m_2 \rangle \end{aligned} \tag{2.9}$$

These equations give the following atomic selection rules:

$$\begin{aligned} &\Delta l = \pm 1 \\ &\Delta m = 0 \text{ (polarized along } z) \\ &\Delta m = \pm 1 \text{ (polarized along } x \text{ or } y) \\ &\text{parity changes, for 1-electron transitions} \end{aligned} \tag{2.10}$$

As Figure 1 shows, the ground state of magnesium is $3s^2\,{}^1S_0$ (l=0, m=0), and the first excited state is $3s3p\,{}^1P_1$ (l = 1, m=0, ±1). Therefore an electric dipole transition from the ground state to the first excited state, with linearly polarized light defining a z direction, excites the m=0 sublevel of the first excited state. The atom can decay to its ground state only by emitted light that is linearly polarized

along the z axis, since for this transition the change in m is zero. Similarly, the atom can be excited further to an upper S state, for example the 3s5s $^1S_0$ state (l = 0, m=0), by light of the appropriate wavelength that is polarized along the z axis. If the light exciting the second transition has no component along the z axis, it cannot be absorbed. However, the atom can be excited to an upper D state, for example the 3s4d $^1D_2$ state (l=2, m=0, ±1, ±2), by light of the appropriate frequency and any polarization, because this upper state permits a change in m to be ±1 as well as zero. For z polarization the m=0 sublevel will be populated; for x or y polarization the m = ±1 sublevels will be populated. Thus the distribution of population in m sublevels in excited states depends on the polarization of the light used to excite the atom.

The relative populations of the sublevels of an atom can be determined by the light it emits. Figure 4 shows the atom in the collision frame and a detector, with an associated detector frame, to intercept the light emitted by the atom. The intensity of detected light for a given transition depends on the location of the detector, the polarization of the detected light, and the orientation of the detector frame. For linearly polarized light, with a detector placed an angle θ from the z axis equipped with a linear polarizer with orientation angle χ, the detected intensity can be written as [2]

$$I(\theta,\chi) = \frac{I_0}{4\pi}[1-\frac{1}{2}h^{(2)}(j,j')\langle A_0\rangle P_2(\cos\theta) + \frac{3}{4}h^{(2)}(j,j')\langle A_0\rangle \sin^2\theta\cos 2\chi] \qquad (2.11)$$

where $h^{(2)}$(j,j') is a function that depends on the upper (j') and lower (j) states

FIGURE 4

Geometry for detecting fluorescence. x, y, and z are laboratory coordinates, and x', y', and z' are detector coordinates related to the laboratory coordinates by Euler angles θ, ϕ, and χ.

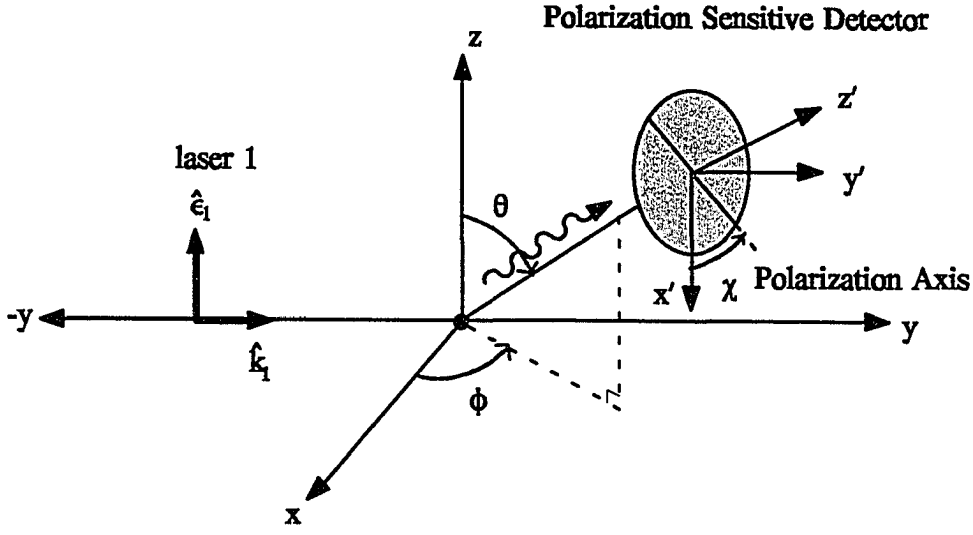

involved in the emission of light, $P_2(\cos\theta)$ is the second order Legendre polynomial, and $\langle A_0 \rangle$ is the upper state alignment, a parameter that measures the differences in population of the sublevels.

$$\langle A_0 \rangle = \sum_{m'} \frac{[3m'^2 - j'(j'+1)]n_{m'}}{j'(j'+1)\sum_{m'} n_{m'}} \tag{2.12}$$

where $n_{m'}$ is the relative population of a given sublevel. It is convenient to locate the detector at 90° from the z axis. Then χ is the angle between the linear polarization of the detector and the z axis. This gives a modified intensity

$$I(\chi) = \frac{I_0}{4\pi}[1 + \frac{1}{4}h^{(2)}(j,j')\langle A_0 \rangle(1+3\cos 2\chi)] \tag{2.13}$$

To determine both I_0 and $\langle A_0 \rangle$ it is necessary to measure the intensity for two values of χ. Convenient values are $\chi = 0°$ and $\chi = 90°$. A useful quantity to calculate is the degree of linear polarization, P_L:

$$P_L = \frac{I(\chi=0°) - I(\chi=90°)}{I(\chi=0°) + I(\chi=90°)} \tag{2.14}$$

Comparing equations (2.14) and (2.13), it is clear that the degree of linear polarization of a state is related to its alignment by the following equation

$$P_L = \frac{3h^{(2)}\langle A_0 \rangle}{4 + h^{(2)}\langle A_0 \rangle} \tag{2.15}$$

If only the total intensity is desired, it can be measured by setting χ at its so-

called magic angle, such that $1 + 3\cos 2\chi = 0$; this equation holds for $\chi = 54.7°$. An equivalent manner of measuring state properties is to probe to a higher state using a linearly polarized light source, for example a laser. Figure 5 shows the geometry for this pump-probe arrangement. The intensity is then measured using cascade fluorescence from the upper state. Since the intensity in equation (2.13) depends on j but not on the principal quantum number n, it will have the same χ dependence regardless of whether the transition is to a lower state or to a higher state, as long as the states have the same j.

For these experiments the $3s3p\,^1P_1$ state is studied, using a probe to the $3s5s\,^1S_0$ state or the $3s4d\,^1D_2$ state. For the first case, $h^{(2)}(0,1) = -2$ (Table 2.1); for the second, $h^{(2)}(2,1) = -1/5$. This gives the following equations for P_L:

$$3s3s\,^1P_1 \rightarrow 3s5s\,^1S_0: \quad P_L = \frac{-3\langle A_0\rangle}{2-\langle A_0\rangle}$$
$$3s3p\,^1P_1 \rightarrow 3s4d\,^1D_2: \quad P_L = \frac{-3\langle A_0\rangle}{20-\langle A_0\rangle} \qquad (2.16)$$

For atomic transitions, if the polarization of light involved in the transition is known, the alignment of the excited state can be calculated using the matrix elements in equation (2.9). Therefore the degree of linear polarization for a transition from the excited state can be predicted. For a $3s^2\,^1S_0 \rightarrow 3s3p\,^1P_1$ transition excited with a linearly polarized laser, $\langle A_0\rangle = -1$ for the $3s3p\,^1P_1$ state. If the excited state is then probed by a second linearly polarized laser set at the $3s3p\,^1P_1 \rightarrow 3s5s\,^1S_0$ transition frequency, the degree of linear polarization is 100%. When the probe is reset to the $3s3p\,^1P_1 \rightarrow 3s4d\,^1D_2$ transition, the polarization

FIGURE 5
Geometry of the probe beam. The shaded plane is parallel to the x-z plane.

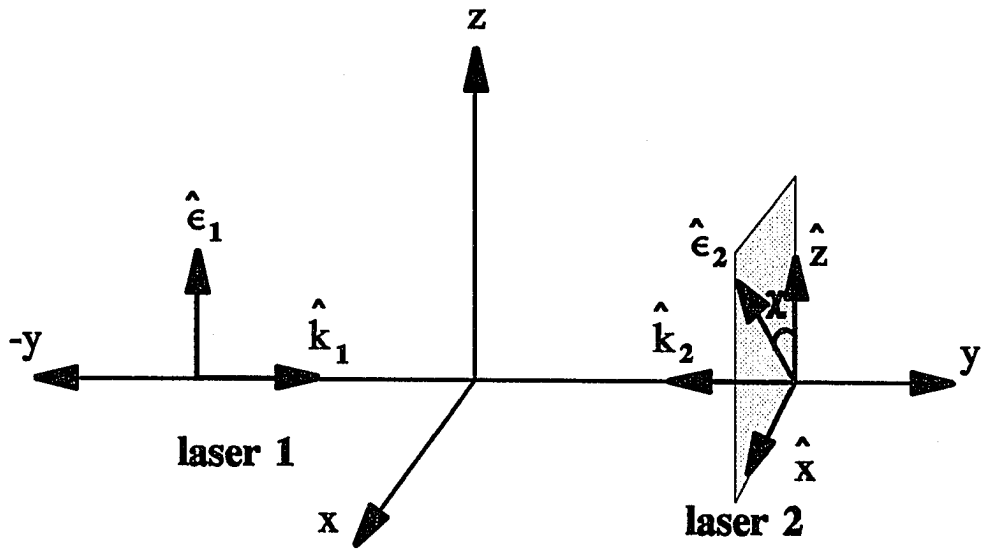

TABLE 1
Formulae for $h^{(2)}(j,j')$.

j	$h^{(2)}(j,j')$
$j'-1$	$-(j'+1)/(2j'-1)$
j'	1
$j'+1$	$-j'/(2j'+3)$

changes to 14.3%. These are atomic polarization values. During a collision, the polarization produced by optical excitation is modified by recoupling of electronic angular momentum into the molecular frame, by the molecular potential structure, and by evolution of the alignment during the collisions. These effects are discussed in the following two sections.

Molecular Selection Rules

Molecular selection rules differ from atomic selection rules because a diatomic molecule has a natural axis of symmetry, its internuclear axis, while a free atom has no special axis of symmetry. For a molecule, then, it is necessary to take into account not only the polarization of the light with respect to a laboratory, space-fixed frame, but also its polarization with respect to the molecular frame. The interaction operator in the spaced fixed frame, $O' = \hat{\varepsilon}\cdot\vec{r}$, is related to the interaction operator in the molecular frame, O, by the relation

$$O'_q = \sum_{k=-1}^{1} D^1_{qk}(\phi,\theta,\chi) O_k \qquad (2.17)$$

where $O'_q = \varepsilon_q r^1_q$ and $D^1_{qk}(\phi,\theta,\chi)$ is a rotation matrix that depends on the Euler angles connecting the two reference frames (Figure 6). The rotation matrix can be written as [28]

FIGURE 6

The molecular and laboratory reference frames. The Euler angles θ, ϕ, and χ connect the two frames.

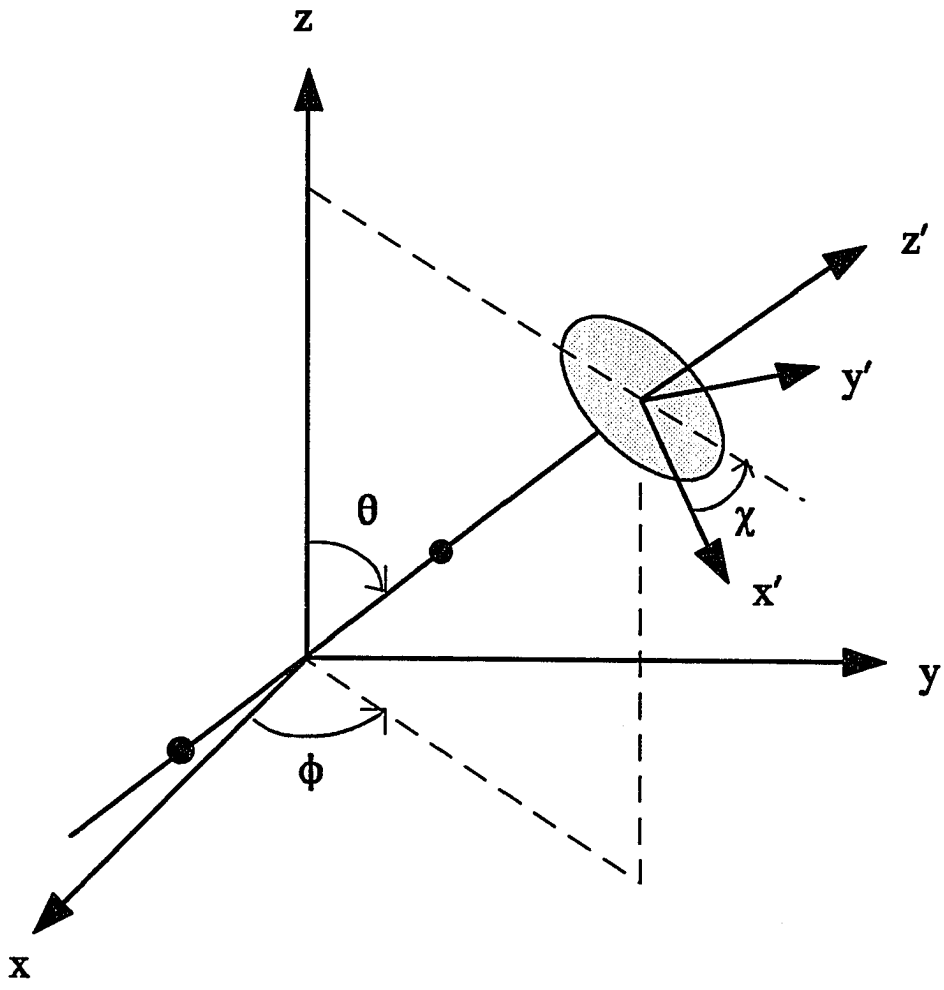

$$D^1_{qk} = \begin{pmatrix} e^{-i\phi}\frac{1}{2}(1+\cos\theta) & -e^{-i\phi}\frac{1}{\sqrt{2}}\sin\theta & e^{-i\phi}\frac{1}{2}(1-\cos\theta) \\ \frac{1}{\sqrt{2}}\sin\theta & \cos\theta & -\frac{1}{\sqrt{2}}\sin\theta \\ e^{i\phi}\frac{1}{2}(1-\cos\theta) & e^{i\phi}\frac{1}{\sqrt{2}}\sin\theta & e^{i\phi}\frac{1}{2}(1+\cos\theta) \end{pmatrix} \tag{2.18}$$

Notice that when $k = q$, the rotation matrix contains a cos θ, where θ is the angle between the laboratory z axis and the molecular z' axis; cos θ is largest when z and z' are parallel. But when $k = q \pm 1$, the rotation matrix contains a sin θ, which is largest when z and z' are perpendicular. The molecular states are not the same as the atomic states; when the orbital angular momentum is coupled to the internuclear axis, the good quantum numbers are total angular momentum J; the projection Λ of orbital angular momentum L on the internuclear axis; the projection Σ of spin on the internuclear axis; the sum Λ+Σ = Ω, which is the projection of J on the internuclear axis; and M, the projection of J on the space-fixed z axis. Thus molecular states can be written as $|J\Lambda M\rangle$ for the spatial coordinates. The radiative transition amplitude between the two states $|J_1\Lambda_1 M_1\rangle$ and $|J_2\Lambda_2 M_2\rangle$ is then

$$\langle J_1\Lambda_1 M_1 | \sum_{k=-1}^{1} D^1_{qk} O_k | J_2\Lambda_2 M_2 \rangle \tag{2.19}$$

This gives the following selection rules

$$\begin{aligned} &\Delta M = q = 0, \pm 1 \\ &\Delta\Lambda = k = 0, \pm 1 \\ &\Delta J = 0, \pm 1 \\ &\text{parity changes} \end{aligned} \tag{2.20}$$

As in the atomic case, the change in M depends on the direction of the laser's

polarization vector. The difference lies in the connection between these quantum numbers and the states the constituent atoms are left in after the molecule dissociates. For example, a Σ molecular state can dissociate to an atomic d state, with a higher polarization than would be generated in an isolated atomic d state. Also, for a molecule there are parallel and perpendicular transitions, as noted above. For $\Delta\Lambda = 0$, the transition dipole moment is parallel to the internuclear axis; for $\Delta\Lambda = \pm 1$, the transition dipole moment is perpendicular to the internuclear axis. Light is absorbed only if its polarization has a component along the direction of the transition dipole moment.

Adiabatic Reorientation Model

The adiabatic reorientation model, developed by Lewis and coworkers [22], takes advantage of the fact that during a collision, the orbital angular momentum of the electrons couples with the internuclear axis of the molecule. In Figure 7 the magnesium atom is excited to the $3s3p\,^1P_1$ state by a linearly polarized laser. The p orbital's long axis is along the polarization direction of the laser, which is labeled the z axis. The magnesium atom approaches the rare gas atom, and when the internuclear separation is less than the decoupling radius R_{dec} (where $\Delta \sim t_c$) the orbital couples to the internuclear axis, shown as a Σ state. As the magnesium atom continues in its trajectory, the p orbital changes its direction so that it is no longer along the laboratory z axis, but is reoriented by an angle ϕ. After the

FIGURE 7

Adiabatic reorientation of a 3p Σ level for a full collision. The heavy line represents the magnesium trajectory.

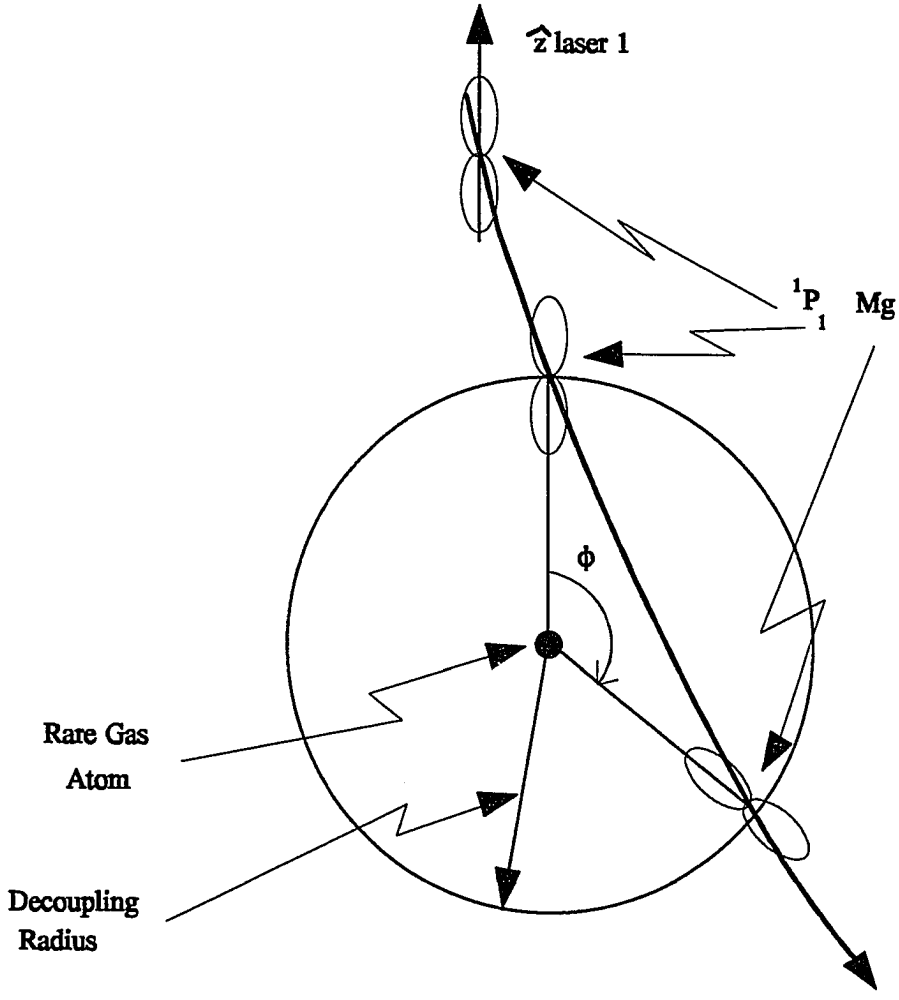

atoms separate past R_{dec}, the p orbital is again fixed in space, but not in the same direction as before the collision. The reorientation angle ϕ depends on the impact parameter and the molecular potentials. Figure 7 shows a repulsive trajectory, since the Σ state associated with the $3s3p\,^1P_1$ state is repulsive. If the magnesium atom is probed to the $3s5s\,^1S_0$ state after the collision, it will no longer have a polarization of 100%. Since the orbital is no longer aligned along the z axis, there can be excitation even when $\chi = 90°$, so that the polarization is lower. The magnesium atom can be probed during a collision, by tuning the probe laser off resonance (Figure 8). Then the reorientation is incomplete, so that there is less depolarization. Thus the polarization measured depends on the time in the collision that the atom was probed. As seen in the previous section, it also depends on what state is probed. Figure 9 shows reorientation for a π state. The $3s3p\,^1\pi_1$ state is attractive, so that the reorientation for a complete collision would be more than that for a repulsive Σ state. However, two π state orientations exist, one in the collision plane and one perpendicular to it. The out of plane orbital is not reoriented during a collision. The net effect is that a π state experiences less reorientation during a collision than a Σ state. It is also possible to both pump and probe the magnesium atom during a collision, by tuning both lasers off atomic resonance. Since light from both lasers is absorbed during a single collision, the effect is examining a fraction of a collision. This process is known as a fractional collision.

Figure 10 shows a collision with a Σ state probed to the $3s4d\,^1D_2$ Σ state.

FIGURE 8

Adiabatic reorientation of the 3p Σ level probed to the 5s Σ level during a collision. *R* represents the Condon point for the laser 2 detuning.

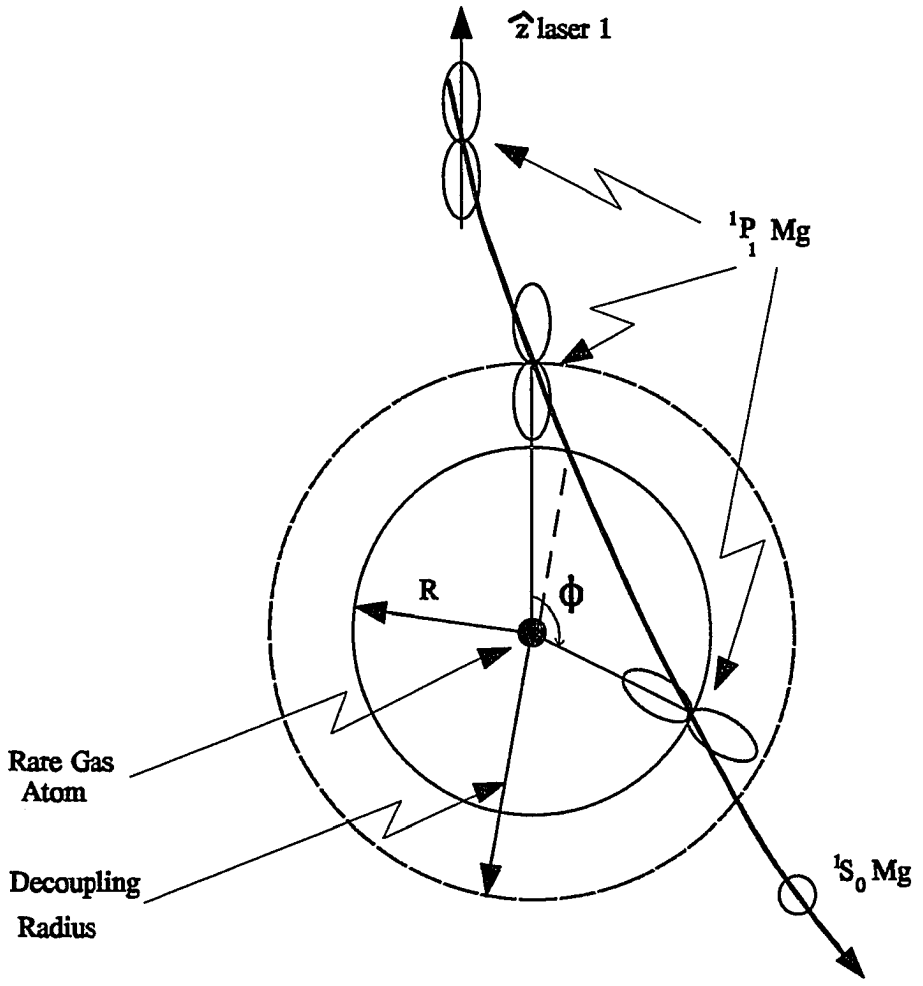

FIGURE 9

Adiabatic reorientation of the 3p π level probed to the 5s Σ level during a collision. R represents the Condon point for the laser 2 detuning.

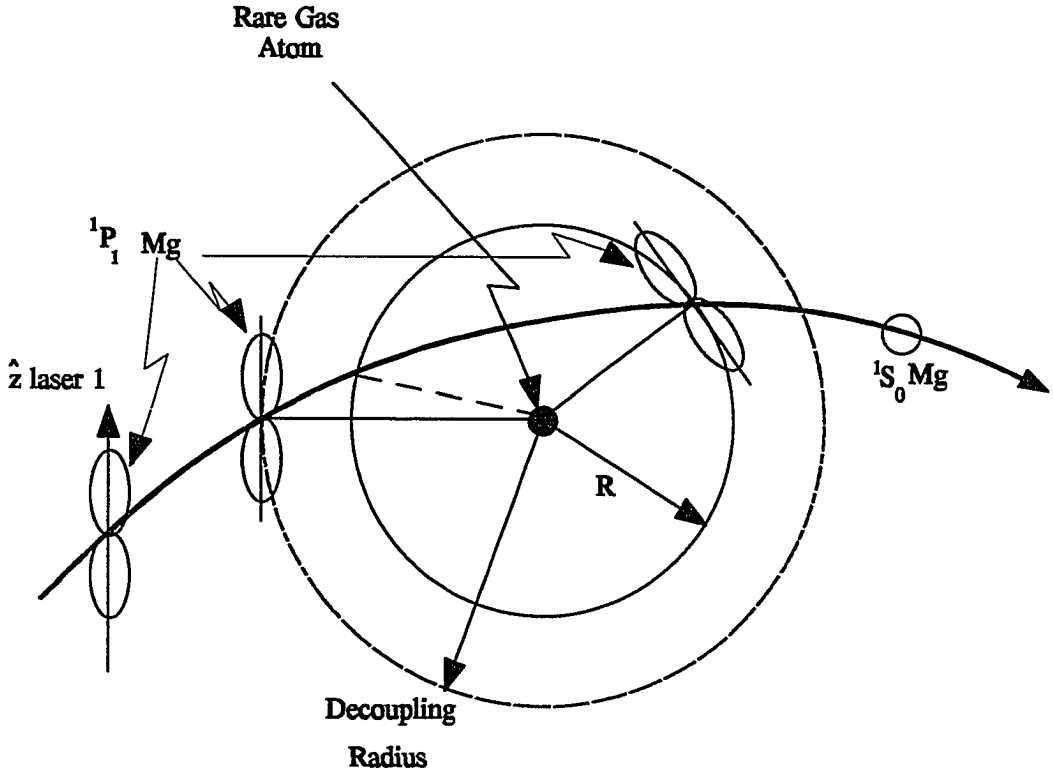

FIGURE 10

Adiabatic reorientation of the 3p Σ level probed to the 4d Σ level during a collision. R represents the Condon point for the laser 2 detuning.

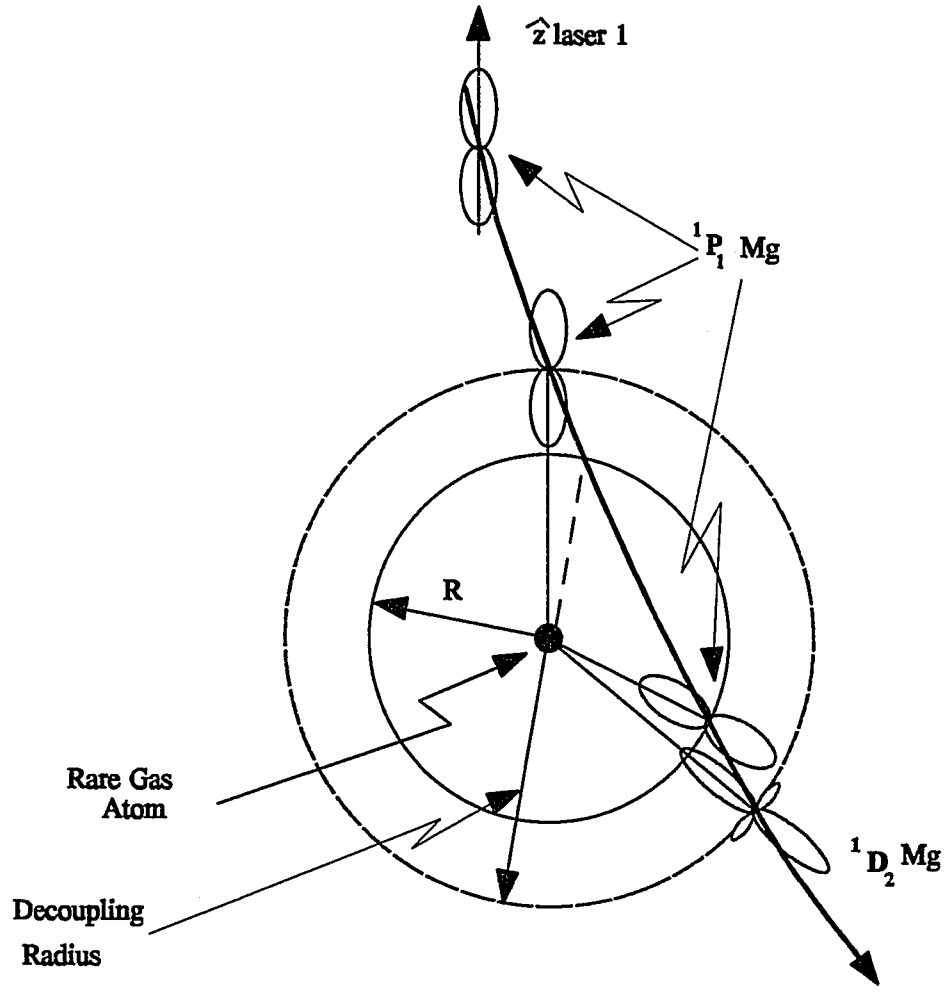

This has generally the same characteristics as a Σ state probed to the 3s5s $^1S_0$ Σ state, except that the initial polarization is smaller. As seen in the previous section, transitions with $\Delta\Lambda = 0$ have transition moments along the internuclear axis, and depolarize like the Σ-Σ transitions pictured, while transitions with $\Delta\Lambda = \pm 1$ have transition moments perpendicular to the internuclear axis, and depolarize like the π-Σ transitions pictured. It is clear from the above discussion that a polarization spectrum, showing P_L versus detuning, can give qualitative information about the dynamics of the collision. For these experiments, the relative velocities of the colliding pair are randomly distributed, and the molecular potentials of the upper states are not well known, making it difficult to extract quantitative information about the collision dynamics.

Inelastic Branching

The upper molecular states' populations are monitored in the experiment by cascade fluorescence from the associated atomic states. In the previous section, it was assumed that excited molecular states will dissociate to the related atomic state. That is, it was assumed that the molecular 3s5s $^1\Sigma_0^+$ state dissociates to the atomic 3s5s $^1S_0$ state, and the 3s4d $^1\Sigma_0^+$, 3s4d $^1\pi_1$, and 3s4d $^1\Delta_2$ states dissociate to the atomic 3s4d $^1D_2$ state (Figure 2). However, these atomic states are separated by only a few hundred wavenumbers, and the molecular 3s4d $^1\pi_1$ and 3s4d $^1\Delta_2$ states may have deep potential wells. Therefore there can be curve

crossings between these states. Similarly, the $3s5s\,^3\Sigma_1$ state is also close in energy to the other two. If curve crossings exist, there may be inelastic branching between states. For example, a magnesium atom may be excited during a collision to a $3s4d\,^1\pi_1$ state, encounter a curve crossing to the $3s5s\,^1\Sigma_0^+$ state, and dissociate to the $3s5s\,^1S_0$ state instead of the expected $3s4d\,^1D_2$ state.

A convenient model for describing inelastic transitions at curve crossings is the Landau-Zener model [29, 30]. This model assumes two states $|a\rangle$ and $|b\rangle$, which are eigenstates of a Hamiltonian $H = H_0+H_1$, where H_0 is an unperturbed Hamiltonian and H_1 is a perturbation between the states. The eigenstates of H have eigenvalues $E_a(R)$ and $E_b(R)$, where R may be any parameter; for the experiment, it is the internuclear separation. The unperturbed Hamiltonian H_0 has eigenstates $|1\rangle$ and $|2\rangle$ with eigenvalues $E_1(R)$ and $E_2(R)$; these eigenvalues are equal for some R_0. For the total Hamiltonian, these states give

$$\begin{aligned} H|1\rangle &= E_1|1\rangle + E_{12}|2\rangle \\ H|2\rangle &= E_{12}|1\rangle + E_2|2\rangle \end{aligned} \tag{2.21}$$

The Landau-Zener model makes two assumptions: (1) R is a known function of time; here, that means for the region of the crossing the collision follows straight-line trajectories; and (2) the region for the crossing is small enough to assume that E_1-E_2 is a linear function of time and that the interaction energy E_{12} and the two unperturbed states do not depend on time there. Assumption (2) can be written as

$$E_1 - E_2 = \hbar\alpha t$$
$$\frac{dE_{12}}{dt} = \frac{d|1\rangle}{dt} = \frac{d|2\rangle}{dt} = 0 \qquad (2.22)$$

With these assumptions, $E_a(R)$ and $E_b(R)$ are hyperbolae with asymptotes $E_1(R)$ and $E_2(R)$ and minimum separation $2E_{12}(R_0)$, as shown in Figure 11. If R changes infinitely slowly, a molecule that starts in state $|a\rangle$ will stay in that state, and a molecule that starts in state $|b\rangle$ will stay there. But if R changes at a finite rate, there is some probability that a molecule that starts in state $|a\rangle$ will end in state $|b\rangle$. The purpose of the model is to calculate the probability of a change.

The calculation begins with the Schrödinger wave equation, with the eigenfunction of H written as a linear combination of $|1\rangle$ and $|2\rangle$, in the form

$$(H-\frac{\hbar}{i}\frac{\partial}{\partial t})[C_1(t)e^{\frac{i}{\hbar}\int E_1 dt}|1\rangle + C_2(t)e^{\frac{i}{\hbar}\int E_2 dt}|2\rangle] = 0 \qquad (2.23)$$

If the system is initially prepared in state $|b\rangle$, then the initial conditions are

$$C_1(-\infty) = 0$$
$$|C_2(-\infty)| = 1 \qquad (2.24)$$

The probability of a transition to state $|a\rangle$ is then

$$P = |C_2(\infty)|^2 = 1 - |C_1(\infty)|^2 \qquad (2.25)$$

Therefore the wave equation (2.23) must be solved to give the asymptotic value of C_1. Using the assumptions, the equation can be rewritten as a second order differential equation in C_1

FIGURE 11

An avoided crossing of two interacting energy levels E_a and E_b, with unperturbed energies E_1 and E_2 as asymptotes.

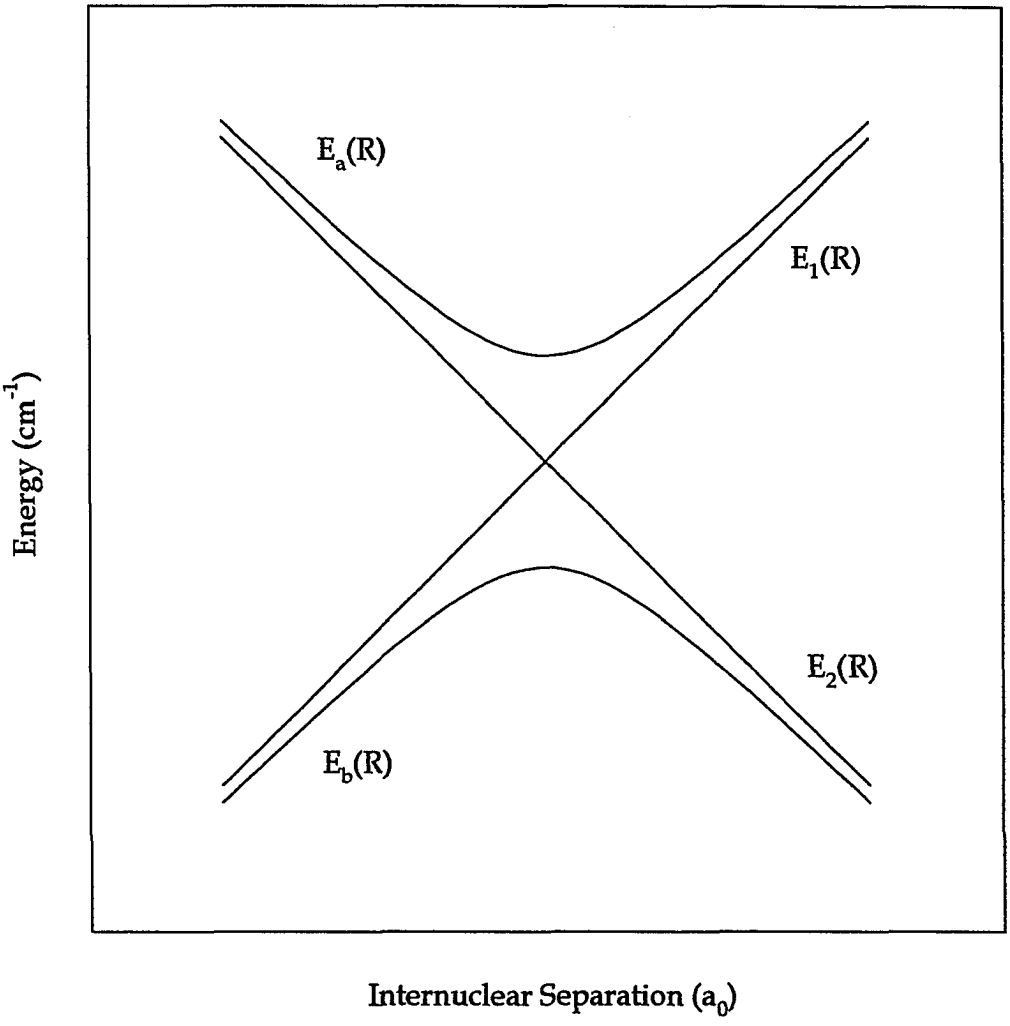

$$\frac{d^2C_1}{dt^2} + \frac{i}{\hbar}(E_1-E_2)\frac{dC_1}{dt} + \frac{E_{12}^{\ 2}}{\hbar^2}C_1 = 0 \qquad (2.26)$$

This can be put into the form for the Weber equation and solved to give

$$|C_1(\infty)|^2 = 1 - e^{-2\pi\gamma}$$

$$\gamma = \frac{E_{12}^{\ 2}/\hbar}{|\frac{d}{dt}(E_1-E_2)|} \qquad (2.27)$$

Which gives a transition probability of

$$P = e^{-2\pi\gamma} \qquad (2.28)$$

Thus the probability of a curve crossing is related to the size of the interaction between the states, E_{12}, and the time rate of change of the eigenvalues of the unperturbed states, which in turn is related to the rate of change of R. Taking the derivative of the upper equation (2.22) gives

$$\frac{d}{dt}(E_1-E_2) = \hbar\alpha$$

$$\frac{dE_1}{dR}\frac{dR}{dt} - \frac{dE_2}{dR}\frac{dR}{dt} = \hbar\alpha \qquad (2.29)$$

Substituting equation (2.29) into equation (2.28) gives

$$P = e^{-\frac{2\pi E_{12}^2/\hbar}{\frac{d}{dR}(E_1-E_2)\frac{dR}{dt}}} \tag{2.30}$$

Figure 12 plots the probability of a curve crossing versus the time derivative of *R*. For infinitely slow changes, there is no transition; for faster changes, the probability increases.

To test for these curve crossings experimentally, branching ratios are measured. The 5s/4d branching ratio is the ratio of population ending in the 3s5s $^1S_0$ state to the population ending in the 3s4d $^1D_2$ state. If the branching ratio is measured at different detunings, it should increase at detunings corresponding to Condon points near curve crossings. Also, the branching ratio for inelastic branching is a single-collision measurement. Therefore it should not depend on the rare gas pressure. Finding curve crossings would give interesting information about the molecular potentials for the upper levels.

FIGURE 12

Probability of a curve crossing versus change in internuclear separation, dR/dt, given by Landau-Zener theory.

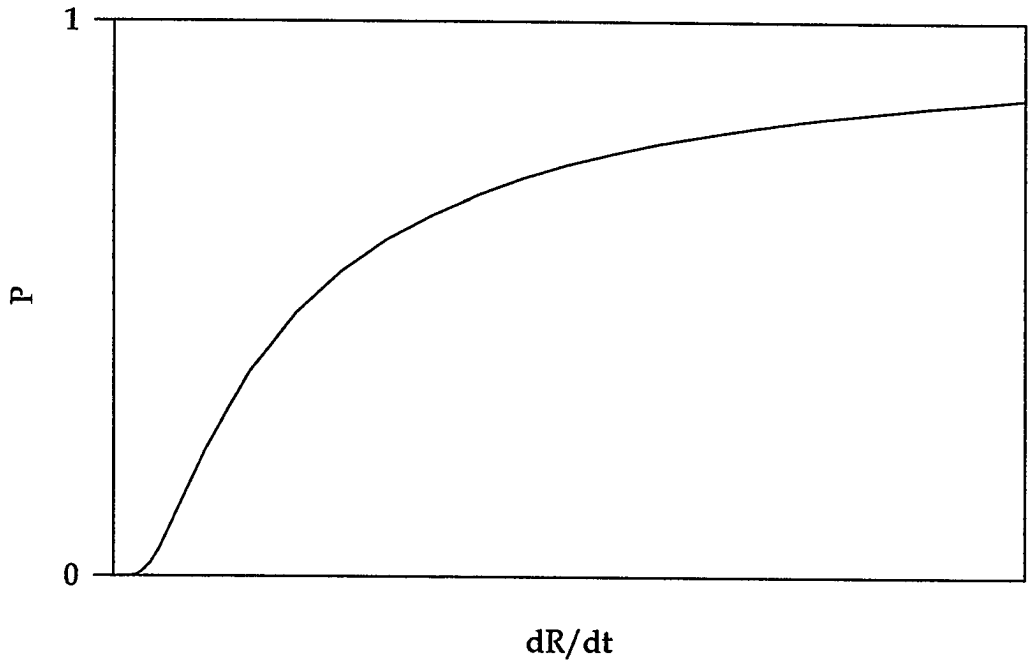

CHAPTER 3

EXPERIMENT

Overview of Experiment

As described in Chapter 2, an excited magnesium atom collides with a rare gas atom, absorbing a photon during the collision. Figure 13 shows the process using molecular potentials, which govern the absorption of energy during the collision. The magnesium is excited from its ground state ($3s^2\ ^1S_0$) to its first excited state ($3s3p\ ^1P_1$) by a linearly polarized laser (laser 1) tuned to the atomic resonance at 285 nm. A second laser (laser 2) is tuned off the atomic resonance for the $3s3p\ ^1P_1 \rightarrow 3s5s\ ^1S_0$ transition at 571 nm for the first experiment, and it is tuned off the $3s3p\ ^1P_1 \rightarrow 3s4d\ ^1D_2$ transition at 553 nm for the second experiment (Figure 14). Light from laser 2 can be absorbed only during a collision. After the collision the atom is left in the $3s5s\ ^1S_0$ (experiment A) or the $3s4d\ ^1D_2$ state (experiment B), unless inelastic branching occurs. The population of the $3s5s\ ^1S_0$ state or the $3s4d\ ^1D_2$ state is monitored by cascade fluorescence from the $3s4p\ ^1P_1$ state to the ground state, at 203 nm.

If there is inelastic branching in experiment B, that is if curve crossings in the molecular potentials relating to different atomic states exist where the transition occurs, then the atom may be in the $3s5s\ ^1S_0$ state or the $3s5s\ ^3S_1$ state

FIGURE 13

Excitation scheme for excited-state magnesium - rare-gas optical collisions, probing near the Mg 3s5s $^1S_0$ state.

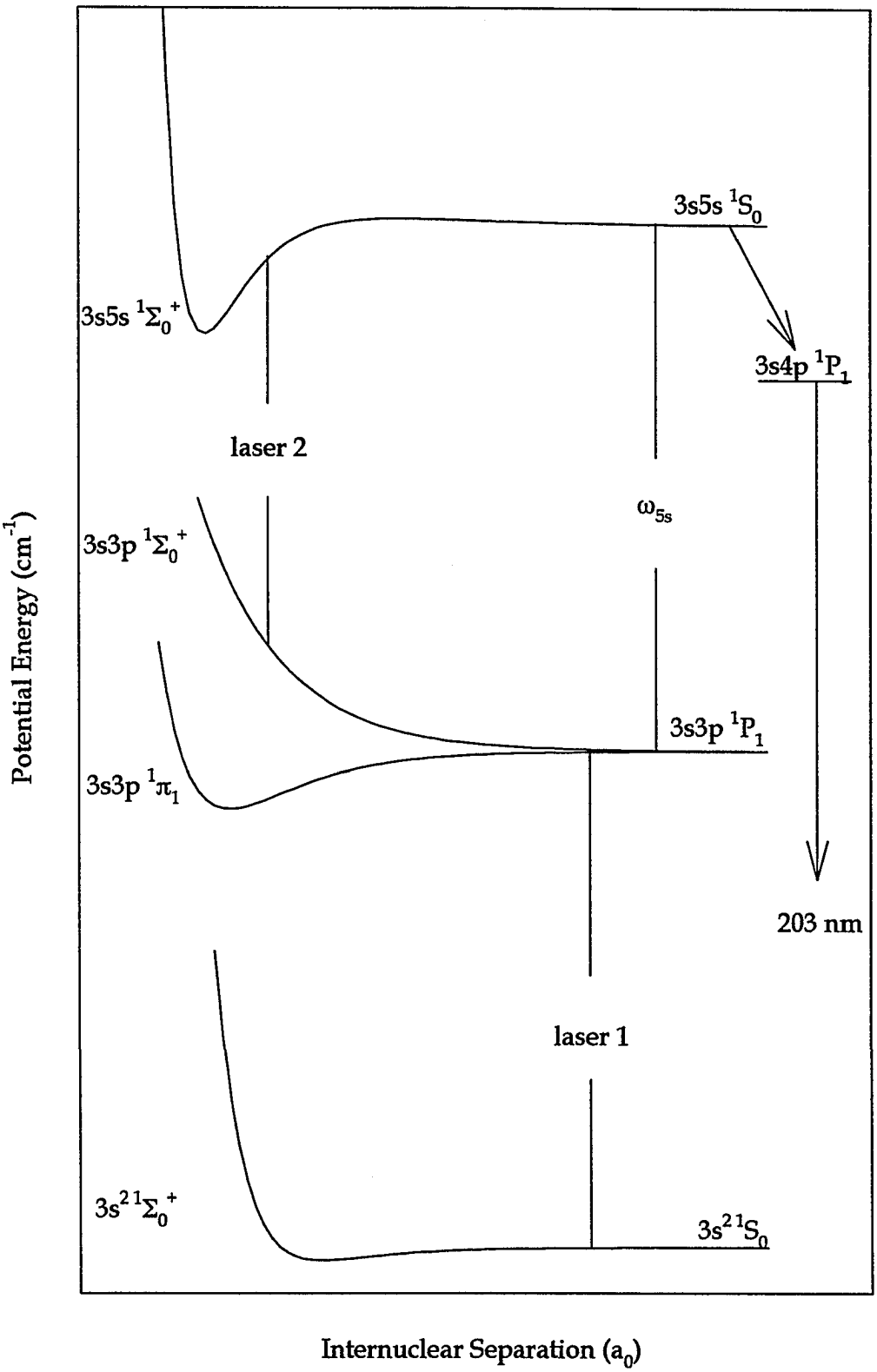

FIGURE 14

Excitation scheme for excited-state magnesium - rare-gas optical collisions, probing near the Mg 3s4d $^1D_2$ state.

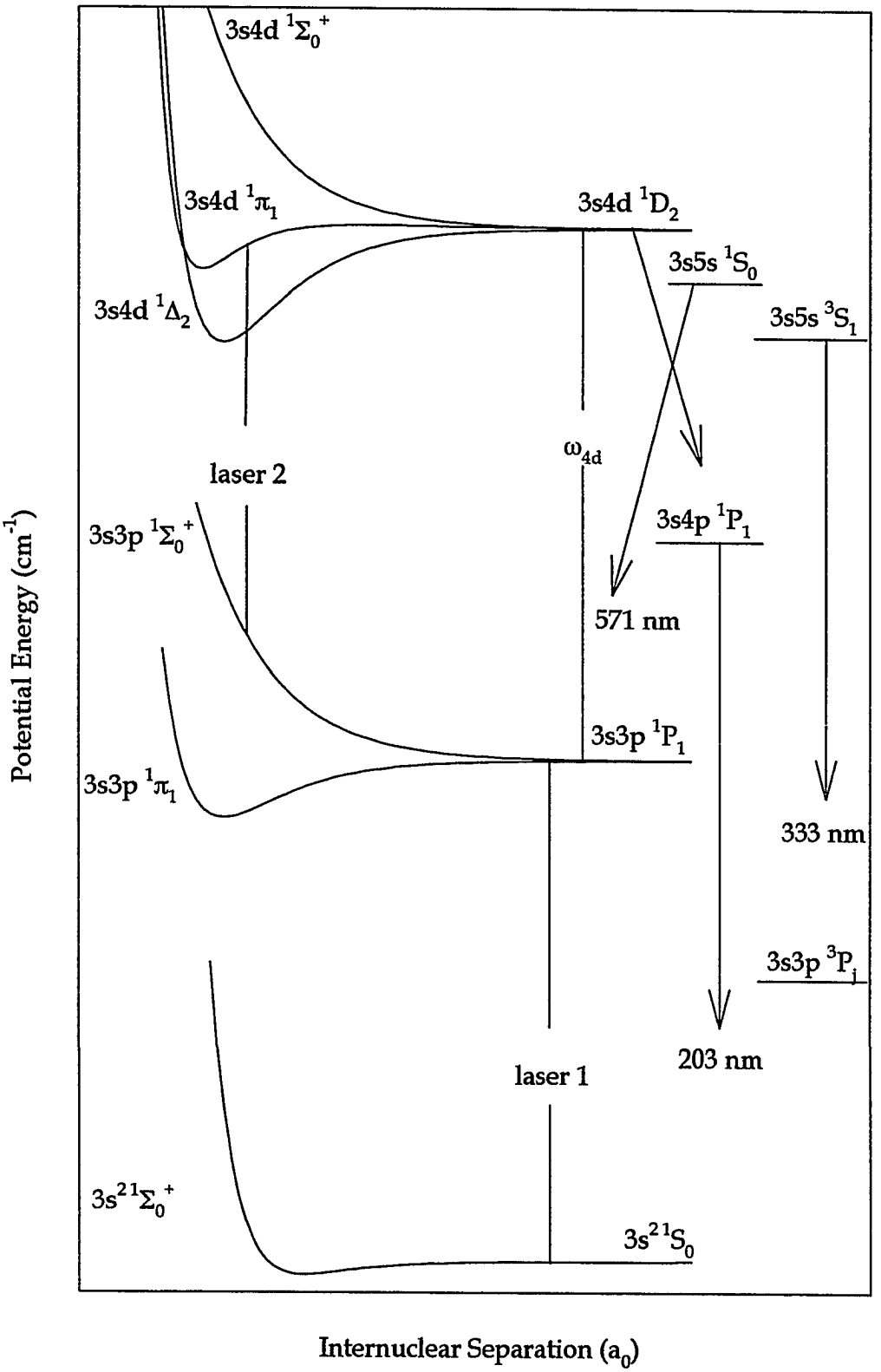

after the collision. The populations in these states can be measured by monitoring the 3s5s $^1S_0 \rightarrow$ 3s3p $^1P_1$ transition at 571 nm, or the 3s5s $^3S_1 \rightarrow$ 3s3p ^3P_j transition near 333 nm. Comparing population in the 3s4d $^1D_2$ state with the population in either the 3s5s $^1S_0$ state or the 3s5s $^3S_1$ state gives a branching ratio, which should change as the detuning of the second laser changes to probe near the internuclear separation at which the curve crossing occurs.

Laser 2 must vary both in frequency and in its linear polarization direction. This direction may be either parallel to the polarization direction of the first laser, or perpendicular to it, as shown in Figure 5. The intensity of fluorescence when the polarization directions of the two lasers are parallel is $I_\parallel$ and the intensity when the polarization directions of the two lasers are perpendicular is $I_\perp$. The intensities will of course vary with experimental factors such as laser intensity, magnesium density, rare gas density, and detector sensitivity. To measure an absolute intensity would require the absolute normalization of the apparatus. However, the degree of linear polarization, given by equation (2.14), which can be rewritten as

$$P_L = \frac{I_\parallel - I_\perp}{I_\parallel + I_\perp} \tag{3.1}$$

is normalized. Therefore the main results of the experiments, the polarization spectra, are normalized by their definition.

The rest of the chapter will cover the apparatus in detail. First the lasers, a tunable ultraviolet laser and a tunable visible laser with a variable polarization,

are described. Next is a discussion of the vacuum system, which makes it easy to adjust the rare gas type and pressure. Then the detection and signal processing system is described. The chapter concludes with a summary of the daily experimental procedure.

Apparatus

The apparatus for experiment A is shown in Figure 15 and the apparatus for experiment B is shown in Figure 16. In both experiments, the apparatus can be divided into three areas: the lasers, the vacuum system, and the detection system.

1. Lasers

Figure 17 shows the lasers, which are both grazing-incidence dye lasers pumped by a 10-Hz neodymium : yttrium aluminum garnet (Nd:YAG) laser (Quantel International, YG660S-10). The Nd: YAG laser's second harmonic, at 532 nm, has about 100 mJ per pulse, and a pulsewidth of 5-6 ns. This output is directed to the dye lasers and amplifiers by four uncoated glass beamsplitters. The reflection from both surfaces of each beamsplitter directs approximately eight percent of the laser towards the dye laser. The remaining energy of the Nd:YAG laser is not used for this experiment.

FIGURE 15
Schematic diagram of the apparatus used for experiment A.

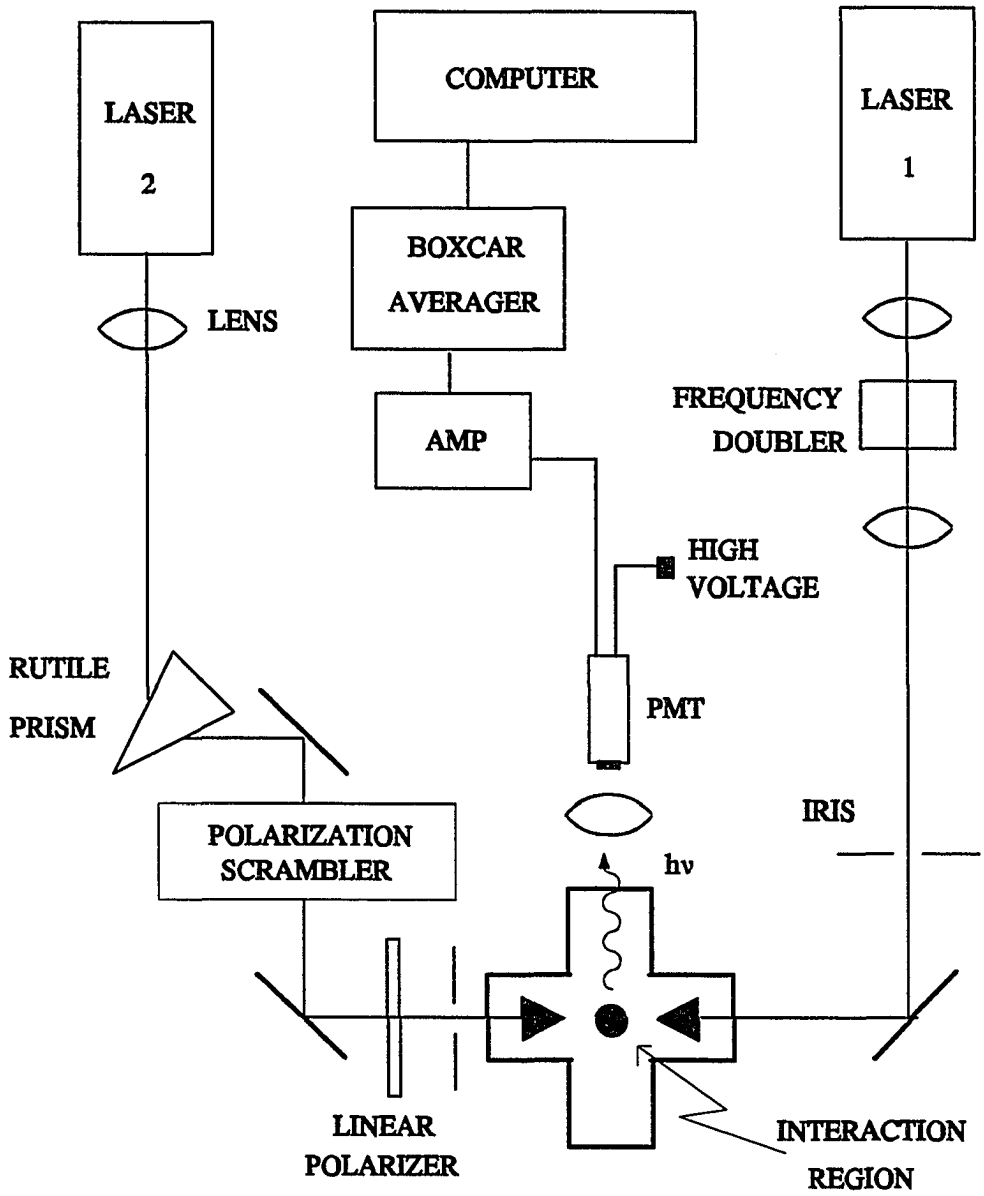

FIGURE 16
Schematic diagram of the apparatus used for experiment B.

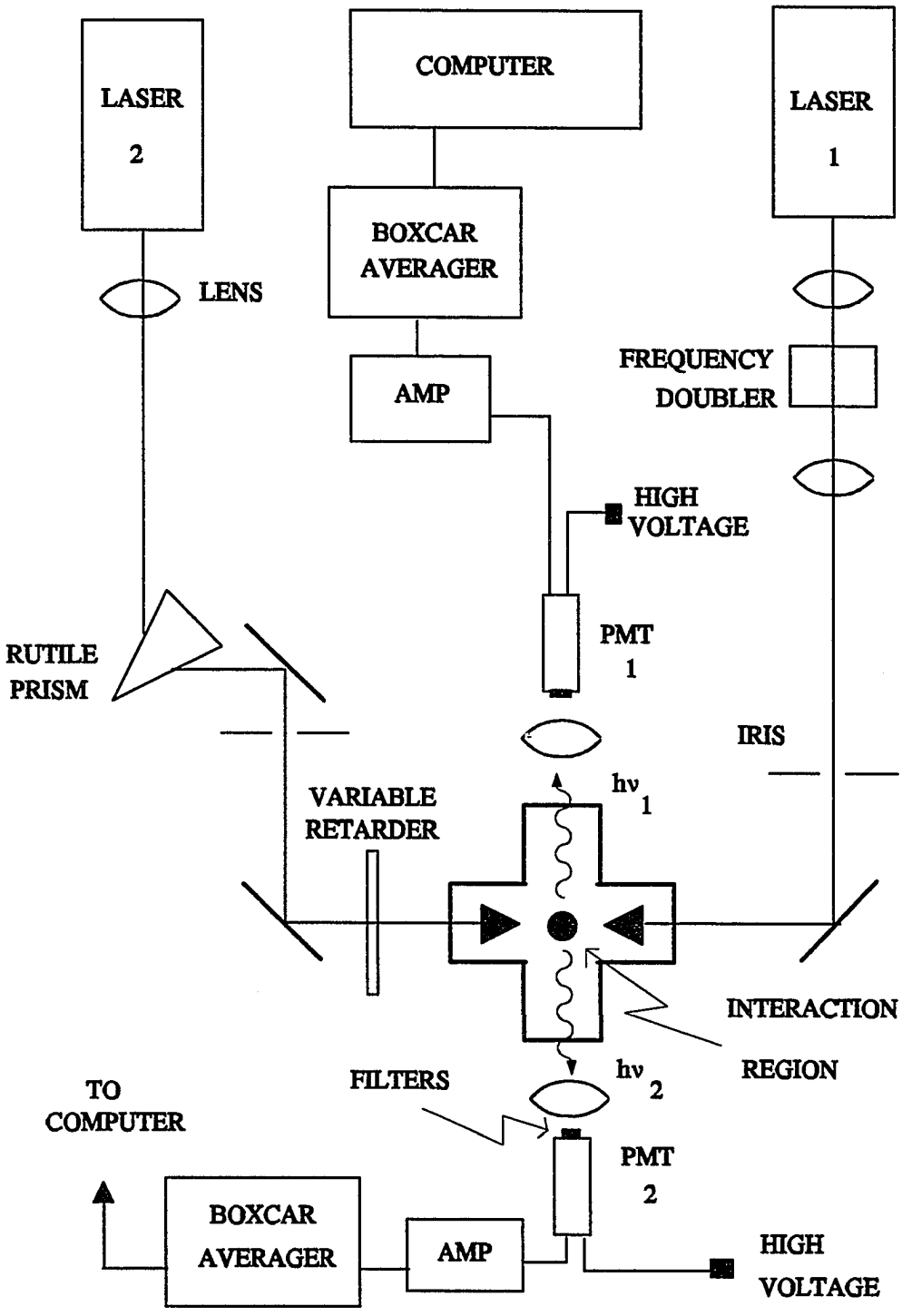

FIGURE 17
Pumping scheme for dye lasers.

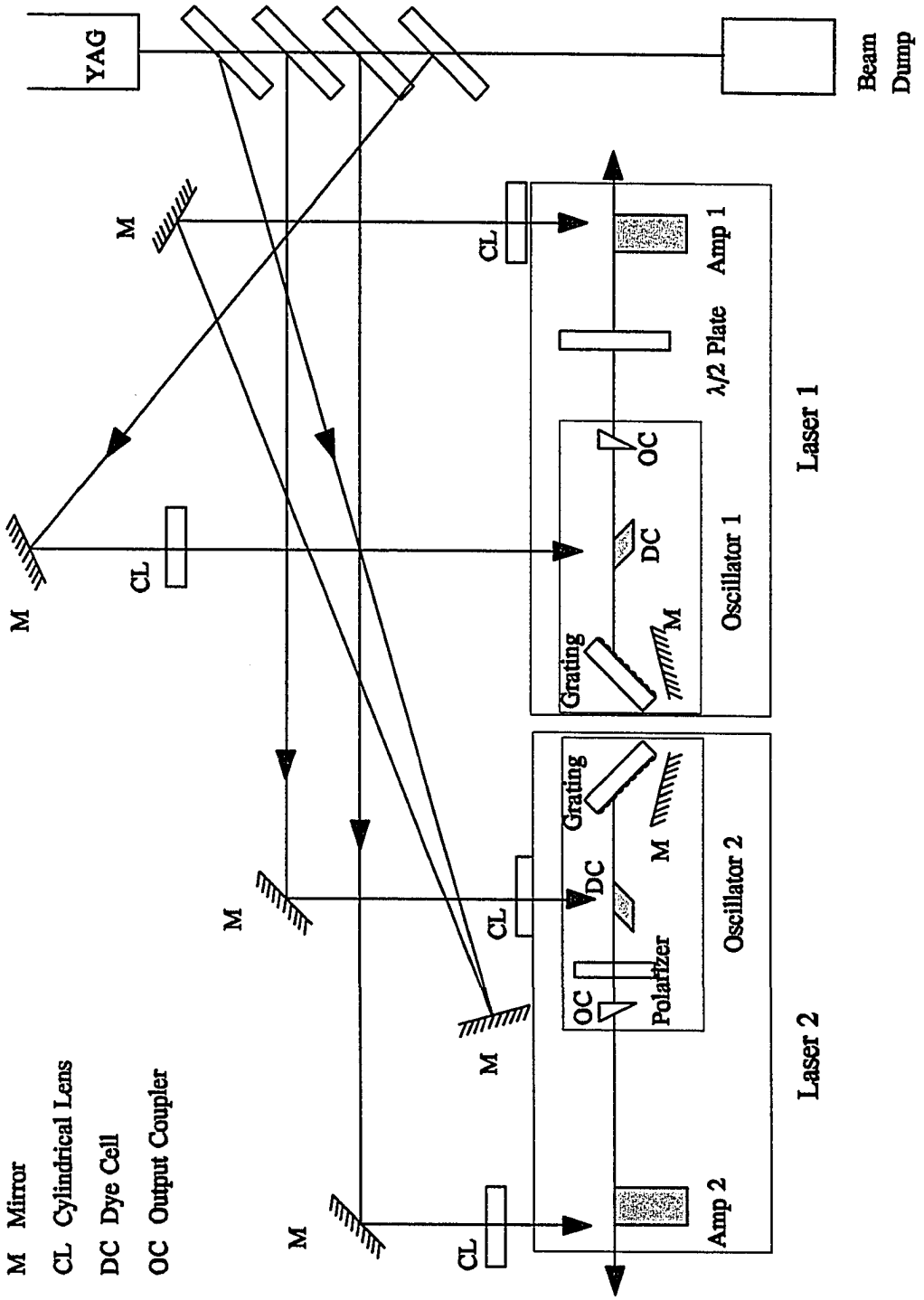

The grazing-incidence dye laser [31] consists of a dye cell, a diffraction grating, a glass wedge, and a mirror with a precision mount, as shown in Figure 18. The dye cell (NSG Precision Cells, Inc, 509H) has a rhombohedral cross-section, to avoid acting as a laser cavity itself. A cylindrical lens focuses the pump laser to a line near the front of the dye cell, where it excites the dye. Some of the resulting fluorescence reflects from the glass wedge and reaches the grating at an angle of incidence near ninety degrees, called grazing incidence. The grating (American Holographic) diffracts the fluorescence at an angle that depends on its wavelength. A tuning mirror is set to intercept the desired wavelength of light and send it back through the grating and cell to the output coupler, the glass wedge. Changing the angle of the mirror changes the amplified wavelength, according to the following equation:

$$\lambda = \frac{x}{m}(\sin\alpha + \cos\beta) \qquad (3.2)$$

where λ is the wavelength in air, x is the line spacing of the grating, m is the order of the diffraction, $\alpha \approx 90°$ is the angle of incidence for the grating, and β is the angle between the normals of the grating and the tuning mirror (Figure 19). For laser 1, x is 1/2400 mm; for laser 2, x is 1/3000 mm; these experiments use first order diffraction; therefore the tuning angles β are in the vicinity of 50°.

The grazing-incidence dye laser has a bandwidth of approximately 0.1 cm^{-1} (3 GHz), an output energy of tens of microjoules per pulse, and a pulsewidth near that of the pump laser; for these experiments, a few nanoseconds. Its light

FIGURE 18
Geometry of the grazing-incidence dye laser.

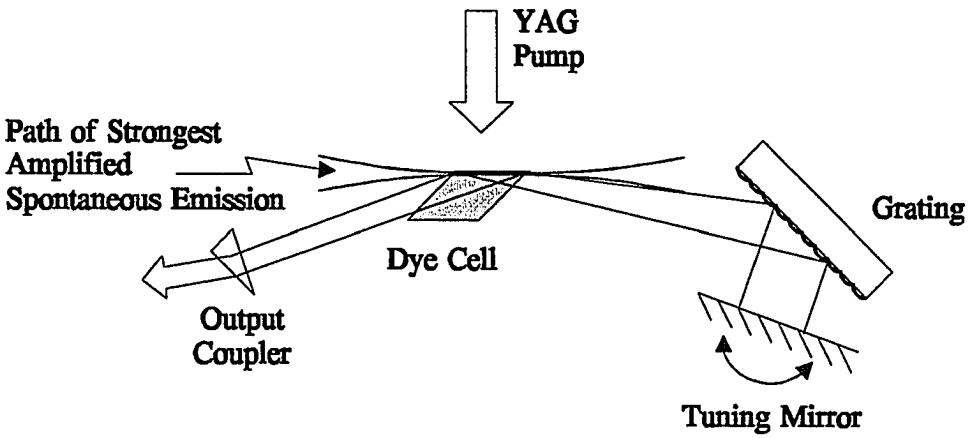

FIGURE 19
Tuning angles for the grazing-incidence dye laser.

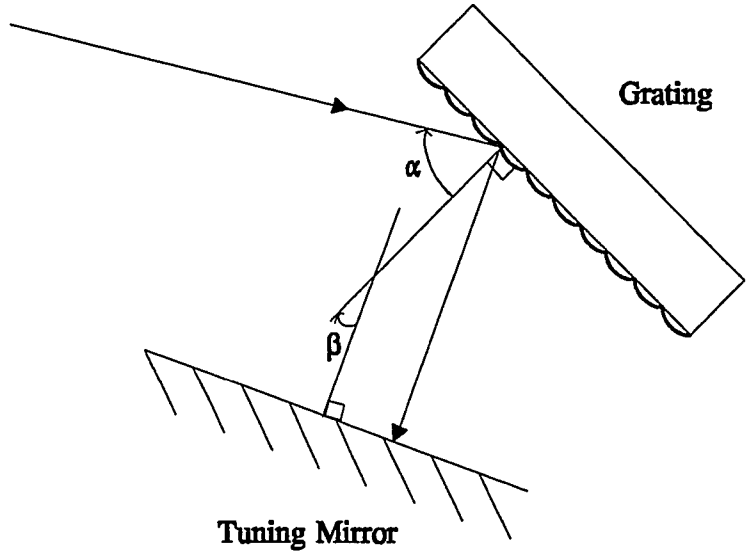

is polarized perpendicular to the lines on the diffraction grating; here, that means it is polarized horizontally.

The amplifier for each laser consists of a dye cell that is pumped by the Nd:YAG laser. This dye cell (NSG Precision Cells, Inc, 23H) has a rectangular cross-section and contains the same dye as the oscillator, but in lower concentration. The paths of the lasers are arranged so that the light from the dye laser reaches the amplifier shortly after it has been excited. The dye laser pulse is amplified by about a factor of ten as it goes through the amplifier.

Laser 1 must have a wavelength of 285 nm, in the ultraviolet. To achieve this, the output of the grazing incidence dye laser is frequency doubled. The laser uses Rhodamine 590 perchlorate dye (Exciton Chemical Company, Inc.) at a concentration of 5×10^{-4} mol in methanol, mixed with a few drops of Rhodamine 610 perchlorate (Exciton) at 5×10^{-3} mol in methanol, to obtain lasing in the range 565-575 nm. The concentration of Rhodamine 610 dye is adjusted by maximizing the laser energy at 570 nm. The amplifier uses approximately 1×10^{-4} molar Rhodamine 590 concentration, mixed with about a drop of Rhodamine 610. These concentrations also are adjusted by maximizing the amplified laser's energy at 570 nm. A half-wave plate (Geartner Scientific Company) between the oscillator and amplifier rotates the polarization vector of the laser by 90°. The amplified beam passes through a potassium dihydrogen phosphate (KDP) crystal (Molectron, DL070), which doubles the frequency with an efficiency near five percent, narrows the time width of the pulse to about 3 ns, and rotates the polarization of

the doubled laser by 90°, back to horizontal. The remaining fundamental beam is blocked with a colored glass filter, Schott type UG11, which reduces the fundamental by more than a factor of 10^5, but leaves more than 85 percent of the ultraviolet light at 285 nm. The energy of the doubled laser beam ranges from 25 to 50 μJ per pulse. However, since laser 1 is set on atomic resonance, it must be attenuated to less than 1 μJ per pulse to avoid saturating the transition.

For experiment A, laser 2 is tuned near the 3s3p $^1P_1 \rightarrow$ 3s5s $^1S_0$ atomic resonance at 571 nm. For this wavelength, as for laser 1, Rhodamine 590 perchlorate at a concentration of 5×10^{-4} mol in methanol, mixed with a few drops of Rhodamine 610 perchlorate 5×10^{-3} mol in methanol, is used. The concentration of Rhodamine 610 is adjusted by maximizing the energy of the laser at 571 nm. In the amplifier, the same dye at a concentration of about 1×10^{-4} is used, with the concentration adjusted by maximizing the energy of the amplified laser at 571 nm; typically, the laser energy is 1 or 2 mJ per pulse.

For experiment B, laser 2 is tuned near the 3s3p $^1P_1 \rightarrow$ 3s4d $^1D_0$ resonance at 553 nm. For this wavelength, Rhodamine 560 chloride dye (Exciton Chemical Company, Inc.), 5×10^{-3} molar in methanol, is used in the oscillator and about half that concentration is used in the amplifier. The amplifier concentration is adjusted by maximizing the energy of the amplified laser; typically, the energy is 600-700 μJ per pulse. The laser range is about 550-560 nm for energy at least 90 percent of the maximum; however, the laser has an energy of ~100 μJ per pulse at 571 nm, allowing some overlap in the data from the two experiments.

Since laser 2's wavelength is tuned off resonance, its wavelength must be measured. The tuning mirror mount has a fine and a coarse micrometer for horizontal adjustments. A 0.5 m monochromator (Jarrell Ash, 82-000), which has a resolution of about an angstrom at the narrowest useable slit width, is used to measure the wavelength of the laser at evenly spaced settings for the fine micrometer or, for large detunings, the coarse micrometer. The accuracy of the monochromator is checked by measuring the wavelength of each laser at its atomic resonance. This allows absolute calibration to vacuum wavelengths for atomic resonances. For laser 1, the atomic resonance is found, then the UG11 filter is removed from the laser and the wavelength of the fundamental beam is measured. Then the corrected wavelength measurements are used to calculate wavenumbers for each measurement. The wavenumbers are plotted versus micrometer reading. This gives a straight line whose slope is used to calibrate the micrometer. Each time the coarse micrometer is changed, the fine micrometer is calibrated before and after taking data, using a monochromator and atomic resonances; the coarse micrometer is also calibrated before and after taking measurements requiring large detunings. The calibration is linear to an excellent approximation over the whole 600 cm^{-1} range of the measurements for experiment B, as Figure 20 shows. Using this calibration, it is possible to determine the wavelength of the laser by the micrometer setting, to within the laser's bandwidth.

Since laser 2 is tuned off atomic resonance, and since molecular signals are

FIGURE 20
Calibration curve for laser 2. Uncertainty is smaller than the dot size.

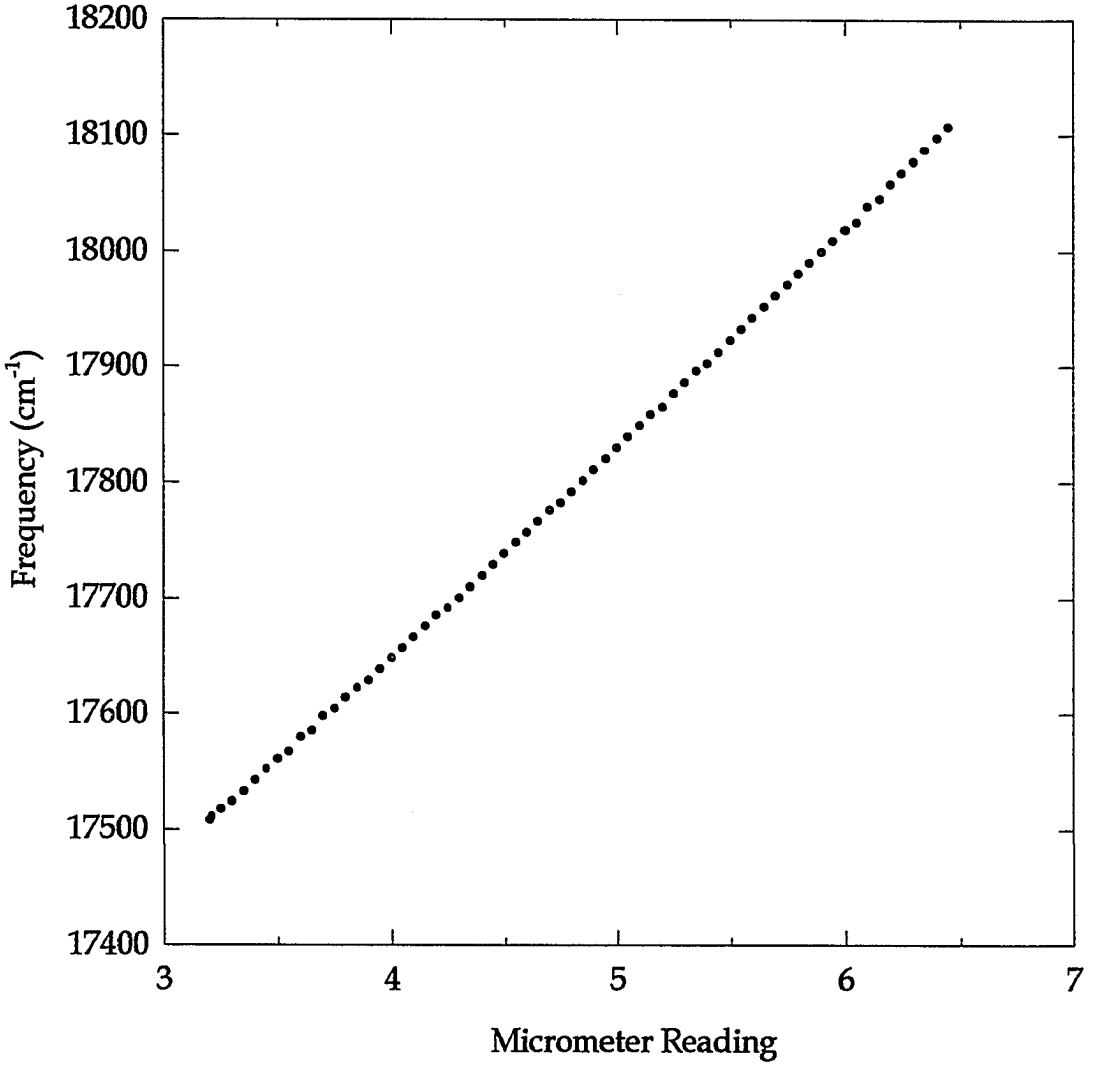

at least four orders of magnitude weaker than atomic signals, it is necessary to be certain that no stray broadband fluorescence, which includes the atomic resonance wavelength, reaches the interaction region. An intracavity polarizer reduces the fluorescence, which is not polarized, without greatly reducing the laser output. A rutile prism (TiO_2, index of refraction $\approx$ 2.6) in the beam path, followed by an iris about a meter away, further spectrally purifies the beam (Figure 21). As the laser is tuned, the prism moves the beam. If the prism is adjusted so that the beam goes through the iris, the fluorescence more than 20 cm^{-1} from the laser frequency will not pass through the iris. This strategy keeps the fluorescence background, which is measured at each point, to less than one percent of the signal size.

In the experiments, it is also necessary to change the linear polarization direction of Laser 2. A grazing-incidence dye laser is naturally polarized perpendicular to the rulings on the grating; in this case, horizontally polarized. The intracavity linear polarizer further purifies the polarization. The two experiments use slightly different methods for providing vertical polarization.

In experiment A, laser 2 passes through a Babinet-Soleil compensator (Geartner Scientific Company, L-133A) set at 45° to the laser's polarization, which produces a beam that has varying polarization across its width, so that the average beam is unpolarized. Then, just before entering the sample cell, the laser passes through a linear polarizer in a mount with a fine angular scale. The polarizer can be set to pass light polarized horizontally, parallel to the

FIGURE 21
Prism arrangement for spectral purification of laser 2.

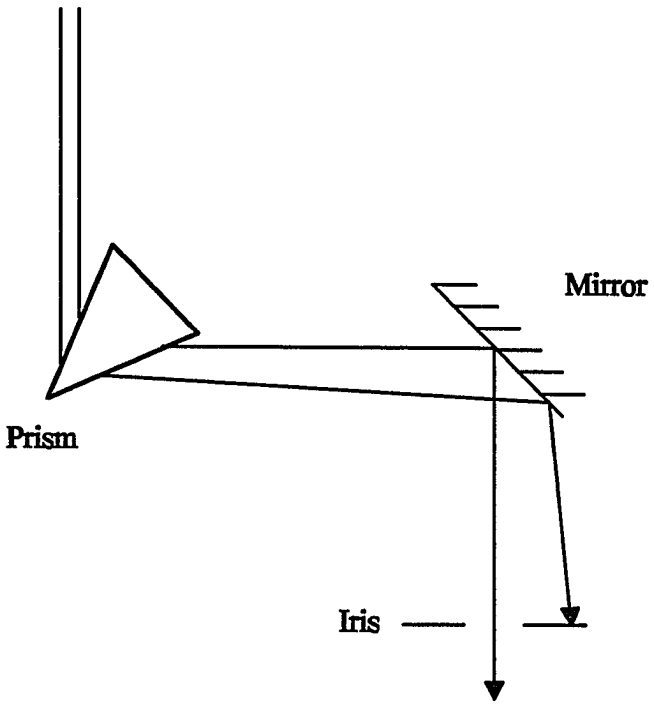

polarization direction of laser 1, or vertically, perpendicular to the polarization direction of laser 1. It can also be set at an angle 54.7° to the polarization direction of laser 1 to make total intensity measurements. The uniformity of the beam intensity with varying polarizer angles is measured regularly; the intensity does not vary more than two percent as the polarizer is rotated. The polarizer's angular scale is calibrated by placing a Glan laser prism polarizer (Spindler & Hoyer, 03-3210) in the path of laser 1, adjusting it for maximum transmission, then measuring the transmission of laser 2 through it going the other way. The linear polarizer in the path of laser 2 is adjusted for maximum transmission through the prism and the angle on its scale for which this occurs is considered to be zero. Since the Glan laser prism has an extinction ratio on the order of 10,000:1, the accuracy limit for the zero setting for laser 2 is the polarizer in its path, with an extinction ratio on the order of 100:1. Thus the polarization measurements have an uncertainty of about two percent from the polarizer-compensator system.

In experiment B, on the other hand, a liquid crystal variable retarder (Meadowlark Optics, LC1090-PC-VIS, with compensator) is used in place of the Babinet-Soleil compensator and linear polarizer. The liquid crystal device acts as a waveplate with a retardance that varies with an applied voltage. It consists of a nematic liquid crystal cell with transparent electrodes over its windows. When there is no voltage across the cell, the liquid molecules line up along the windows, and the retardance is a maximum. With increasing voltage, the liquid

molecules line up more with the applied field, decreasing the retardance. With only one cell, the retardance would not reach zero except at very high voltages, because of surface pinning effects. However, with a negative-retardance compensator, the device can change from half-wave retardance to zero retardance, both with voltages between zero and twenty volts. Thus this system has the advantages of a Pockels cell--variable retardance--without its disadvantage--high voltage. The voltage needed to obtain a desired retardance varies with wavelength and cell temperature as well as retardance. The liquid crystal variable retarder comes with a calibration for a range of wavelengths, retardances, and temperatures. It does have its own disadvantages. One is that it takes up to 40 ms to change its retardance. To make sure that the retardance has time to change, a delay is included in the operating program. Another disadvantage is that the liquid crystal can be damaged by ultraviolet light. To avoid damage by laser 1, a cutoff filter (Schott, GG 470 3 mm) that blocks laser 1 by at least a factor of 10^5 but passes 99 percent of laser 2 is placed between the sample cell and the liquid crystal variable retarder.

The liquid crystal retarder is set with its optic axis 45° from the polarization direction of the laser. For parallel measurements, the retardance is set to zero, so that the laser passes through with its polarization unchanged. For perpendicular measurements, the retardance is set to half-wave, so that the polarization direction of the laser is rotated by 90°. The contrast ratio measured by placing the Glan laser prism after the liquid crystal and setting it for

maximum transmission of the horizontal polarization, then measuring the transmitted laser intensity for retardance set at zero and half-wave, is on the order of 1000:1. The uncertainty in polarization introduced by the variable retarder is less than one percent. For total intensity measurements, the retardance is set to half-wave and the optic axis is set 27.35° from the initial polarization direction of the laser, so that the polarization direction of the laser is rotated by 54.7°. The variable retarder is controlled by a laboratory computer, so that the polarization may be rotated every few laser shots if necessary.

For both experiments, the lasers are focused so that within the cell their diameter is about 0.5 cm, with laser 1 slightly larger than laser 2. The laser beams overlap for a least half a meter each side of the sample cell to insure full overlap within the cell. The spatial overlap of the lasers is checked daily by observing both beams on a single white card. Ordinary file cards fluoresce in the visible range when exposed to ultraviolet light, and laser 2 is strong enough to be seen through the card. Thus it is possible to determine whether the lasers overlap properly. The lasers must also overlap in time. Therefore their paths are carefully planned and measured so that laser 2, the longer pulse, arrives about two nanoseconds before laser 1. Variations of a nanosecond or so are acceptable, but must be known since they affect the interpretation of the data. For experiment A, the path of laser 1 is five inches longer than the path of laser 2; for experiment B, it is three inches longer. Since the KDP crystal narrows laser 1 about its center in time, in both experiments this gives just under 2 ns difference

in arrival time.

2. Vacuum System

The optical collisions take place inside a sample cell, which consists of a 250 ml glass bulb with six projections (Figure 22). The lower projection, about 15 cm long, contains an iron boat supported by a quartz tube. A coaxial heater (ARi Industries, BXX04B8-6K), with the hot part coiled around magnesium chips, fits inside the boat. The coil is connected to a temperature controller (Cole Parmer, 2168-80), and a chromel-alumel thermocouple (Cole Parmer K-type) attached to the boat monitors the temperature. The controller keeps the boat temperature stable to 0.1° C, at 300°C for experiment A and at 320°C for experiment B. This temperature is not high enough to melt the magnesium, but it does provide a vapor pressure around 10^{-4} torr [24], sufficient for the experiment. The top of the boat is about a centimeter below the interaction region, where the lasers meet.

The cell has four sidearms spaced at 90-degree intervals in a horizontal plane. Two of these, 180 degrees apart, allow the lasers to enter the cell. The other two allow the fluorescence to reach the photomultiplier tubes (PMTs). For experiment A, only one PMT is used, so one sidearm is unused. These sidearms have the advantage of being far enough from the interaction region to minimize plating with magnesium vapor. In normal operation, the approximately spherical body of the cell is completely plated with magnesium, but the sidearms are still clear. However, they have been externally coated with graphite paint, except for

FIGURE 22
Design of the sample cell. Fluorescence is observed through the view port.

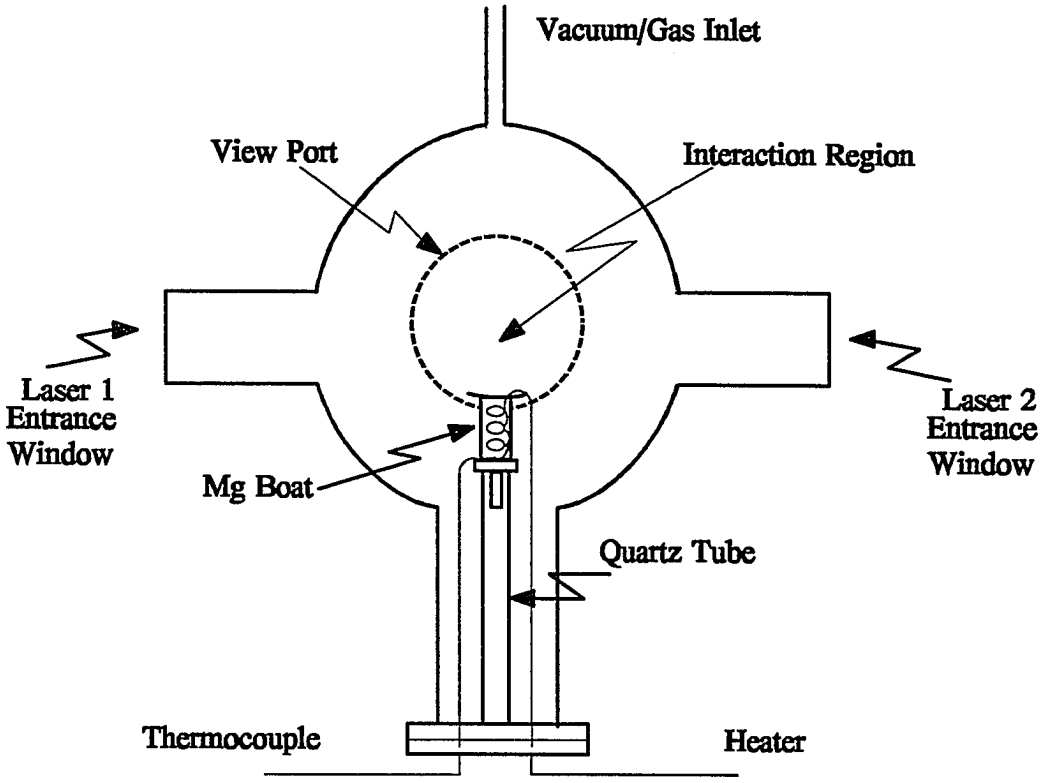

the ends, to keep unwanted laser reflections from the PMTs. All of the sidearms are fitted with quartz plates sealed with vacuum sealant (Varian, Torr Seal), so that ultraviolet light may pass.

The top of the cell is a tube connecting the cell to a vacuum system (Figure 23). The cell is usually isolated by a high-vacuum valve. The vacuum system includes a mechanical pump to provide a rough vacuum and an ion pump to evacuate the cell. It also includes a connection for a bottle of rare gas. This arrangement makes it easy to adjust the pressure of the rare gas, to change rare gases, and to evacuate the cell.

The rare gases used in the experiment are argon and neon. The neon (Air Products) is 99.999 percent pure; the argon (Spectra Gases), 99.9999 percent pure (Table 2). Both come in lecture bottles which connect to a regulator to allow controlled flow of gas to the cell. A capacitance manometer (MKS Baratron, 221A) monitors the pressure of the rare gas while the cell is filled; at this gauge, the temperature is about 295 K. The capacitance manometer has been calibrated using an oil manometer; its readings are correct to within the 0.2 torr combined uncertainty of the calibration measurement. After the cell has the correct pressure of rare gas--usually 20 torr--the cell valve is closed.

Two pumps are needed to evacuate the cell. The mechanical pump (Welch Scientific Company, 1402) can pump from atmospheric pressure down to 10^{-2} torr. The pressure in this range is measured by a Hastings DV-6 thermocouple pressure gauge. The ion pump (Varian, 911-5030) works in the range of 10^{-3} to

FIGURE 23
Schematic diagram of the vacuum system connected to the cell.

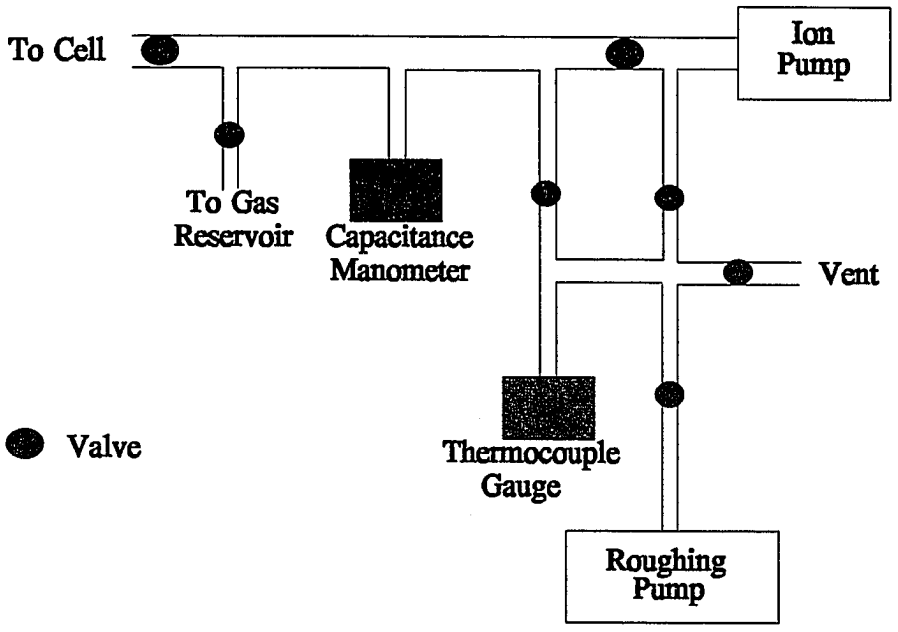

TABLE 2

Maximum levels of impurities, in parts per million (ppm) in the argon and neon as supplied by the gas manufacturer.

Typical Impurities	Argon	Neon
Acetylene		0.05
Carbon Dioxide	0.1	0.5
Carbon Monoxide	0.1	1.0
Helium		2
Hydrogen	0.2	2
Methane		0.5
Nitrogen	0.4	5
Nitrous Oxide		0.1
Oxygen	0.1	0.5
Total Hydrocarbons	0.1	0.2
Water	0.2	0.15

10^{-8} torr. Its pressure is measured by a gauge on the pump control unit (Varian, 921-0062). Exposing the ion pump while it is working to a pressure much higher than 1×10^{-2} can damage it. Therefore the procedure for pumping out the system is as follows: first, the sample cell and surrounding areas are pumped out using the mechanical pump, with the ion pump valves closed. When the thermocouple pressure gauge reads less than 1×10^{-2} torr, the mechanical pump valve is closed and the ion pump valve to the system is opened slowly. The ion pump is connected to a valve that leads directly to the mechanical pump, so that if the pressure in the ion pump rises above the critical level, it can be immediately pumped out by the mechanical pump. When the ion pump valve is fully open, the mechanical pump may be turned off and vented.

The cell is evacuated once each week during normal operation, to avoid build-up of outgassing contaminants. Every six months or so, the system is evacuated and baked, using heating tapes, for several hours to drive out accumulated impurities. This procedure is also followed whenever the cell has been opened, for example to add magnesium chips. The base pressure for the system is about 2×10^{-8} torr.

3. Detection System

The optical collision signals are generated in PMTs (EMI 9814QB). For experiment A, there is only one PMT, but for experiment B, there are two PMTs. The basic measurement for both experiments is intensity of the cascade

fluorescence from the $3s4p\,^1P_1 \rightarrow 3s^2\,^1S_0$ transition at 203 nm, which indicates population in the $3s5s\ ^1S_0$ state or the $3s4d\ ^1D_2$ state. PMT1 therefore has two interference filters centered at 200 nm (Acton Research Corporation, 201-N-1D* and OCA Microcoatings, MC-200). These filters block the resonance scattering at 285 nm by about a factor of 10^{-8}, and pass about two percent of the desired 203 nm radiation.

For experiment B, the secondary measurement may be either the $3s5s\ ^1S_0 \rightarrow 3s3p\,^1P_1$ fluorescence at 571 nm, or the $3s5s\ ^3S_1 \rightarrow 3s3p\,^3P_j$ fluorescence at 333 nm. In the first case, PMT2 uses three interference filters (one Ealing Electro-Optics, Inc, 35-3730 and two Oriel, 53905) centered at 570 nm and two cutoff filters (Schott, OG 570 3 mm). The main background for this PMT is the scattering from the Nd:YAG laser at 532 nm. This is very intense; to remove it the cell and both PMTs must be covered with black cloths with small holes to let the lasers through. Laser 2, near 553 nm, is less of a problem because it is less intense, but it does provide a strong background for the fluorescence. When laser 2 is tuned near (within 200 cm^{-1}) the 5s-3p resonance, the background from laser 2 is extremely high unless the laser is attenuated. The output for PMT2 at this wavelength is low partly because of the necessary filters which pass less than ten percent of the 571 nm fluorescence. Only detunings less than 25 cm^{-1} have a large enough signal-to-noise ratio to obtain reliable polarization or intensity measurements.

When PMT2 is set up to measure the triplet resonance at 333 nm, the

background is less important. Here, as for PMT1, the main background is resonance scattering from laser 1. The filters are an interference filter centered at 333 nm, an ultraviolet colored glass filter (Schott, UG11 1 mm), and a short wave cutoff filter (Schott, WG335 1 mm). This arrangement passes about 15 percent of the desired wavelength while blocking visible and 285 nm light by at least a factor of 10^{-5}. However, the signal-to-noise ratio for this channel is prohibitively high; no reliable polarization or intensity measurements can be made.

The output signal from each PMT is amplified using a timing-filter amplifier (EG&G Ortec 474). The amplified signal goes to a boxcar averager (Stanford Research SR250), which integrates the signal over a specified time. The gate is triggered by a photodiode that detects light from the Nd:YAG laser. It opens 45 ns after the trigger and stays open for 300 ns for experiment A and 200 ns for experiment B (Figure 24). These settings were chosen by observing the PMT output signal and the gate simultaneously on an oscilloscope and placing the gate to include most of the signal, while excluding the noise. Most of the laser scattering reaches the PMT immediately after the laser pulses, while fluorescence depends on the lifetimes of the states. The 3s4d $^1D_2$ state lifetime is 55 ± 3 ns, and the 3s5s $^1S_0$ state is 100 ± 5 ns [32]. Thus allowing the 45 ns delay blocks most of the laser scattering while passing most of the fluorescence.

The boxcar sends a voltage to an analog-to-digital board (MetraByte DAS20) in a laboratory computer (Win 386). This board has eight analog-to-digital channels; experiment A requires two channels, one for the boxcar voltage

FIGURE 24
Timing diagram for signal detection; Gate 1 is the gate for experiment A, and Gate 2 is the gate for experiment B.

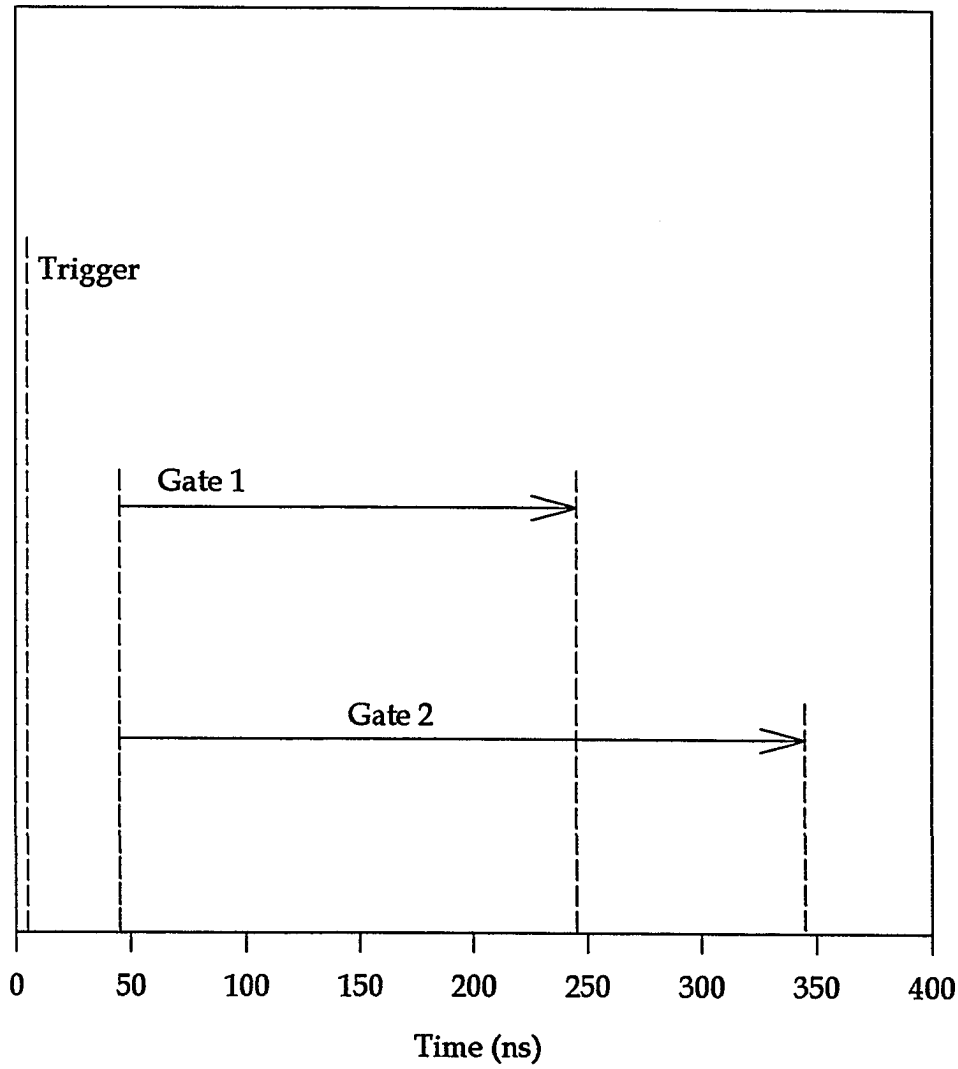

and one for a trigger, the busy output of the boxcar averager; experiment B requires a third channel for the second boxcar voltage. The program that runs the experiment, written in QuickBASIC 4.0, accumulates the data for many shots (typically 1000 for each polarization), then calculates the intensities, polarizations, and statistical errors. It also prompts the user to block or unblock the lasers. For experiment A, it prompts the user to rotate the linear polarizer to the necessary angle; for experiment B, it controls the liquid crystal variable retarder. The A-to-D board came with QuickBASIC subprograms to use with a data collection program. The variable retarder came with a calibration file and C subprograms to use with a data collection program. Because of the difficulty of combining QuickBASIC and C subprograms, I translated the C subprograms to QuickBASIC for use in this program.

Experimental Procedure

The experimental routine begins with finding the atomic resonance for the experiment by watching the PMT output on an oscilloscope (Tektronix, 7488) while adjusting the micrometers for the lasers. The oscilloscope shows a signal of several hundred millivolts on resonance. The resonance signal decreases noticeably in amplitude for detunings about 1 cm^{-1} for both experiments. The temporal full width at half maximum on the oscilloscope is about 150 ns for the $3s3p\ ^1P_1 \leftarrow 3s5s\ ^1S_0$ resonance and about 75 ns for the $3s3p\ ^1P_1 \leftarrow 3s4d\ ^1D_2$

resonance. With no attenuation in laser 1, it is often possible to observe the laser scattering with laser 2 blocked. This makes it possible to tune to the $3s^2\,{}^1S_0 \leftarrow 3s3p\ {}^1P_1$ resonance alone. Tuning laser 1 by itself avoids the problem of 2-photon resonances, where the lasers are detuned from atomic resonance by equal and opposite amounts, so that an isolated magnesium atom can absorb two photons at once. After the laser 1 resonance has been found, laser 2 is unblocked and tuned for a maximum negative peak on the oscilloscope.

The next step is optimizing the dye lasers and recording the output beam energy, measured with a Molectron J3-02 pyroelectric energy meter, which has a 2-mm diameter aperture. Typical measured energies for laser 2, with a beam diameter of about 0.5 cm at the detector, are 300 μJ per pulse for experiment A and 150 μJ per pulse for experiment B; the shot-to-shot variation is about ten percent. For laser 1, with a beam diameter of about 2 mm at the detector, the measured energy is typically 30 μJ per pulse. Then the electronic signal at the computer is checked for saturation of the $3s^2\,{}^1S_0 \rightarrow 3s3p\ {}^1P_1$ transition by laser 1. That is, this signal must be linear in laser 1 power. The signal is measured, then laser 1 is attenuated by a known factor. A second measurement of the signal should show a reduction of the signal by the same factor that the laser is attenuated. If it does not, the laser is attenuated further and the measurement repeated until the signal response is linear. This usually means attenuating laser 1 to an energy of around 1 μJ per pulse. When laser 2 is set to an atomic resonance, it must also be attenuated, usually by a factor of 10^4 for both

experiments, to avoid saturation.

The data is collected in runs of about 2000 data shots each, with slight variations for the two experiments. For experiment A, a data run consists of a baseline measurement, with both lasers blocked, a background measurement, with only laser 2 blocked, a parallel data measurement, with neither laser blocked and the laser polarizations parallel, and a perpendicular data run with the neither laser blocked and the laser polarizations perpendicular. Usually the background and baseline measurements consist of 250 laser shots each and the data runs consist of 1000 shots each, for a total of 2500 laser shots, which takes about 5 minutes. To avoid effects of drifting laser intensity, an even number of data runs is taken for each point, with the order of the parallel and perpendicular measurements alternating. The computer displays the background minus baseline figure for diagnostic purpose. When the background becomes comparable to the signal size, the data is no longer reliable.

For experiment B, a data run is divided into two halves. The first half has this order: first baseline, then laser 1 background (laser 2 blocked), then parallel laser 2 background (laser 1 blocked, laser 2 polarized horizontally), then parallel data, then perpendicular laser 2 background (laser 1 blocked, laser 2 polarized vertically), then perpendicular data. The second half-run has the same measurements in the opposite order. Thus if the laser intensity increases or decreases monotonically during a run, the effect should be averaged out by the two halves of the run. A typical run has 250 shots for each baseline or

background measurement (a total of 500 shots per type of measurement per run), and 500 shots for each data measurement (a total of 1000 shots per polarization per run), for a grand total of 4000 laser shots per run, which takes about 15 minutes. The computer displays the background minus baseline figure for both channels.

For both experiments, the average background in each PMT for a run is subtracted from the raw intensity to give a net intensity. This net intensity is used to calculate polarization. The background subtracted, for experiment B, depends on the PMT. When PMT2 is set for 571 nm, the laser 2 background is significant, and changes with laser 2 polarization. Therefore laser 2 backgrounds are included in each run and subtracted from PMT2 signals. Laser 1 backgrounds for PMT2 are negligible, and Laser 2 backgrounds for PMT1 are negligible; therefore, these are not subtracted from raw signals. However, when PMT2 is set for 333 nm, the laser 2 background is negligible for both PMTs. After ascertaining this, the laser 2 background measurements were dropped. However, the laser 1 background is now significant for PMT2 as well as for PMT1. Therefore the average laser 1 background is subtracted from each PMT.

At each detuning, the polarization is measured with two to six runs. The total polarization is calculated using the total parallel and perpendicular intensities.

The relative intensity spectrum is measured using one run, with the polarization vector of laser 2 set at 54.7° to that of laser 1. As explained in

chapter 2, this is the "magic angle" at which the total intensity for electric dipole radiation can be measured without polarization effects. To avoid as much as possible the effects of laser intensity drifts, a reference point not too near resonance is chosen and measured several times during the intensity spectrum measurement, which is done on a single day for each spectrum.

In addition to polarization and intensity spectra, the dependence of polarization on rare gas pressure is measured for several detunings. For each pressure-dependence run, the polarization is measured at four to six different pressure, selected from the following 5, 7.5, 10, 12.5, 15, 17.5, 20, 25, and 30 torr. Plotting inverse polarization versus pressure gives a straight line, to a good approximation. This measurement permits the extrapolation of the polarization results to a single-collision limit, as explained in the next chapter. For experiment B, the PMT2/PMT1 signal ratio as a function of pressure is also measured to determine the single-collision limit. Detailed analysis of pressure dependence is discussed in Chapter 4.

Chapter 4

Experimental Results

The results for the excitation near the 3s5s $^1\Sigma_0^+$ state consist of polarization spectra, intensity spectra, and pressure dependence data for magnesium-argon and magnesium-neon collisions. For the excitation near the 3s4d $^1\Sigma_0$, 3s4d $^1\pi_1$, and 3s4d $^1\Delta_2$ states, the results comprise a polarization spectrum, an intensity spectrum, pressure dependence data, and inelastic branching data for magnesium-argon collisions. This chapter begins by presenting the pressure dependence data, then discusses the polarization spectra and intensity spectra, and concludes by mentioning other observations.

Pressure Dependence

The measured polarization can be affected by several factors besides the optical collision dynamics. The most important of these in the experiments is collisional disalignment. An aligned, excited state magnesium atom collides with a rare gas atom, absorbing a photon during the collision. In these experiments the magnesium atoms are initially in the 3s3p $^1P_1$ level. But if the atom collides with one or more rare gas atoms before the optical collision, the atom may be partially disaligned. The number of collisions the magnesium atom undergoes is

related to the number of rare gas atoms available for collision; in other words, it is related to the pressure of rare gas in the sample cell. The degree of linear polarization measured therefore depends on the rare gas pressure. As shown in an appendix, for low pressures, ≤ 35 torr, inverse polarization has an approximately linear dependence on rare gas pressure,

$$P_L^{-1}(P) = P_{L0}^{-1}(1+\alpha P) \qquad (4.1)$$

where α is a constant that is related to the collisional disalignment rate coefficient k and the lifetime of the state τ, $\alpha P = Nk\tau$. This constant does not depend directly on detuning. Therefore it is possible to extrapolate each data point to a single-collision limit (at 0 torr) by making pressure dependence measurements at several detunings.

A pressure dependence measurement consists of polarization measurements made at the same detuning, but different rare gas pressures. The inverse polarization data are then plotted versus pressure. Figure 25 shows several such plots for Mg-Ar, with detunings near the 3s5s $^1\Sigma_0^+$ state. The intercept of the best straight line through the points, calculated using a least squares fit, is the inverse polarization for 0 torr, the single collision limit. The slope of the line divided by the intercept gives α. Once α has been determined by taking the average α from several pressure dependence runs, it is possible to use equation (4.1) to calculate the inverse polarization at 0 torr for each detuning at which a polarization measurement at finite rare gas pressure has been made. Figures 26 and 27 show pressure-dependent plots for Mg-Ne near the 5s state and

FIGURE 25

Pressure dependence of inverse polarization for Mg-Ar in experiment A. Representative error bars are shown.

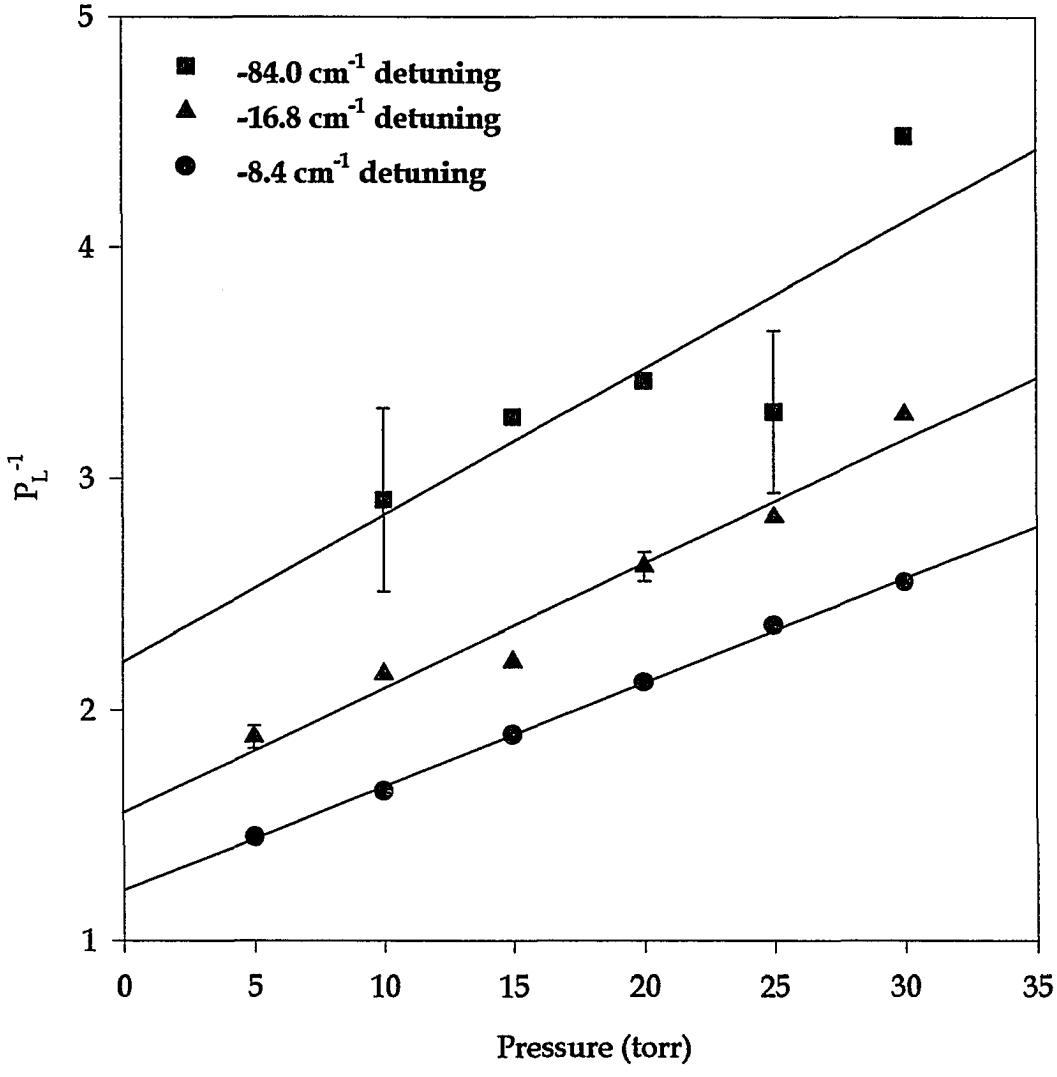

FIGURE 26
Pressure dependence of inverse polarization for Mg-Ne in experiment A. Representative error bars are shown.

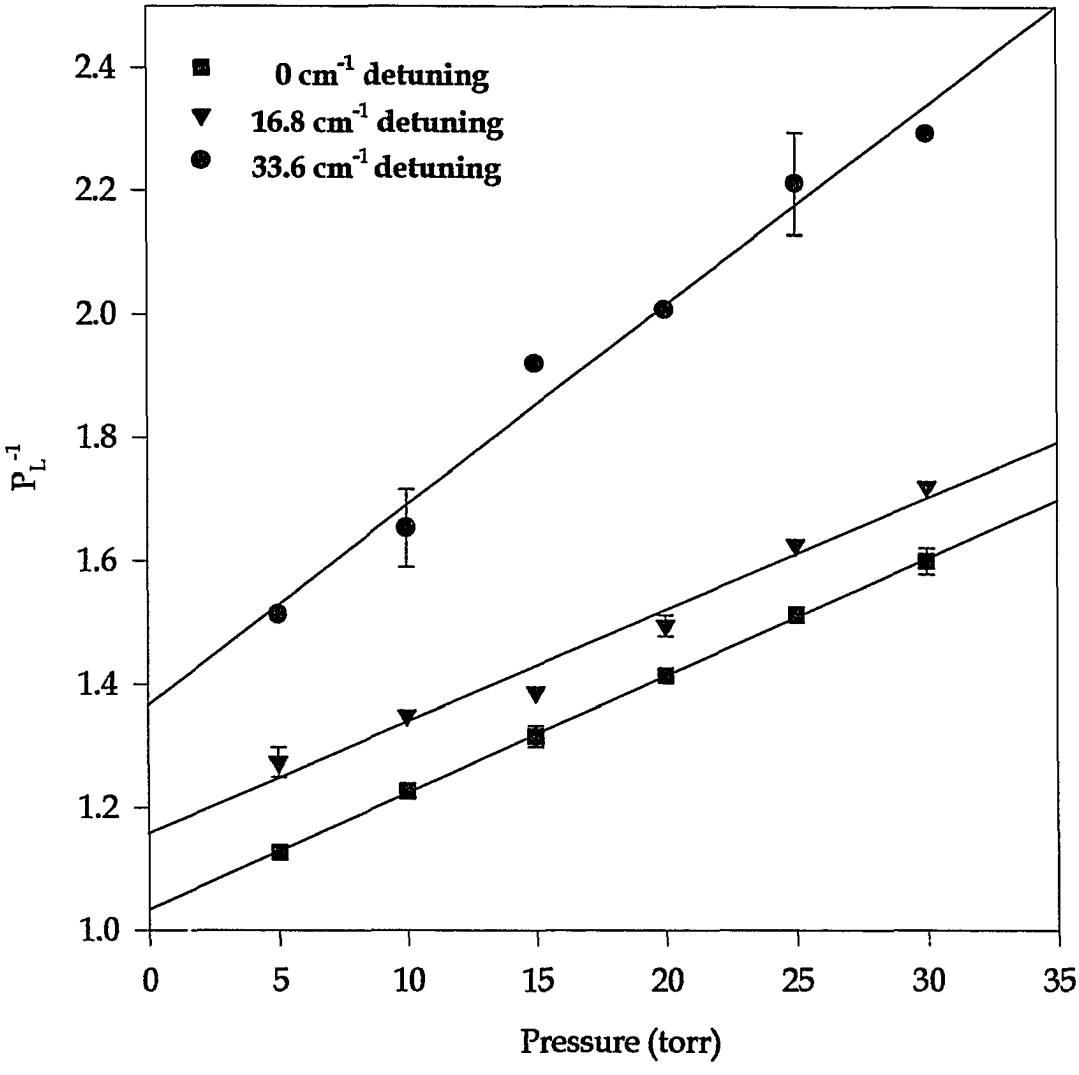

FIGURE 27
Pressure dependence of inverse polarization for Mg-Ar in experiment B. Representative error bars are shown.

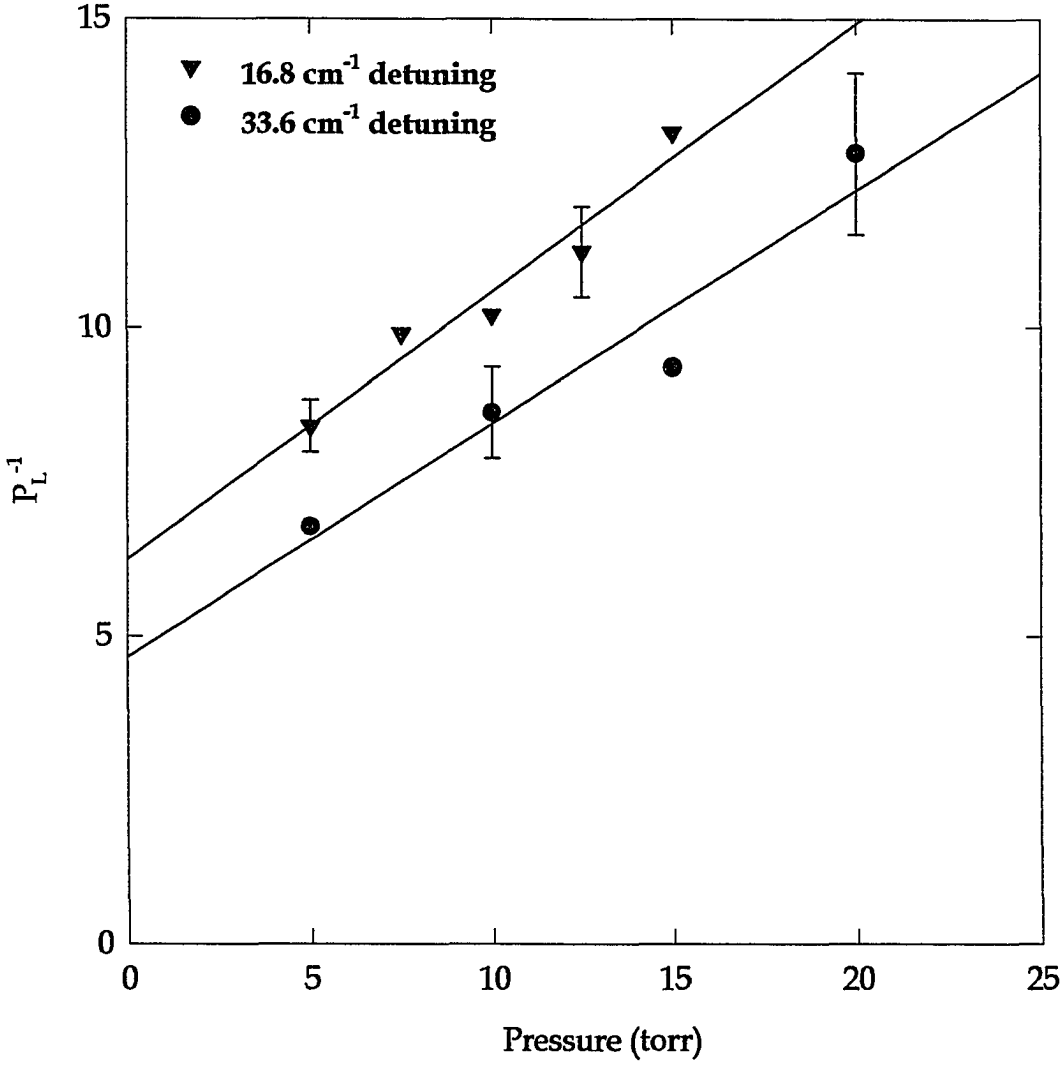

Mg-Ar near the 4d state, respectively.

The actual dependence of alignment, $\langle A_0 \rangle$, on pressure is far from linear for arbitrary pressures. Using a rate equation analysis (see Appendix) and assuming the lasers are square pulses gives

$$\langle A_0 \rangle = -\Gamma_r \left[\frac{1.4}{x} + \frac{1.05}{x^2} e^{-1.90x}(1 - e^{1.43x}) \right] \tag{4.2}$$

where $x = 1 + Nk\tau$, where N is the number of rare gas atoms present and k is a rate coefficient for collisional disalignment. For the 5s state, this gives for P_L, using equation (2.16)

$$P_L = \frac{3\Gamma_r \left[\frac{1.45}{x} + \frac{1.05}{x^2} e^{-1.90x}(1 - e^{1.43x}) \right]}{2 + \Gamma_r \left[\frac{1.45}{x} + \frac{1.05}{x^2} e^{-1.90x}(1 - e^{1.43x}) \right]} \tag{4.3}$$

For the 4d state, using equation (2.16), P_L is given by

$$P_L = \frac{3\Gamma_r \left[\frac{1.45}{x} + \frac{1.05}{x^2} e^{-1.90x}(1 - e^{1.43x}) \right]}{20 + \Gamma_r \left[\frac{1.45}{x} + \frac{1.05}{x^2} e^{-1.90x}(1 - e^{1.43x}) \right]} \tag{4.4}$$

These equations can be fit to the data for each pressure dependence run, using k as a parameter, to determine k. The derivation was repeated assuming triangular pulses. Although the equation for P_L in this case is much more complicated, the resulting k is the same within the uncertainties. Table 3 gives the rate coefficients for collisional depolarization determined by these fits.

TABLE 3

Rate coefficients for collisional disalignment calculated from the pressure dependence data, in units of cm^3/s.

MgAr: k	Mg-Ne: k	Model for Calculations
12.4 (7) x 10^{-10}	8.3 (9) x 10^{-10}	Square Pulse
15.4 (1) x 10^{-10}	10.8(1) x 10^{-10}	Triangular Pulse
13.9(7) x 10^{-10}	9.6(9) x 10^{-10}	Average

Polarization Spectra

Most of the physical information comes from interpretation of polarization spectra. The interpretation of these spectra requires some knowledge of qualitative molecular potentials. The polarization spectra usually have a peak at atomic resonance and decrease for larger detunings. The main measurements are taken at 20 torr of rare gas pressure, then the results are extrapolated to a single collision limit as explained above. Figure 28 shows the polarization spectrum for magnesium-argon optical collisions for an excitation of upper 3s5s $^1\Sigma_0$ molecular state. The figure displays data for 20 torr argon and also the extrapolations to a single collision. In this context, detuning Δ_{5s} is defined by

$$\Delta_{5s} = \omega - \omega_{5s} \tag{4.5}$$

where ω is the laser frequency, and ω_{5s} is the 3s3p $^1P_1$ - 3s5s $^1S_0$ transition frequency. For the single-collision limit, at atomic 5s resonance the polarization is 100 percent, as expected from calculations in chapter 2. This value decreases rapidly for positive detunings from the 5s, reaching zero percent by $\Delta_{5s} \approx 50$ cm^{-1}. For negative detunings from the 5s state, the polarization decreases more slowly, eventually reaching zero percent at $\Delta_{5s} \approx 150$ cm^{-1}. The molecular potential diagram in Figure 2 can help to interpret these findings. Positive detunings mostly connect the 3s3p $^1\pi_1$ state to the 3s5s $^1\Sigma_0$ state. This transition has a dipole moment that is perpendicular to the internuclear axis, and so from the arguments

FIGURE 28

Polarization spectrum for Mg-Ar, experiment A, at 20 torr. Data are extrapolated to the single-collision limit (zero pressure limit). Representative error bars are shown.

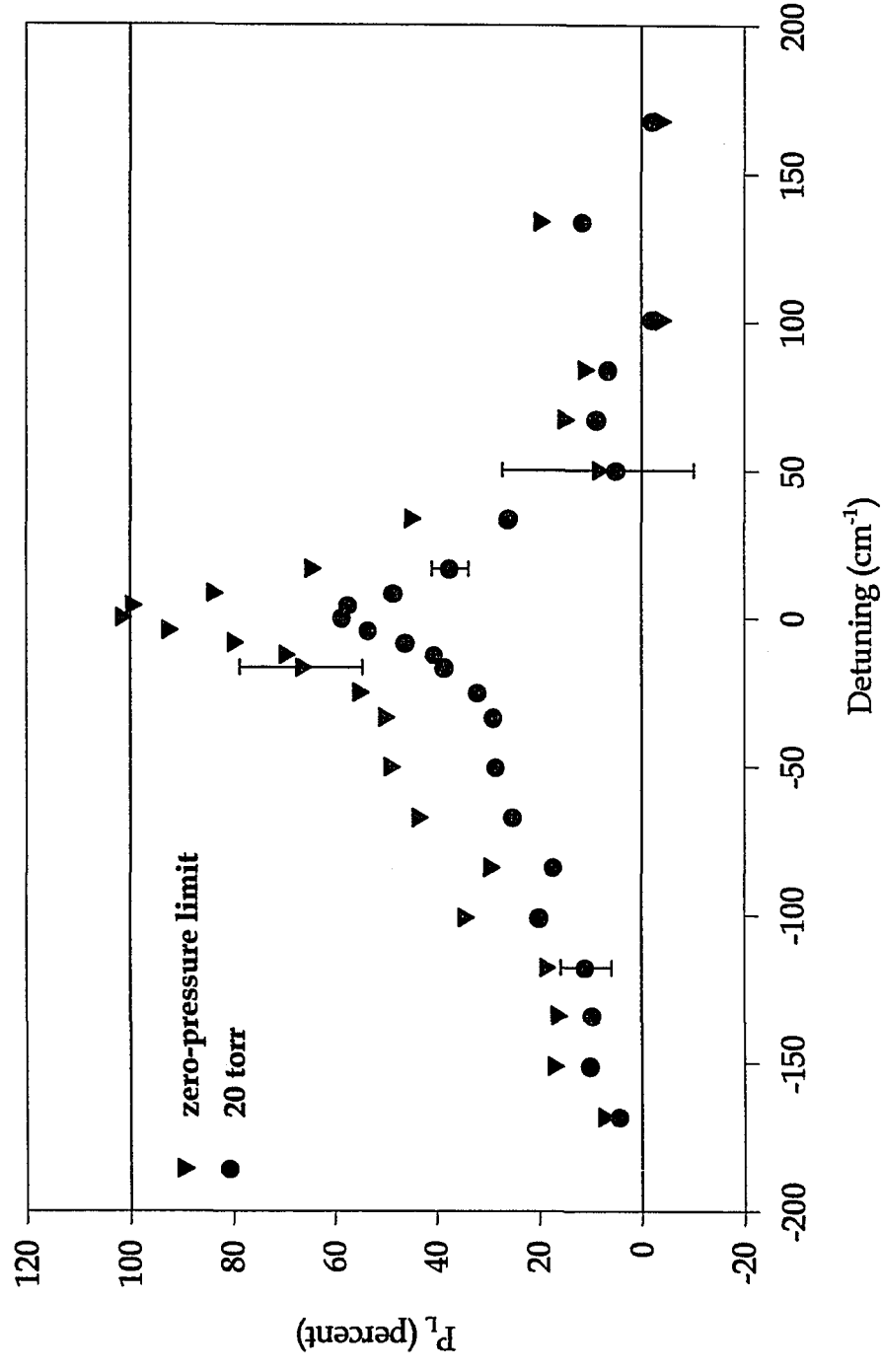

in chapter 2 a relatively high polarization would be expected. However, the positive detunings show rapidly decreasing polarization. Two effects might account for this. First, both the 3s3p $^1\pi_1$ state and the 3s5s $^1\Sigma_0$ state have potential wells. Therefore the transition may involve bound states, which have lifetimes longer than collision times. The bound molecule is likely to undergo depolarizing three-body collisions. The signal from bound states should show a nonlinear dependence on laser power, which cannot be ruled out because of the low signal to noise ratio in this region. Second, if the 3s4d $^1\pi_1$ has a deep enough well, it may be excited for large positive detunings. This π-π transition has a parallel transition dipole moment, and therefore should show low polarization.

Negative detunings involve transitions from both the 3s3p $^1\Sigma_0^+$ and the 3s3p $^1\pi_1$ states to the 3s5s $^1\Sigma_0^+$ state. The π-Σ transitions are perpendicular, and would show relatively high polarization. However large negative detunings are likely to end up deep in the 5s $^1\Sigma_0^+$ potential well, where they are bound so that they do not dissociate soon enough to be detected within the gate time, or they may radiatively decay outside the spectral band pass of the interference filters. Therefore for larger negative detunings the parallel Σ-Σ transitions dominate. These have lower polarization, especially for larger detunings which indicate stronger collisions with greater reorientation.

Figure 29 shows the polarization spectrum near the 5s state for Mg-Ne optical collisions. This is similar to the Mg-Ar spectrum, except that the polarization drops more slowly with increasing detuning. For negative detunings,

FIGURE 29

Polarization spectrum for Mg-Ne, experiment A, at 20 torr. Data are extrapolated to the single-collision limit (zero pressure limit). Representative error bars are shown.

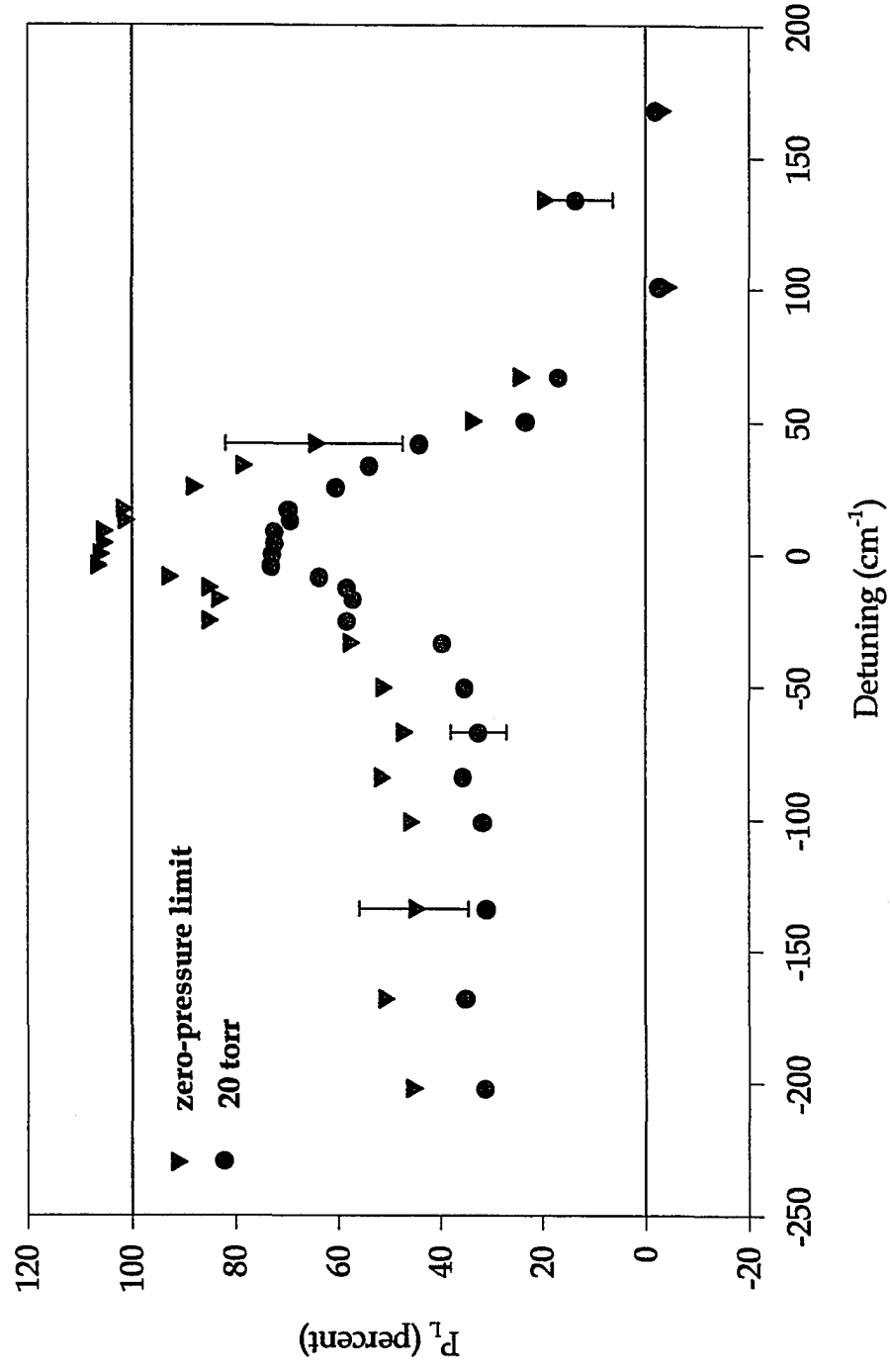

the polarization levels off around 50 percent for $\Delta_{5s} \approx 50$ cm^{-1}. The Mg-Ne potentials show shallower wells than the Mg-Ar potentials; therefore the π-Σ transitions reach free states for larger negative detunings. The perpendicular transitions show less reorientation than parallel transitions, which agrees with the observation that the Mg-Ne polarization remains higher than the Mg-Ar for large negative detunings. For positive detunings, the polarization remains high longer than in Mg-Ar, which suggests that the depolarizing mechanism for Mg-Ar is related to its greater well depth.

Figure 30 shows the polarization spectrum near the 4d state for Mg-Ar optical collisions. Here detuning Δ_{4d} is defined by the equation

$$\Delta_{4d} = \omega - \omega_{4d} \tag{4.6}$$

where ω is the frequency of the laser and ω_{4d} is the frequency of the 3s3p $^1P_1$ - 3s4d $^1D_2$ transition. Near the atomic resonance, the polarization is the expected 14 percent, within the uncertainty. The polarization drops for negative detunings, going to zero percent near $\Delta_{4d} = -150$ cm^{-1}. It stays low as far as the signal is strong enough to measure, $\Delta_{4d} \approx -300$ cm^{-1}. This is consistent with the low polarization for $\Delta_{5s} \approx 150$ cm^{-1}. The polarization is slightly negative in the region midway between the two atomic resonances. For positive detunings, the polarization rises slightly, an occurrence not before observed in optical collision experiments. Referring again to the molecular potentials, negative detunings involve transitions from the 3s3p $^1\pi_1$ and the 3s3p $^1\Sigma_0^+$ states to the 3s4d $^1\pi_1$ state. For large negative detunings, the parallel π-π transition dominates, giving a low

FIGURE 30

Polarization spectrum for Mg-Ar, experiment B, at 20 torr. Data are extrapolated to the single-collision limit (zero pressure limit). Representative error bars are shown.

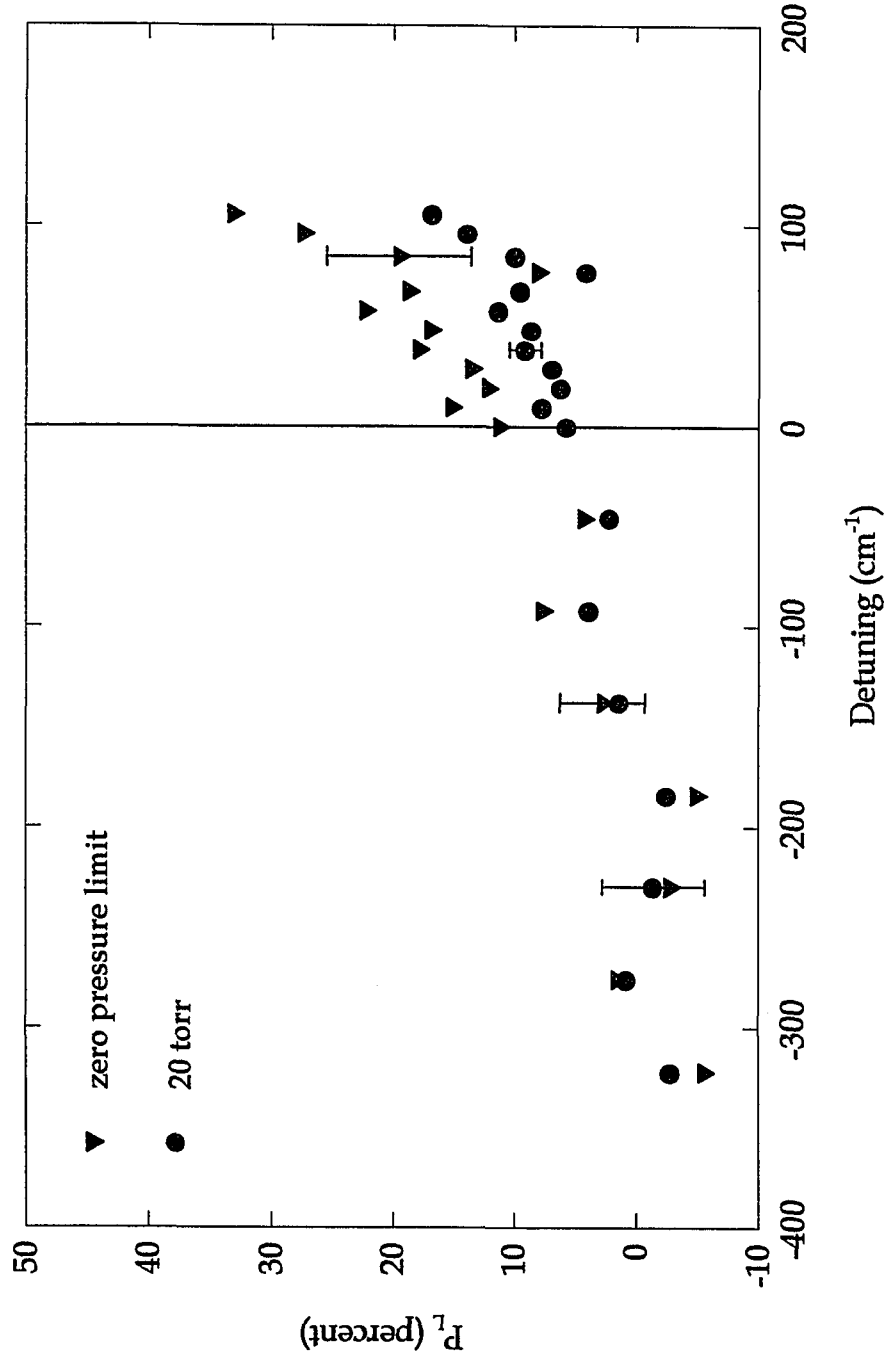

polarization. Near resonance the perpendicular π-Σ transition contributes, so that the polarization rises. Also near resonance there are transitions from the 3s3p $^1\pi_1$ and the 3s3p $^1\Sigma_0^+$ states to the 3s4d $^1\Sigma_0^+$ state. For positive detunings, these transitions are the important ones, with the π-Σ transition becoming more important for large detunings, so that with the Σ-Σ transition becoming less important, the polarization rises. The polarization can rise above the atomic resonance polarization because, as explained in chapter 2, the molecular levels have an axis of symmetry that affects the angular momentum so that, for example, a molecular Σ level may dissociate to an atomic d level with different polarization characteristics.

Intensity Spectra

Relative intensity spectra were also measured for experiment A for each rare gas collision partner (Figures 30 and 31). For each intensity spectrum a nonresonant detuning was chosen as a reference point, and measured several times while the spectrum was obtained and interpolated to normalize the measurements. The measured intensity at each point is divided by the intensity at the reference point. As expected, the spectra show a sharp peak at the atomic resonance and rapid decreases with increasing detuning.

A relatively simple model [1] of the intensity of absorption or emission between two energy levels at a given detuning takes into account the number of

FIGURE 31
Relative intensity spectrum for Mg-Ar, experiment A, at 20 torr. Connecting lines have been added to guide the eye. Representative error bars are shown.

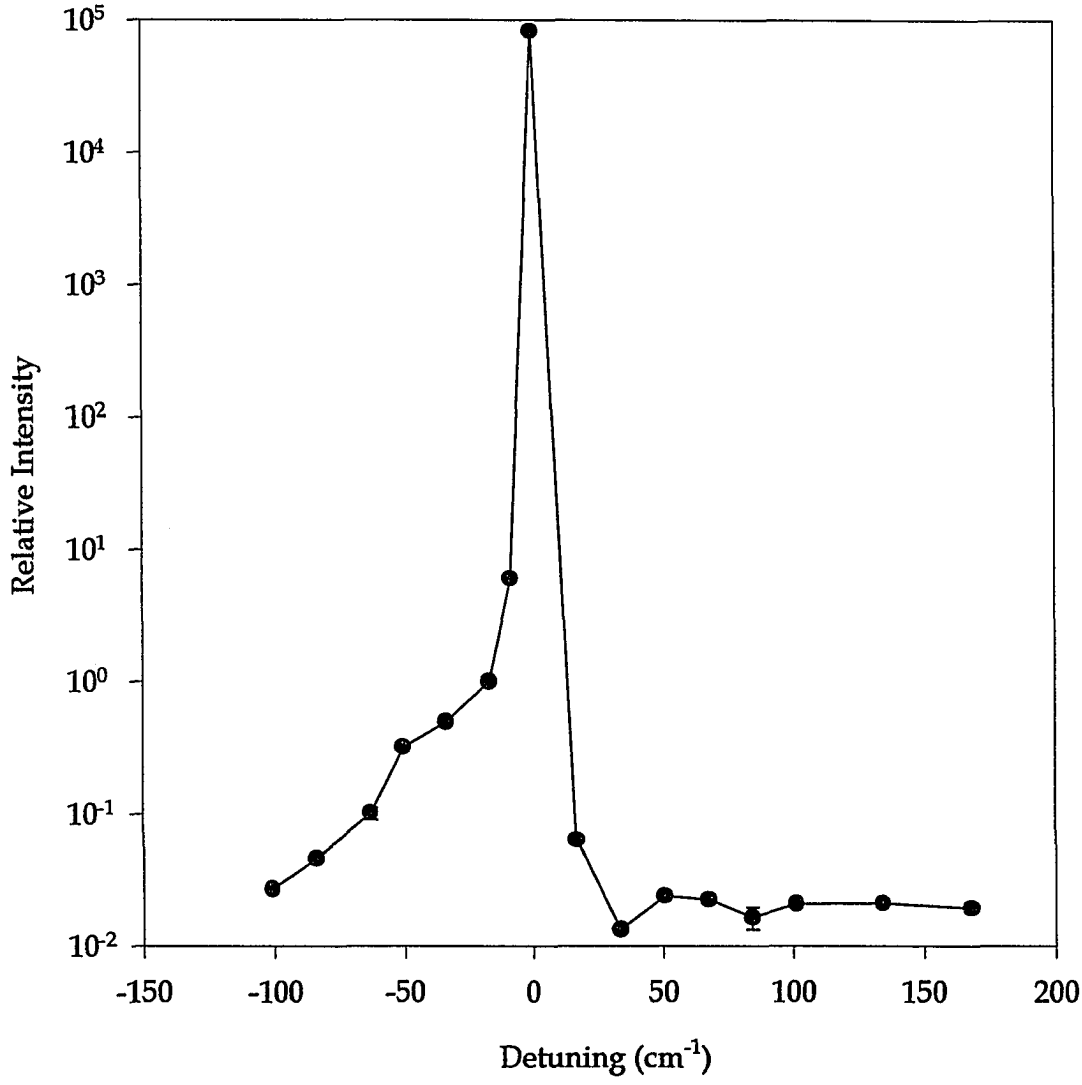

FIGURE 32
Relative intensity spectrum for Mg-Ne, experiment A, at 20 torr. Connecting lines have been added to guide the eye. Representative error bars are shown.

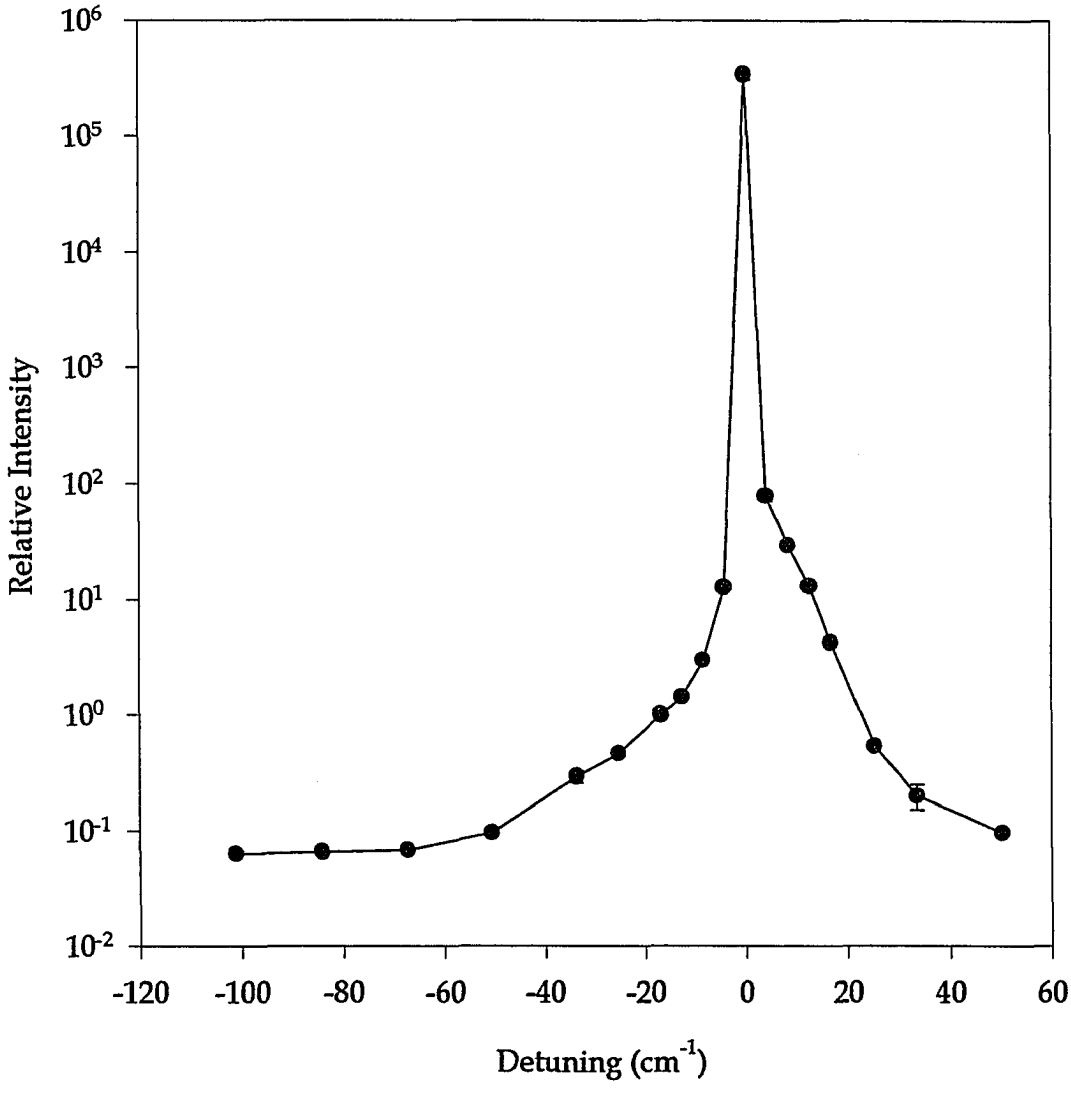

colliding partners available within a spherical shell whose radius is given by the Condon point for the detuning, and the spontaneous decay rate $A(R)$,

$$I(\omega)d\omega = N(R)4\pi R^2 dR \times A(R)\hbar\omega(R) \tag{4.7}$$

Using the Classical Franck-Condon Principle (equation 2.2) and assuming thermal equilibrium, this can be rewritten

$$I(\omega) = N_0 \frac{g_2}{g_1} e^{-\frac{\Delta V}{kT}} 4\pi R^2 \hbar \left[\frac{d(\Delta V)}{dR}\right]^{-1} \times A(R)\hbar\omega(R) \tag{4.8}$$

where ΔV is the difference in potential energy between the two levels and g_1 and g_2 are the degeneracies of the two levels. Therefore the intensity spectrum depends on the details of the potentials. For rapidly changing ΔV, for example where the potential curves have opposite slopes, the intensity is small. But for a slowly changing difference potential, where the potential curves are roughly parallel for some range of R, the intensity is large.

Inelastic Branching

The inelastic branching to the 5s $^1\Sigma_0^+$ and 5s $^3\Sigma_1^+$ triplet states during a single collision was not observed. Figure 33 shows the pressure dependence of the 5s/4d intensity ratio. It is a straight line, with an intercept near zero. This shows that the population monitored in the 5s $^1\Sigma_0^+$ state comes from subsequent collisions, not from the optical collision in which the 4d state was excited. If the

FIGURE 33

Pressure dependence of the ratio of the intensity in the $3s3p\ ^1P_1 \leftarrow 3s5s\ ^1S_0$ fluorescence channel to the intensity in the $3s^2\ ^1S_0 \leftarrow 3s4p\ ^1P_1$ fluorescence channel in Mg-Ar, experiment B, at a laser 2 detuning of 57.3 cm^{-1}.

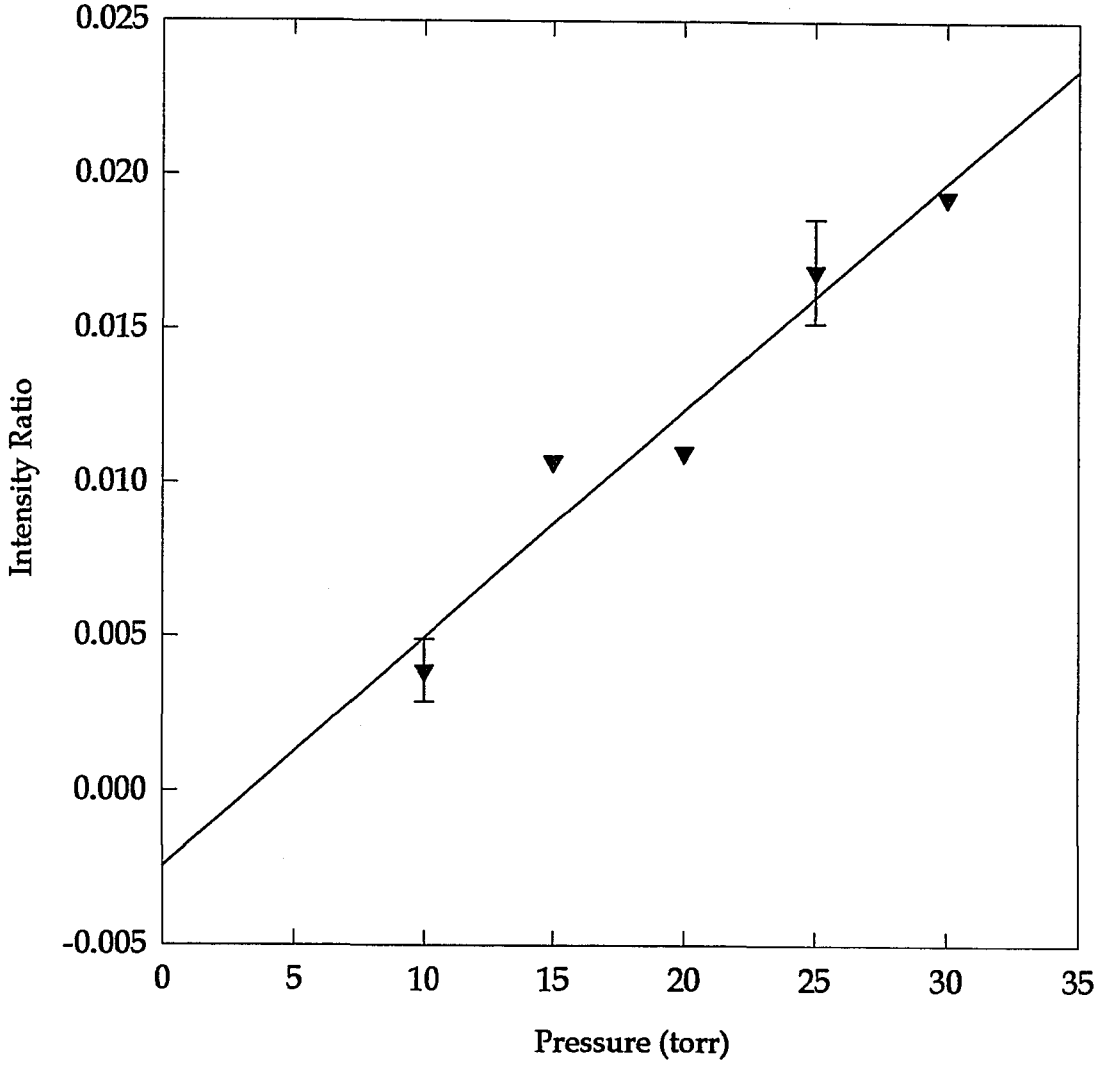

data were in the vicinity of a curve crossing, the population in the 5s $^1\Sigma_0^+$ state would not depend on rare gas pressure , and the line would be horizontal. However, the signal in the 5s channel was significant only for $\Delta_{4d} < 25$ cm^{-1}. There may have been significant branching to the 5s $^1\Sigma_0^+$ state for detunings at which the signal in the main channel was so small that any fraction of it in the 5s channel was unmeasurable; also, the curve crossings may be outside the range that was covered. There must be some curve crossings, or there would be no signal in the 5s channel. This experiment did not locate them.

Inelastic branching to the triplet 5s $^3\Sigma_1^+$ state was not observed. With both lasers set on resonance, there was a small amount of signal in the triplet 5s channel, but the signal to noise ratio was not large enough to make measurements practical. However, with laser 2 set to the atomic 3s3p $^1P_1 \rightarrow$ 3s5s $^1S_0$ transition, fluorescence can be observed at 553 nm (the 3s3p $^1P_1 \rightarrow$ 3s4d $^1D_2$ frequency) and at 333 nm (the 3s3p $^1P_1 \rightarrow$ 3s5s $^3S_1$). Therefore there must be some inelastic branching among these levels.

Other Effects

The polarization can be affected by several experimental factors. These factors tend to decrease the measured polarization. Radiation trapping occurs when the fluorescence from one atom is absorbed by a second atom before it leaves the cell; an environment in which the probability for reabsorption is

significant is said to be optically thick. The second atom fluoresces also, but its fluorescence is in an arbitrary direction. Therefore the fluorescence becomes unpolarized, and also less likely to reach the PMT within the gate time. The density of the magnesium, adjusted by the temperature of the sample cell, determines whether the medium is optically thick or thin. To eliminate radiation trapping, the polarization for one detuning--usually 0 cm^{-1}--was measured at several cell temperatures. The selected cell temperature of 320 °C was chosen because changes of ±20 °C, a factor of two in signal, did not affect polarization measurably at this temperature. Another thing that can decrease polarization is saturation of the transition by one of the lasers; saturation is a problem only on atomic resonance because the lasers are not intense enough to saturate a molecular transition. If the transition is saturated, additional laser intensity will not provide additional signal. The transition may be saturated when the lasers have their polarizations parallel but not when they are perpendicular, so that the weaker transition increases its signal relative to the stronger transition, thus lowering the polarization. To avoid saturation, the linearity of the PMT output with laser energy was measured every day and the lasers were attenuated to remove any saturation, as described in chapter 3. Atomic hyperfine interactions can also affect alignment. Hyperfine interactions occur when the electronic angular momentum J couples to the nuclear spin I to form total angular momentum F. J then precesses around F, resulting in an oscillating alignment. Magnesium has three stable isotopes, ^{24}Mg (I=0, relative abundance .79), ^{25}Mg

(I=5/2, relative abundance .1), and ^{26}Mg (I=0, relative abundance .11). Only the ^{25}Mg will contribute to the hyperfine interaction. The precession frequencies for ^{25}Mg are unknown, but the effect should be strongest on atomic resonance. However, the polarization on atomic resonance, extrapolated to a single collision limit, is 100 percent, as calculated by ignoring the hyperfine effect. Therefore disalignment by hyperfine interaction is negligible for these experiments.

Some interesting observations do not directly contribute to the experiment. When both lasers are tuned to atomic resonance, and the temperature is increased to 380 °C and the attenuation in the lasers is reduced, Dicke superradiance occurs. This is a result of a population inversion between the 4d (or 5s) state and the 4p state in an optically thick medium. A spontaneous emission then stimulates neighboring atoms to radiate, and the upper level depopulates rapidly. Since the emission is infrared (~2.5 μm), it cannot be observed directly, but its effect of the PMT output displayed on an oscilloscope is obvious. Normally the 3s4d $^1D_2$ resonance trace on the oscilloscope is about 75 ns wide, consistent with the 3s4d $^1D_2$ lifetime of 55 ns. When the superradiance occurs, the trace narrows rapidly and increases in amplitude. The narrowing occurs because the 3s4p $^1P_1$ level has a lifetime of only 9.7 ns, so the rapid transition caused by superradiance is not broadened much by the $3s^2\,^1S_0 \leftarrow 3s4p\,^1P_1$ transition by which it is observed. By adjusting the attenuation in the lasers, it is possible to see the trace oscillate between normal resonance and superradiance.

Another interesting effect occurs when laser 1 is tuned to the 3s-3p

resonance, and is ≥ 50 μJ. Then instead of one resonance peak, three are present. This Mollow triplet is a result of the dynamic Stark effect [33]. That is, the laser is a strong field, and splits each level into two components separated by the Rabi frequency ω_R, which is related to the strength of the laser field. There are then four possible transitions with three distinct frequencies: ω_0, the weak-field resonance, and $\omega_0 \pm \omega_R$. The Mollow triplet appears only for strong laser fields; in ordinary data taking, the laser is attenuated so that the transition is not even saturated.

Chapter 5

Conclusions

In this dissertation, optical collisions of excited-state ($3s3p\ ^1P_1$) magnesium and rare gas atoms have been discussed. Transitions to the molecular 3s5s $^1\Sigma_0^+$state in Mg-Ne and Mg-Ar and the 3s4d $^1\Sigma_0^+$, 3s4d $^1\pi_1$, and 3s4d $^1\Delta_2$ states in Mg-Ar were studied. For each transition, a polarization spectrum, an intensity spectrum, and a collisional disalignment rate for the Mg $3s3p\ ^1P_1$ level were obtained. In addition, for the transition to the 3s4d $^1\Sigma_0^+$, 3s4d $^1\pi_1$, and 3s4d $^1\Delta_2$ states inelastic branching to the $3s5s\ ^1\Sigma_0^+$ state and the $3s5s\ ^3\Sigma_1^+$ state was looked for but not observed. This null result is important in restricting theoretical modelling of the process. These data provide a test for theories of collision dynamics for these collisions. Where comparisons have been made, they are in good agreement with the qualitative results of Kupriyanov, an extension of the adiabatic reorientation theory of Lewis et. al.

Although these experiments have provided valuable information, it is possible to improve the apparatus to make possible more sensitive measurements. The dye lasers would be improved by changing to flowing dye cells. The current dye cells must be changed about every two weeks and cannot support more pumping from the Nd:YAG laser. A flowing dye system could be pumped by higher power from the Nd:YAG beam and would only need to be changed once

a year or so. This would increase the intensity of the off-resonance laser and enable the measurement of polarizations at larger detunings, where the signals are very weak. An improvement for the inelastic branching measurements could be obtained using spectrally narrower filters, to exclude more of the background without significantly reducing the desired fluorescence. Further automating the experiment would also be desirable, to allow more systematic background measurements. The experiment would also benefit from a change to atomic beams, which would allow the selection of initial velocities and eliminate averaging over collision angles.

Further experiments that would be interesting include a fractional collision study in the vicinity of the 4d state. Fractional collisions use two lasers that are off atomic resonance, so that two photons must be absorbed during a single optical collision. The reorientation that takes place then depends on the time between the absorption of the two lasers, which is related to the distance between the two Condon points. This method gives finer detail about the collision dynamics, similar to the information available from experiments using femtosecond lasers.

Since no inelastic branching was observed in the regions accessible to this experiment, it would be interesting to measure inelastic branching among the 3s6s $^1\Sigma_0^+$, 3s5d $^1\pi_1$ and 3s5d $^1\Sigma_0^+$, and the 3s6s $^3\Sigma_1^+$. These states are closer together in energy than the 3s5s $^1\Sigma_0^+$, 3s4d $^1\pi_1$ and 3s4d $^1\Sigma_0^+$, and the 3s5s $^3\Sigma_1^+$. Perhaps the curve crossings occur at accessible detunings from atomic resonance for these

higher states.

So far measurements of polarization spectra in alkaline earth-rare gas optical collisions have concentrated on magnesium, calcium, and strontium. However, the lightest alkaline earth metal is beryllium; it is therefore the simplest to make exact calculations for. Beryllium-rare gas optical collisions would be a natural extension of this work, provided that certain difficulties could be overcome. For example, beryllium has a low vapor pressure at temperatures easily reached by a resistance heater.

The experiments discussed in this dissertation provided some useful new information and insights about alignment effects in atomic collisions. However, they did not exhaust the possibilities of the field. Further experiments and calculations should continue to provide insights into collision dynamics for alkaline earth metal--rare gas optical collisions.

REFERENCES

1. N. Allard and J. Kielkopf, *Rev. Mod. Phys.* **54**, 1103 (1982).

2. C. H. Greene and R.N. Zare, *Ann. Rev. Phys. Chem.* **33**, 119 (1982).

3. R.L. Robinson, L.J. Kovalenko, and S.R. Leone, *Phys. Rev. Lett.* **64**, 388 (1990).

4. L.J. Kovalenko, R.L. Robinson, and S.R. Leone, *J. Chem. Soc. Faraday Trans. 2* **85**, 939 (1989).

5. K. Burnett, *Phys. Rep.* **118**, 339 (1985).

6. W. Behmenburg, *Phys. Scr.* **36**, 300 (1987).

7. P.D. Kleiber, W.C. Stwalley, and K.M. Sando, *Annu. Rev. Phys. Chem.* **44**, 13 (1993).

8. R.E.M. Hedges, D.L. Drummond, and A. Gallagher, *Phys. Rev. A* **6**, 1519 (1972).

9. J.L. Carlsten, A. Szöke, and M.G. Raymer, *Phys. Rev. A* **15**, 1029 (1977).

10. W.J. Alford, N. Andersen, K. Burnett, and J. Cooper, *Phys. Rev. A* **30**, 2366 (1984).

11. W.J. Alford, N. Andersen, M. Belsley, J. Cooper, D.M. Warrington, and K. Burnett, *Phys. Rev. A* **31**, 3012 (1985).

12. D.A. Olsgaard, M.D. Havey, A. Sieradzan, and R.A. Lasell, *Phys. Rev. Lett.* **69**, 1745 (1992).

13. D.A. Olsgaard, R.A. Lasell, M.D. Havey, and A. Sieradzan, *Phys. Rev. A* **48**, 1987 (1993).

14. S. Yeh and P.R. Berman, *Phys. Rev. A* **22**, 1403 (1980).

15. A.H. Zewail, *Science* **242**, 1645 (1988).

16. S.J. Singer and K.F. Freed, *J. Chem. Phys.* **79**, 6060 (1983).

17. V. Zarfiropulos, P.D. Kleiber, K.M. Sando, X. Zeng, A.M. Lyyra, and W.C. Stwalley, *Phys. Rev. Lett.* **61**, 1485 (1988).

18. J.H. Schloss, R.B. Jones, and J.G. Eden, *Chem. Phys. Lett.* **191**, 195 (1992).

19. K. Burnett, J. Cooper, R.J. Ballagh, and E.W. Smith, *Phys. Rev. A* **22**, 2005 (1980).

20. K. Burnett and J. Cooper, *Phys.Rev. A* **22**, 2027 (1980).

21. K. Burnett and J. Cooper, *Phys. Rev. A* **22**, 2044 (1980).

22. E.L. Lewis, M. Harris, W.J. Alford, J. Cooper, and K. Burnett, *J. Phys. B* **16**, 553 (1983).

23. D. Kupriyanov, to appear in *Chem. Phys.*

24. A.A. Radzig and B.M. Smirnov, *Reference Data on Atoms, Molecules, and Ions* (Springer-Verlag, Berlin, 1985).

25. R.R. Bennett, J.G. McCaffrey, I. Wallace, D.J. Funk, A. Kowalski, and W.H. Breckenridge, *J. Chem. Phys.* **90**, 2139 (1989).

26. I. Wallace and W.H. Breckenridge, *J. Chem. Phys.* **98**, 1 (1993).

27. M. Hliwa and J. Daudey, *Chem. Phys. Lett.* **153**, 471 (1988).

28. M.E. Rose, *Elementary Theory of Angular Momentum* (John Wiley and Sons, New York, 1957).

29. C. Zener, *Proc. Roy. Soc. (London)* **A137**, 696 (1932).

30. W.M. Finlay, unpublished, MIT undergraduate thesis (1979).

31. M.G. Littman and H.J. Metcalf, *Applied Optics* 17 2224 (1978).

32. T.N. Chang, *Phys. Rev. A* **41**, 4922 (1990).

33. R. Loudon, *The Quantum Theory of Light* (Clarendon Press, Oxford, 1992).

APPENDIX 1

The computer program used to control experiment B follows. The specific subprograms that control the liquid crystal variable retarder were adapted from C code written by Meadowlark Optics, and contain proprietary information owned by Meadowlark Optics. They are described in general terms but not reproduced here.

```
'*****************************************************************************
'*****************************************************************************
'**                          POLAR.BAS                                      **
    '** Formerly PMAN2.BAS : accumulates data for polarization
measurements**
    '** prompting for background and manual changing of polarization      **
    '** Changed so that it reverses the order of data taking to average out  **
    '** drifts. Adds channel for second PMT and background for yellow laser
    '** Further modified to use liquid crystal variable retarder and shutters. **
    '** That is, it no longer requires manual polarization changes.       **
    '** programmer: dave o.; modified by RAL                              **
    '**                                                                   **

'*****************************************************************************
'*****************************************************************************

    'Dimension arrays and declare subprograms. Subprogram DAS20 operates
the
    'A to D board. Subprogram reader reads the liquid crystal data file.
    'Subprogram ReadHeader helps it. Subprogram RetControl runs the liquid
    'crystal variable retarder. The other subprograms are called by RetControl
    'to help control the retarder.
    DIM DIO%(10)
    COMMON SHARED DIO%()
    DIM SHARED wavelength%(13), temp%(7), retardance%(135)
    DECLARE SUB DAS20 (MODE%, BYVAL dummy%, flag%)
    DECLARE SUB reader ()
    DECLARE SUB ReadHeader (A%, b%)
DECLARE SUB RetControl (wavelength!, waveretardance!, VoltErr%,
      TempErr%)
    DECLARE SUB ReadTemp (BaseAddr, temperature!)
DECLARE SUB CalcVoltage (wavelength!, waveretardance!, temperature!,
```

```
    SendVolts%)
DECLARE SUB FindIndex (array%(), maxind%, param%, thisind%, perdiff!)
DECLARE SUB OutVoltage (BaseAddr, SendVolts%)
DIM setp$(0 TO 2), bbg$(0 TO 2), pmt%(5)

'Declare the following arrays to be dynamic. That way they can occupy far
'memory. Otherwise this program can't be compiled.
REM $DYNAMIC
DIM SHARED voltage%(13, 7, 135)

'These arrays must be less than 10,000 if the file is to be compiled, unless
'the arrays are dynamically allocated.
DIM IIraw%(10000), LLraw%(10000)
DIM YIIraw%(10000), YLLraw%(10000)
DIM BLraw%(10000), BL2raw%(10000), BGraw%(10000)
DIM YBIraw%(10000), YBLraw%(10000)
DIM IIsub&(500), LLsub&(500)
DIM YIIsub&(500), YLLsub&(500)


CALL reader
Begn:

'Clear the screen.
SCREEN 0, 0, 0: CLS : KEY OFF: WIDTH 80

GOSUB Init          'mode 0-initialize the DAS20 board

'Get information about the run.
5 INPUT "Number of shots each for baseline/background:", Bshots%
10 INPUT "Number of shots per polarization: ", Pshots%
20 INPUT "Number of polarization cycles :", Pcycles%
  IF Pshots% * 2 * Pcycles% > 10000 THEN
    PRINT "Maximum allowed data points is 10000.  Reenter correct
values."
    GOTO 5
  END IF
30 INPUT "Gain (1=x.5, 3=x1, 5=x10, 7=x100): ", gain%
IF gain% <> 1 AND gain% <> 3 AND gain% <> 5 AND gain% <> 7 THEN
    BEEP: GOTO 30
40 INPUT "Name of file to store data: ", filenam$
45 INPUT "Does this file exist yet? ", fis$
50 INPUT "Laser 1 detuning: ", UVdet
55 INPUT "Laser 2 detuning: ", yelldet
```

```
'56 INPUT "Parallel is what retardance (in nm)? ", ParRet!
'57 INPUT "Perpendicular is what retardance(in nm)? ", PerRet!

GOSUB FileOpen    'open the file to store data
GOSUB LambdaCalc  'calculate laser 2 wavelength

q% = Pcycles%
P% = Pshots%


60 'accumulate polarization data

setp$(0) = "PARALLEL"
setp$(1) = "PERPENDICULAR"

FOR k% = 1 TO q%     'no. of times polarization is switched

 'First, this order: baseline, background, parallel, perpendicular
  fst% = 0:   lst% = 1: stp% = 1

  IF Bshots% > 0 THEN  'determine baseline offset and UV background
    GOSUB Back
  END IF
   FOR j% = 0 TO 1      'to take data for each polarization

       'PRINT "set polarization "; setp$(j%);
       GOSUB SetRetardance    'set polarization parallel or perpendicular
    IF Bshots% > 0 THEN GOSUB YellBack  'determine yellow laser
     background
       PRINT "prepare for data measurement"
       INPUT " (press 'Enter' to start)", Enter
            kind% = j% + 4    'identify as parallel or perpendicular data
     FOR i% = 1 TO P%     'no. of shots for each polarization

    IF i% MOD 20 = 0 THEN GOSUB SetRetardance  'read temp every 2
     seconds
       GOSUB trig          'mode 16:analog trigger
       GOSUB AtoD           'mode 3:single A/D conversion in each
channel

      NEXT i%
      BEEP
      shotcount% = 0
    NEXT j%
```

```
        ' GOSUB Calc          'calculate and display polarization

    'Now this order: perpendicular, parallel, background, baseline
      FOR j% = 1 TO 0 STEP -1
        GOSUB SetRetardance
        'print "set polarization "; setp$(j%)
        PRINT "prepare data measurement"
        INPUT " (press 'Enter' to start)", Enter

        kind% = j% + 4

       FOR i% = 1 TO P%

         IF i% MOD 20 = 0 THEN GOSUB SetRetardance  'read cell temp.
often
         GOSUB trig
         GOSUB AtoD

       NEXT i%
       BEEP
       shotcount% = 0
       IF Bshots% > 0 THEN GOSUB YellBack
      NEXT j%
     fst% = 1: lst% = 0: stp% = -1
     IF Bshots% > 0 THEN GOSUB Back 'run background, then baseline

        GOSUB Calc
       IF Bshots% > 0 THEN GOSUB BackDev: GOSUB YellDev
       GOSUB Pdev    'error analysis
       GOSUB FileWrite

    NEXT k%

    PRINT

    corq:
      GOSUB Null
      PRINT
   INPUT "Enter 'c' to change parameters 'n' for new detunings 'q' to quit: ",
        cq$
      IF UCASE$(cq$) = "C" THEN CLEAR : CLOSE #2: GOTO Begn
      IF UCASE$(cq$) = "N" THEN GOSUB NewDetunings
      IF UCASE$(cq$) <> "Q" THEN GOTO 60
```

```
CLOSE #2
END

'*************************************************************************
'*                    END OF MAIN PROGRAM                                *
'*                  BEGINNING OF SUBROUTINES                             *
'*************************************************************************

'*****************************SUBROUTINE INIT*****************************
'* Initializes the DAS20 board. Called once at the program's beginning.  *
'*************************************************************************
Init:
  OPEN "DAS20.ADR" FOR INPUT AS #1
  INPUT #1, DIO%(0)
  CLOSE #1
  DIO%(1) = 2
  DIO%(2) = 1
  flag% = 0
  MD% = 0
  CALL DAS20(MD%, VARPTR(DIO%(0)), flag%)
  IF flag% <> 0 THEN PRINT "INSTALLATION ERROR": STOP
  RETURN

'*************************SUBROUTINE FILEOPEN*****************************
'* Opens a file to store polarization data. Called once at the program's *
'* beginning.   6/9/93                                                   *
'*************************************************************************
FileOpen:
filepath$ = "c:\lasell\dstate\" + filenam$
IF UCASE$(fis$) = "YES" OR UCASE$(fis$) = "Y" THEN
   OPEN filepath$ FOR APPEND AS #2
  ELSEIF UCASE$(fis$) = "NO" OR UCASE$(fis$) = "N" THEN
   OPEN filepath$ FOR OUTPUT AS #2
  ELSE
   BEEP: GOTO 45
  END IF
  RETURN

'*************************SUBROUTINE LAMBDACALC***************************
'* Calculates air wavelength in nm from the given detuning.Called once at*
'* the beginning of the program.    6/13/94                              *
'*************************************************************************
LambdaCalc:
```

```
    reswav! = 53134.7 - 35051.36       '4d-3p levels
    'reswav! = 52556.37 - 35051.36     '5s-3p levels
    wavenumber! = reswav! + yelldet
    centimeters! = 1 / wavenumber!
    vaclambda! = centimeters! * 1E+07
    sig! = 1E-10 * wavenumber! ^ 2
  indref! = 1 + .0001 * (.834213 + (2.40603 / (1.3 - sig!)) + (.015997 / (.389 -
      sig!)))
    lambda! = vaclambda! / indref!
    RETURN


  '*****************************SUBROUTINE BACK*****************************
  '* Takes data for baseline and UV background runs. Uses subroutines trig
*'
'* and AtoD to get data from the DAS20 board, and subroutine BackCalc to
      *'
  '* calculate average signal. Called once at the beginning and once at the  *'
  '* end of each data set.                                                    *'
  '*************************************************************************'
  Back:
    bbg$(0) = "BASELINE"
    bbg$(1) = "UV BACKGROUND"
    PRINT


    FOR j% = fst% TO lst% STEP stp%
      IF j% = 1 THEN
      PRINT "prepare for "; bbg$(j%); " measurement ";
      INPUT "(press 'Enter' to start)", Enter
      kind% = j%
      FOR m% = 1 TO Bshots%

        GOSUB trig
        GOSUB AtoD

      NEXT m%
      BEEP

    NEXT j%

    IF Bshots% > 0 THEN GOSUB BackCalc
      shotcount% = 0
    RETURN
```

```
'**********************SUBROUTINE SETRETARDANCE**********************
'* Sets the retardance by calling the RetControl subroutine.  Called 4 times
*'
'* in each set of data runs.  6/13/94                                  *'
'*************************************************************************
SetRetardance:
  RetWaves! = j% / 2
  'IF j% = 0 THEN RetNm! = ParRet!
  'IF j% = 1 THEN RetNm! = PerRet!
  RetNm! = RetWaves! * lambda!
  CALL RetControl(lambda!, RetNm!, VoltErr%, TempErr%)
  IF VoltErr% = 1 THEN
    PRINT "Error: Retardance or wavelength out of range"
    STOP
  END IF
  IF TempErr% = 1 THEN
    PRINT "Error:  temperature out of range or faulty sensor."
    STOP
  END IF
  RETURN

'**************************SUBROUTINE YELLBACK**************************
'* Takes data for parallel and perpendicular yellow background. Uses subs
*'
'* trig and AtoD to get data from the DAS20 board, and YellCalc to
calculate*'
'* total signal.  Called either twice for parallel, twice for perpendicular *'
'* in each data set.  6/9/93                                           *'
'*************************************************************************
YellBack:
  kind% = j% + 2
  PRINT

    PRINT "prepare for yellow background measurement ";
    INPUT "(press 'Enter' to start)", Enter
    FOR m% = 1 TO Bshots%

   IF m% MOD 20 = 0 THEN GOSUB SetRetardance  'Read cell temp.
    often
      GOSUB trig
      GOSUB AtoD

    NEXT m%
```

```
    BEEP

  GOSUB YellCalc
   shotcount% = 0
  RETURN


'*****************************SUBROUTINE TRIG*****************************
'* Uses the DAS20 board (channel 6) to check for a trigger indicating that
*'
'* data is present;  or to check for a keyboard signal to interrupt the    *'
'* program. Called every time data is taken.                               *'
'*************************************************************************

trig:
   channel% = 6
   level% = 300          '1.5V
   slope% = 1            'negative
   DIO%(0) = channel%
   DIO%(1) = level%
   DIO%(2) = slope%
   MD% = 16
   CALL DAS20(MD%, VARPTR(DIO%(0)), flag%)
   SELECT CASE flag%
     CASE 0
       shotcount% = shotcount% + 1
     CASE 160
       INPUT "abort run or restart from last 'Enter'?(a/r):"; abrst$
       IF UCASE$(abrst$) = "A" THEN GOTO corq
       IF UCASE$(abrst$) = "R" THEN GOSUB Rstrt
       GOSUB trig
     CASE ELSE
       PRINT "MODE 16 ERROR= "; flag%
   END SELECT
   RETURN

'*****************************SUBROUTINE ATOD*****************************
'* Takes data from channels 5 and 7 of the DAS20 board.  Called every
time  *'
'* data is taken.  Modified 6/13/94.                                       *'
'*************************************************************************

AtoD:
   pmtnum% = 0
   FOR channel% = 5 TO 7 STEP 2
    MD% = 3
```

```
DIO%(0) = gain%
DIO%(1) = channel%
CALL DAS20(MD%, VARPTR(DIO%(0)), flag%)
IF flag% <> 0 THEN PRINT "MODE 3 ERROR= "; flag%
pmtnum% = pmtnum% + 1
pmt%(pmtnum%) = DIO%(0)
IF DIO%(0) = 2047 THEN COLOR 4: over = over + 1
NEXT channel%

SELECT CASE kind%
  CASE 0
    BLcount% = BLcount% + 1
    BLraw%(BLcount%) = pmt%(2)
    BLsub& = BLsub& + BLraw%(BLcount%)
    BL2raw%(BLcount%) = pmt%(1)
    BL2sub& = BL2sub& + BL2raw%(BLcount%)
  CASE 1
    BGcount% = BGcount% + 1
    BGraw%(BGcount%) = pmt%(2)
    BGsub& = BGsub& + BGraw%(BGcount%)
  CASE 2
    YBIcount% = YBIcount% + 1
    YBIraw%(YBIcount%) = pmt%(1)
    YBIsub& = YBIsub& + YBIraw%(YBIcount%)
  CASE 3
    YBLcount% = YBLcount% + 1
    YBLraw%(YBLcount%) = pmt%(1)
    YBLsub& = YBLsub& + YBLraw%(YBLcount%)
  CASE 4
    IIcount% = IIcount% + 1
    IIraw%(IIcount%) = pmt%(2)
    IIsub&(k%) = IIsub&(k%) + IIraw%(IIcount%)
    YIIraw%(IIcount%) = pmt%(1)
    YIIsub&(k%) = YIIsub&(k%) + YIIraw%(IIcount%)
  CASE 5
    LLcount% = LLcount% + 1
    LLraw%(LLcount%) = pmt%(2)
    LLsub&(k%) = LLsub&(k%) + LLraw%(LLcount%)
    YLLraw%(LLcount%) = pmt%(1)
    YLLsub&(k%) = YLLsub&(k%) + YLLraw%(LLcount%)
  CASE ELSE
    PRINT "Error in kind%-not one of the assigned numbers."
    STOP
END SELECT
```

```
    PRINT shotcount%, j%, pmt%(2), pmt%(1)
    COLOR 7
    RETURN

'*****************************SUBROUTINE CALC*******************************
'* Calculates total signal after a set of data runs and prints it to the   *'
'* screen.  Called once every data set.                                     *'
'*************************************************************************'
Calc:
    IItot& = IItot& + IIsub&(k%)
    LLtot& = LLtot& + LLsub&(k%)
    IIsub&(k%) = 0: LLsub&(k%) = 0
    IImean = IItot& / IIcount%
    LLmean = LLtot& / LLcount%
    YIItot& = YIItot& + YIIsub&(k%)
    YLLtot& = YLLtot& + YLLsub&(k%)
    YIIsub&(k%) = 0: YLLsub&(k%) = 0
    YIImean = YIItot& / IIcount%
    YLLmean = YLLtot& / LLcount%
    PRINT
    PRINT "IItotal1="; IItot&, , "LLtotal1="; LLtot&
    PRINT "IItotal2="; YIItot&, , "LLtotal2="; YLLtot&
    PRINT "IImean1="; IImean, , "LLmean1="; LLmean
    PRINT "IImean2="; YIImean, , "LLmean2="; YLLmean
    PRINT
    RETURN

'*************************SUBROUTINE BACKDEV*******************************
'* Calculates the standard deviation in the baseline and UV background
data.*'
'* Called once every data set.                                             *'
'*************************************************************************'
BackDev:
    BLvar = 0: BL2var = 0
    FOR bl% = 1 TO BLcount%
        BLvar = BLvar + (BLraw%(bl%) - BLmean) ^ 2
        BL2var = BL2var + (BL2raw%(bl%) - BL2mean) ^ 2
    NEXT bl%
    BLdev = SQR(BLvar / BLcount% / (BLcount% - 1))
    BL2dev = SQR(BL2var / BLcount% / (BLcount% - 1))

    BGvar = 0
    FOR BG% = 1 TO BGcount%
        BGvar = BGvar + (BGraw%(BG%) - BGmean) ^ 2
```

```
  NEXT BG%
  BGdev = SQR(BGvar / BGcount% / (BGcount% - 1))

 RETURN

'*****************************SUBROUTINE PDEV*****************************
'* Calculates the standard deviation for the parallel and perpendicular   *'
'* intensity data, calculates polarization (and its error) and total      *'
'* intensity and prints to the screen.  Called once every data set.       *'
'*************************************************************************
Pdev:
  Πvar = 0: YΠvar = 0
  FOR Π% = 1 TO Πcount%
    Πvar = Πvar + (Πraw%(Π%) - Πmean) ^ 2
    YΠvar = YΠvar + (YΠraw%(Π%) - YΠmean) ^ 2
  NEXT Π%
  Πdev = SQR(Πvar / Πcount% / (Πcount% - 1))
  YΠdev = SQR(YΠvar / Πcount% / (Πcount% - 1))

  LLvar = 0: YLLvar = 0
  FOR LL% = 1 TO LLcount%
    LLvar = LLvar + (LLraw%(LL%) - LLmean) ^ 2
    YLLvar = YLLvar + (YLLraw%(LL%) - YLLmean) ^ 2
  NEXT LL%
  LLdev = SQR(LLvar / LLcount% / (LLcount% - 1))
  YLLdev = SQR(YLLvar / LLcount% / (LLcount% - 1))

  ΠBdev = SQR(Πdev ^ 2 + BGdev ^ 2)        'for PMT 1
  LBdev = SQR(LLdev ^ 2 + BGdev ^ 2)
  ΠLdev = SQR(ΠBdev ^ 2 + LBdev ^ 2)

  YΠBdev = SQR(YΠdev ^ 2 + YBΠdev ^ 2)     'for PMT 2
  YLBdev = SQR(YLLdev ^ 2 + YBLdev ^ 2)
  YΠLdev = SQR(YΠBdev ^ 2 + YLBdev ^ 2)

  Πcorr = Πmean - BGmean                   'for PMT 1
  LLcorr = LLmean - BGmean
  Tcorr = Πcorr + (2 * LLcorr)

  YΠcorr = YΠmean - YBΠmean                'for PMT 2
  YLLcorr = YLLmean - YBLmean
  YTcorr = YΠcorr + (2 * YLLcorr)

  Pminus = Πcorr - LLcorr + 1E-10          'for PMT1
```

```
    Pplus = IIcorr + LLcorr + 1E-10
    LP = Pminus / Pplus
  LPdev = SQR((LP ^ 2) * ((ILdev ^ 2 / Pminus ^ 2) + (ILdev ^ 2 / Pplus ^
      2)))

    YPminus = YIIcorr - YLLcorr + 1E-10
    YPplus = YIIcorr + YLLcorr + 1E-10
    YLP = YPminus / YPplus
  YLPdev = SQR((YLP ^ 2) * ((YILdev ^ 2 / YPminus ^ 2) + (ILdev ^ 2 /
      YPplus ^ 2)))

    PRINT "Background corrected results:"
    PRINT
  PRINT "mean baseline1="; BLmean, "mean baseline2="; BL2mean, "mean UV
      background="; BGmean, "mean BG-BL="; BGmean - BLmean
  PRINT "mean II yellow background="; YBImean, "mean LL yellow
      background="; YBLmean
  PRINT "mean YII-BL="; YBImean - BL2mean, "mean YLL-BL="; YBLmean -
      BL2mean
    PRINT
  results1$ = "    IIcorr1=####.#(##.#)   LLcorr1=####.#(##.#)
      Lpol1=###.#(#.#)"
    COLOR 5
    PRINT USING results1$; IIcorr, IBdev, LLcorr, LBdev, LP * 100, LPdev *
100
    PRINT
    COLOR 2
  results2$ = "    IIcorr2=####.#(##.#)   LLcorr2=####.#(##.#)
      Lpol2=###.#(#.#)"
  PRINT USING results2$; YIIcorr, YIBdev, YLLcorr, YLBdev, YLP * 100,
      YLPdev * 100
    PRINT
    COLOR 7
  results3$ = "Total Signal 1 = ####.#  Total Signal 2 = ####.#  Over Range
      shots= ##  A/D gain = #"
    PRINT USING results3$; Tcorr, YTcorr, over, gain%
    PRINT
    RETURN

  '*************************SUBROUTINE FILEWRITE*************************
  '* Writes polarization and intensity data to a file.  Called once every set *'
  '* of data runs.  6/9/93.                                                    *'
  '************************************************************************
  FileWrite:
```

```
      WRITE #2, UVdet
      WRITE #2, yelldet
      WRITE #2, BGmean - BLmean, IIcorr, LLcorr, Tcorr, LP * 100, LPdev *
100
  WRITE #2, YBImean - BLmean, YBLmean - BLmean, YIIcorr, YLLcorr,
        YTcorr, YLP * 100, YLPdev * 100

      RETURN

    '**********************SUBROUTINE NEWDETUNINGS**********************
    '* Changes the detunings recorded for the UV and yellow laser.  Called
only *'
    '* at the user's request.  6/9/93                                    *'
    '*******************************************************************************
    NewDetunings:
      INPUT "Laser 1 detuning: ", UVdet
      INPUT "Laser 2 detuning: ", yelldet
      'INPUT "Parallel is what retardance (in nm)? ", ParRet!
      'INPUT "Perpendicular is what retardance (in nm)? ", PerRet!
      GOSUB LambdaCalc
      RETURN

    '*****************************SUBROUTINE NULL*****************************
    '* Resets all arrays and totals to zero.  Called at the program's end or   *'
    '* cancellation.                                                           *'
    '*******************************************************************************
    Null:
      shotcount% = 0: IIcount% = 0: LLcount% = 0: BLcount% = 0: BGcount%
= 0
      YIIcount% = 0: YLLcount% = 0: YBIcount% = 0: YBLcount% = 0
      FOR NLL% = 0 TO q%
    IIsub&(NLL%) = 0: LLsub&(NLL%) = 0: YIIsub&(NLL%) = 0:
       YLLsub&(NLL%) = 0
      NEXT NLL%
      BLsub& = 0: BGsub& = 0: YBIsub& = 0: YBLsub& = 0: BL2sub& = 0
      IItot& = 0: LLtot& = 0: YIItot& = 0: YLLtot& = 0
      BLtot& = 0: BGtot& = 0: YBItot& = 0: YBLtot& = 0: BL2tot& = 0
      over = 0
      RETURN

    '**************************SUBROUTINE BACKCALC**************************
    '* Calculates total signal for baseline and UV background and prints it on
*'
    '* the screen.  Called by subroutine Back each time it runs.               *'
```

```
'*************************************************************************
BackCalc:
   BLtot& = BLtot& + BLsub&
   BL2tot& = BL2tot& + BL2sub&
   BGtot& = BGtot& + BGsub&
   BLmean = BLtot& / BLcount%
   BL2mean = BL2tot& / BLcount%
   BGmean = BGtot& / BGcount%
   BLsub& = 0: BGsub& = 0: BL2sub& = 0
   PRINT
PRINT "mean baseline1="; BLmean, "mean baseline2="; BL2mean, "mean UV
     background="; BGmean
   PRINT
  RETURN

'************************SUBROUTINE YELLCALC*************************
'* Calculates the total and average signal in yellow background runs.    *'
'* Called by subroutine YellBack each time it runs.  6/9/93              *'
'*************************************************************************
YellCalc:
   IF j% = 0 THEN
     YBItot& = YBItot& + YBIsub&
     YBImean = YBItot& / YBIcount%
     ymean = YBImean
   ELSE
    YBLtot& = YBLtot& + YBLsub&
    YBLmean = YBLtot& / YBLcount%
    ymean = YBLmean
   END IF

   YBIsub& = 0: YBLsub& = 0
   PRINT
   PRINT "mean yellow background="; ymean
   PRINT
  RETURN

'*****************************SUBROUTINE RSTRT*****************************
'* Sets counts and totals to zero in an individual run to restart that run  *'
'* without restarting the whole set of runs.  Called only at the user's     *'
'* request.  Modified 6/13/94 for clarity.                                  *'
'*************************************************************************
Rstrt:
   SELECT CASE kind%
     CASE 0
```

```
      BLcount% = BLcount% - m% + 1
      BLsub& = 0
      BL2sub& = 0
    CASE 1
      BGcount% = BGcount% - m% + 1
      BGsub& = 0
    CASE 2
      YBIcount% = YBIcount% - m% + 1
      YBIsub& = 0
    CASE 3
      YBLcount% = YBLcount% - m% + 1
      YBLsub& = 0
    CASE 4
      IIcount% = IIcount% - i% + 1
      IIsub&(k%) = 0
      YIIsub&(k%) = 0
    CASE 5
      LLcount% = LLcount% - i% + 1
      LLsub&(k%) = 0
      YLLsub&(k%) = 0
    CASE ELSE
      PRINT "error in program; kind% not one of the possible values."
      STOP
    END SELECT

  IF kind% = 4 OR kind% = 5 THEN
     shotcount% = shotcount% - i% + 1
     i% = 1
   ELSE
     shotcount% = shotcount% - m% + 1
     m% = 1
  END IF

  INPUT "RESTART (press 'Enter' to start)"; Enter
  RETURN

'************************SUBROUTINE YELLDEV*****************************
'* Calculates the standard deviation in the yellow background data.  Called
*'
'* at the end of each set of data runs.  6/9/93                          *'
'************************************************************************
YellDev:
  YBIvar = 0
  FOR bl% = 1 TO YBLcount%
```

```
    YBIvar = YBIvar + (YBIraw%(bl%) - YBImean) ^ 2
  NEXT bl%
  YBIdev = SQR(YBIvar / YBIcount% / (YBIcount% - 1))

  YBLvar = 0
  FOR BG% = 1 TO YBLcount%
    YBLvar = YBLvar + (YBLraw%(BG%) - YBLmean) ^ 2
  NEXT BG%
  YBLdev = SQR(YBLvar / YBLcount% / (YBLcount% - 1))

 RETURN



END

REM $STATIC
'************************SUBPROGRAM CALCVOLTAGE************************
'* Calculates the voltage needed to set the liquid crystal at the required  *'
'* retardance for the given wavelength and temperature. Receives            *'
'* wavelength, retardance, and temperature values, and returns the needed
*'
'* voltage. Uses shared arrays for voltage, wavelength, retardance, and     *'
'* temperature. Called each time the retardance changes. Written by RAL,
*'
'* starting 6/16/94. Contains proprietary information.
*'
'************************************************************************

'************************SUBPROGRAM FINDINDEX*************************
'* For wavelength, temperature, and retardance, finds the element of the
*'
'* voltage array that's just less than the required value, and the percent  *'
'* of the difference between voltage values to add in order to interpolate  *'
'* to find the correct voltage. Called every time the retardance changes.   *'
'* Written by RAL, starting 6/16/94. Contains proprietary information.      *'

'************************************************************************

'************************SUBPROGRAM OUTVOLTAGE************************
'* Writes the desired voltage to the digital I/O board, which sends it to  *'
'* the liquid crystal variable retarder controller. Receives the base      *'
```

```
'* address of the I/O card and the required voltage. Called every time
*'
'* the retardance is changed. Written by RAL, starting 6/20/94.  *'
'* Contains proprietary information.
*'
'*************************************************************************'

'*************************SUBPROGRAM READER*************************'
'* Subprogram to read the data file for the pc1090 liquid crystal variable *'
'* retarder. Called once at the program's beginning. Written by RAL  *'
'* 6/15/94. Contains proprietary information.  *'
'*************************************************************************'

'*************************SUBPROGRAM READHEADER*************************'
'* Reads the header for the voltage/retardance table and extracts the  *'
'* wavelength and temperature from the surrounding text. Called for each *'
'* temperature/wavelength combination while reading the data file.
*'
'* Written by RAL starting 6/15/94.  Contains proprietary information.
*'
'*************************************************************************'

'*************************SUBPROGRAM READTEMP*************************'
'* Reads the temperature of the liquid crystal cell, so that the voltage  *'
'* can be calculated. Receives the base address of the I/O board, returns *'
'* cell temperature.  Called each time the retardance changes. Written by
*'
'* RAL, starting 6/20/94. Contains proprietary information.  *'
'*************************************************************************'

'*************************************************************************'
'*************************SUBPROGRAM RETCONTROL*************************'
'** A subprogram to control the liquid crystal variable retarder. Adapted
**'
'** from a C program written by Meadowlark Optics, April 1994.
Adaptation**'
'** by RAL starting 6/15/94. Contains proprietary information.
**'
'*************************************************************************'
'*************************************************************************'
```

APPENDIX 2

A rate equation analysis of collisional depolarization of resonance Mg-rare gas $^1S_0 \rightarrow {}^1P_1$ transitions is presented, followed by a rate equation analysis for off-resonance transitions.

Figure 34 shows the energy levels involved in the transition. First, consider the level when the laser is off. The sublevels have collisional mixing rates of γ_{ij}, where i and j refer to any two different levels, and radiative decay rates of $\gamma = 1/\tau$, where τ is the lifetime of the P state. Then the upper energy sublevels have populations changing at the following rates:

$$\begin{aligned} \dot{N}_c &= -(\gamma+\gamma_{cb}+\gamma_{ca})N_c + \gamma_{bc}N_b + \gamma_{ac}N_a \\ \dot{N}_b &= -(\gamma+\gamma_{bc}+\gamma_{ba})N_b + \gamma_{cb}N_c + \gamma_{ab}N_a \\ \dot{N}_a &= -(\gamma+\gamma_{ac}+\gamma_{ab})N_a + \gamma_{ca}N_c + \gamma_{ba}N_b \end{aligned} \tag{A.1}$$

Detailed balancing gives $\gamma_{ij} = \gamma_{ji}$; assuming an aligned system, $N_c = N_a$. These substitutions allow the equations to be written as

$$\begin{aligned} \dot{N}_a &= -(\gamma+\gamma_{ab})N_a + \gamma_{ab}N_b \\ \dot{N}_b &= -(\gamma+\gamma_{ab})N_b + 2\gamma_{ab}N_a \end{aligned} \tag{A.2}$$

Now, use the definition of alignment, $\langle A_0 \rangle$, and total population N.

$$\langle A_0 \rangle = \frac{\sum_m (3m^2 - j(j+1))N_m}{j(j+1)} \tag{A.3}$$

where N_m is the population of a given sublevel and for the 3s3p $^1P_1$ state, j=1.

FIGURE 34

The energy levels involved in the collisional disalignment of the 3s3p $^1P_1$ level in Mg - rare-gas optical collisions. The collisional mixing rates γ_{ij} and the radiation rate γ are shown.

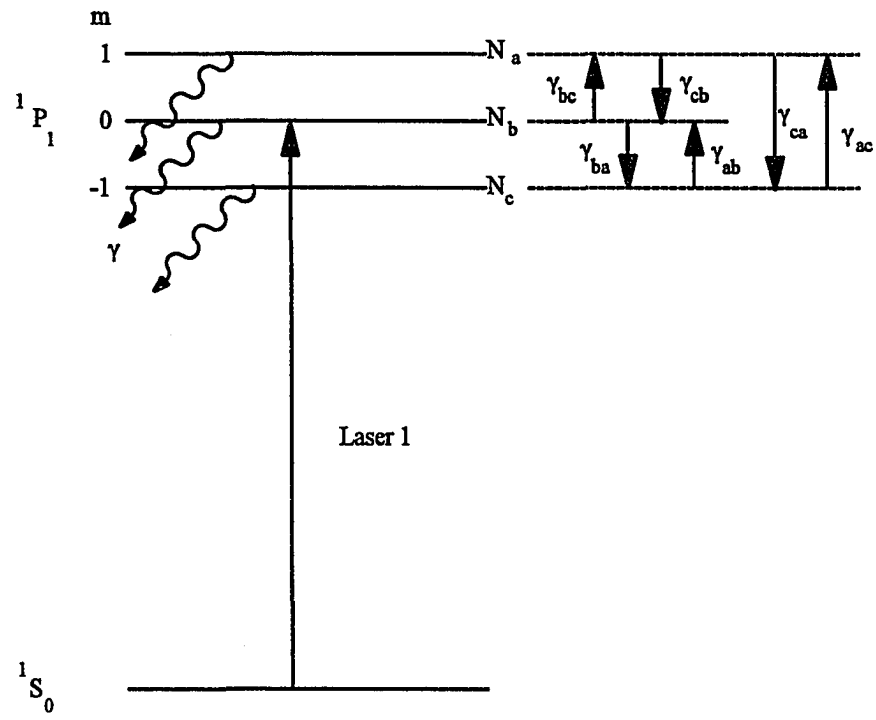

Therefore this can be written as

$$\begin{aligned} \langle A_0 \rangle &= \frac{1}{2}(N_a - 2N_b + Nc) \\ &= N_a - N_b \end{aligned} \tag{A.4}$$

The total population N is just

$$\begin{aligned} N &= N_a + N_b + N_c \\ &= 2N_a + N_b \end{aligned} \tag{A.5}$$

The rates of change are then

$$\begin{aligned} \langle \dot{A}_0 \rangle &= \dot{N}_a - \dot{N}_b \\ \langle \dot{A}_0 \rangle &= -(\gamma + 3\gamma_{ab}) \langle A_0 \rangle \end{aligned} \tag{A.6}$$

and

$$\begin{aligned} \dot{N} &= 2\dot{N}_a + \dot{N}_b \\ \dot{N} &= -(2\gamma N_a + \gamma N_b) \\ \dot{N} &= -\gamma N \end{aligned} \tag{A.7}$$

Integrating these equations gives

$$\begin{aligned} \langle A_0(t) \rangle &= \langle A_0(0) \rangle e^{-(\gamma + 3\gamma_{ab})t} \\ N(t) &= N(0) e^{-\gamma t} \end{aligned} \tag{A.8}$$

Now consider the situation when the laser is on, exciting level *a* at a rate Γ_a and exciting level *b* at a rate Γ_b. The level populations now change at the new rates

$$\begin{aligned} \dot{N}_a &= -(\gamma + \gamma_{ab}) N_a + \gamma_{ab} N_b + \Gamma_a \\ \dot{N}_b &= -(\gamma + 2\gamma_{ab}) N_b + 2\gamma_{ab} N_a + \Gamma_b \end{aligned} \tag{A.9}$$

Substituting for $<A_0>$ and N in these equations and integrating gives

$$\begin{aligned} <A_0(t)> &= \frac{\Gamma_a-\Gamma_b}{\gamma+3\gamma ab}\left(1-e^{-(\gamma+3\gamma ab)t}\right) \\ N(t) &= \frac{2\Gamma_a+\Gamma_b}{\gamma}\left(1-e^{-\gamma t}\right) \end{aligned} \tag{A.10}$$

If the laser is on for a time T_1, then shut off, equations (A.10) hold while it is on, and equations (A.8) hold while it is off. This gives, after the pulse, the expressions

$$\begin{aligned} <A_0(t)> &= \frac{\Gamma_a-\Gamma_b}{\gamma+3\gamma_{ab}}e^{-(\gamma+3\gamma_{ab})t}\left(e^{(\gamma+3\gamma_{ab})T_1}-1\right) \\ N(t) &= \frac{2\Gamma_a+\Gamma_b}{\gamma}e^{-\gamma t}\left(e^{-\gamma T_1}-1\right) \end{aligned} \tag{A.12}$$

If the population distribution is observed only while a gate of width T_2 is open, the observed alignment and population will be averaged, or integrated, over the gate. Integrating equations (A.12) over a gate gives

$$<\bar{A}_0> = \frac{(\Gamma_a-\Gamma_b)T_1}{(\gamma+3\gamma_{ab})T_2}+e^{-(\gamma+\gamma_{ab})T_2}\left(1-e^{(\gamma+3\gamma_{ab})T_1}\right)\frac{\Gamma_a-\Gamma_b}{(\gamma+3\gamma_{ab})^2} \tag{A.13}$$

$$\bar{N} = \frac{(2\Gamma_a+\Gamma_b)T_1}{\gamma T_2}+\frac{2\Gamma_a+\Gamma_b}{\gamma^2 T_2}e^{-\gamma T_2}\left(1-e^{\gamma T_1}\right) \tag{A.14}$$

To get an alignment per atom, as defined in Chapter 2, divide the ensemble $\langle A_0 \rangle$ by the total population. In equation A.14, the variables are all known except for Γ_a and Γ_b. The effective laser pulsewidths are T_1 = 3 ns and T_2 = 4 ns; the lifetime of the 3s3p $^1P_1$ state is 2.1 ns = $\tau = 1/\gamma$. Substituting these numbers into equations (A .13) and (A.14) and dividing (A.13) by (A.14) gives the result mentioned in chapter 4:

$$\langle A_0 \rangle = -\Gamma_r \left[\frac{1.4}{x} + \frac{1.05}{x^2} e^{-1.90x}(1 - e^{1.43x}) \right] \tag{A.15}$$

where $x = 1 + 3\gamma_{ab}\tau$ and $\Gamma_r = (\Gamma_a - \Gamma_b)/(2\Gamma_a + \Gamma_b)$. The disalignment rate k is related by $k = 3\gamma_{ab}/n$, where n is the number density of rare gas atoms. From equations (2.16), this alignment gives a polarization for excitation near the 3s4d $^1D_2$ state of

$$P_L = \frac{3\Gamma_r \left[\frac{1.45}{x} + \frac{1.05}{x^2} e^{-1.90x}(1 - e^{1.43x}) \right]}{20 + \Gamma_r \left[\frac{1.45}{x} + \frac{1.05}{x^2} e^{-1.90x}(1 - e^{1.43x}) \right]} \tag{A.16}$$

For excitation near the 3s5s $^1S_0$ state, the polarization is

$$P_L = \frac{3\Gamma_r \left[\frac{1.45}{x} + \frac{1.05}{x^2} e^{-1.90x}(1 - e^{1.43x}) \right]}{2 + \Gamma_r \left[\frac{1.45}{x} + \frac{1.05}{x^2} e^{-1.90x}(1 - e^{1.43x}) \right]} \tag{A.17}$$

Although this equation has a complex pressure dependence, for small pressures the inverse polarization is nearly linear in pressure. Using the value

of k and P_L^{-1} found for Mg-Ar at a detuning of 16.8 cm^{-1} ($k = 1.33 \times 10^{-9}$ cm^3/s, $P_L^{-1} = 1.91$) as an example, Figure 35 plots $P_L^{-1}(P)$, calculated using the inverse of equation (A.17), versus pressure for 0-30 torr. The line on the graph is a best fit to the points; its correlation is 0.9991. This shows the linear behavior of the equation at low pressures.

FIGURE 35
A plot of P_L^{-1} versus pressure for low pressures, showing its linearity.

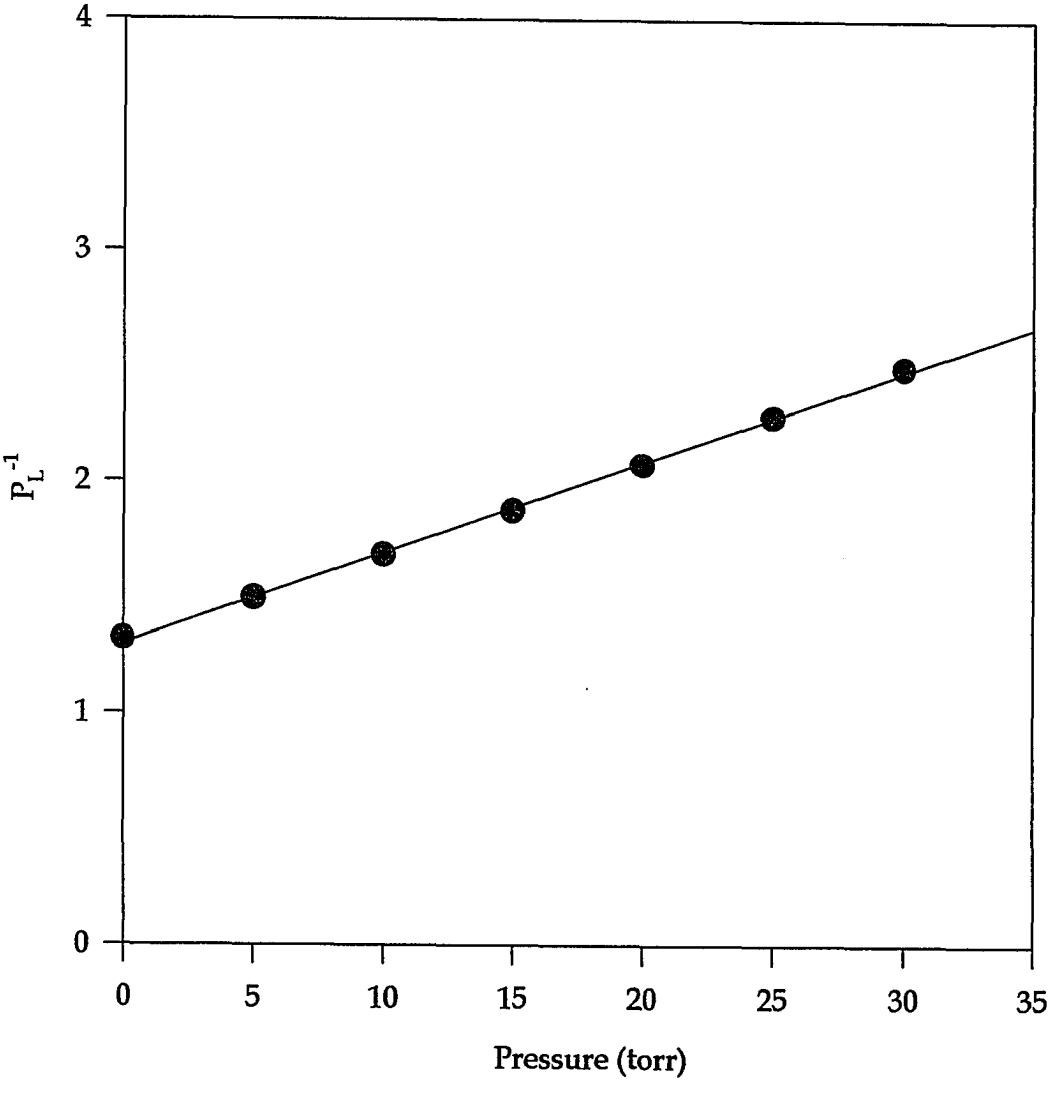

BIOGRAPHY

Rosemary Lasell was born in Montpelier, Vermont on October 24, 1963. She received a B.S. in Physics from Bob Jones University in May of 1985 and entered Old Dominion University as a graduate student in August of 1988. She was a teaching assistant for three years, then received a Patricia Roberts Harris fellowship for 1991-1994, and then was supported by a Graduate Assistance in Areas of National Need fellowship for August 1994-May 1995. During her graduate studies, she worked on three papers that have been published and two others that are in preparation. She is a member of the American Physical Society and the American Association of Physics Teachers.

PUBLICATIONS

R.A. Lasell, D.A. Olsgaard, M.D. Havey, and Dmitriy V. Kupriyanov, "Polarization spectra of excited-state-Mg(3p)--rare-gas-atom optical collisions," Physical Review A50, 423 (1994).

D.A. Olsgaard, R.A. Lasell, M.D. Havey, and A. Sieradzan, "Polarization and intensity spectra for Mg-Ne and Mg-Ar fractional collisions," Physical Review A48, 1987 (1993).

D.A. Olsgaard, M.D. Havey, A. Sieradzan, and R.A. Lasell, "Alignment Spectra of Two-Photon, Magnesium-Rare-Gas-Atom Fractional Collisions," Physical Review Letters 69, 1745 (1992).